

Electronic Thesis and Dissertation Repository

June 2012

Bayesian Analyses of Metal-Loss Corrosion on Energy Pipeline Based on Inspection Data

Mohammad Al-Amin,

Supervisor: Dr. Wenxing Zhou, *The University of Western Ontario*

A thesis submitted in partial fulfillment of the requirements for the Master of Engineering Science degree in Civil and Environmental Engineering

© Mohammad Al-Amin 2012

Follow this and additional works at: <https://ir.lib.uwo.ca/etd>



Part of the [Civil and Environmental Engineering Commons](#)

Recommended Citation

Al-Amin, Mohammad, "Bayesian Analyses of Metal-Loss Corrosion on Energy Pipeline Based on Inspection Data" (2012). *Electronic Thesis and Dissertation Repository*. 588.
<https://ir.lib.uwo.ca/etd/588>

This Dissertation/Thesis is brought to you for free and open access by Scholarship@Western. It has been accepted for inclusion in Electronic Thesis and Dissertation Repository by an authorized administrator of Scholarship@Western. For more information, please contact wlsadmin@uwo.ca.

**BAYESIAN ANALYSES OF METAL-LOSS CORROSION ON
ENERGY PIPELINES BASED ON INSPECTION DATA**

(Spine title: Bayesian Analyses of Metal-loss Corrosion on Energy Pipelines)

(Thesis format: Integrated Article)

by

Mohammad Al-Amin

Graduate Program in Engineering Science
Department of Civil and Environmental Engineering

A thesis submitted in partial fulfillment
of the requirements for the degree of
Master of Engineering Science

The School of Graduate and Postdoctoral Studies
Western University
London, Ontario, Canada

© Mohammad Al-Amin 2012

WESTERN UNIVERSITY
SCHOOL OF GRADUATE AND POSTDOCTORAL STUDIES

CERTIFICATE OF EXAMINATION

Supervisor

Examiners

Dr. Wenxing Zhou

Dr. F. Michael Bartlett

Supervisory Committee

Dr. Hanping Hong

Dr. Hanping Hong

Dr. Jeff T. Wood

The thesis by

Mohammad Al-Amin

entitled:

**Bayesian analyses of Metal-loss Corrosion on Energy Pipelines Based on
Inspection Data**

is accepted in partial fulfillment of the
requirements for the degree of
Master of Engineering Science

Date _____

Chair of the Thesis Examination Board

Abstract

Bayesian models are developed to calibrate the accuracies of high-resolution in-line inspection (ILI) tools for sizing metal-loss corrosion defects and to characterize the growth of individual defects on energy pipelines. Moreover, a methodology is proposed to evaluate the time-dependent system reliability of a segment of a pressurized pipeline containing multiple active corrosion defects. The calibration of ILI tools is carried out by comparing the field-measured depths and ILI-reported depths for a set of static defects. The measurement error associated with the field-measuring tool is found to be negligibly small; therefore, the field-measured depth is assumed to equal the actual depth of the defect. The depth of a corrosion defect reported by an ILI tool is assumed to be a linear function of the corresponding field-measured depth subjected to a random scattering error. The probabilistic characteristics of the intercept and slope in the linear function, i.e. the constant and non-constant biases of the measurement error, as well as the standard deviation of the random scattering error are then quantified using the Bayesian methodology. The proposed methodology is able to calibrate the accuracies of multiple ILI tools simultaneously and quantify the potential correlations between the random scattering errors associated with different ILI tools.

The corrosion growth model is developed in a hierarchical Bayesian framework. The depth of the corrosion defects is assumed to be a power-law function of time characterized by two power-law coefficients and the corrosion initiation time, and the probabilistic characteristics of the parameters involved in the growth model are evaluated using Markov Chain Monte Carlo (MCMC) simulation technique based on ILI data

collected at different times for a given pipeline. The model accounts for the constant and non-constant biases and random scattering errors of the ILI data, as well as the potential correlation between the random scattering errors associated with different ILI tools. The model is validated by comparing the predicted depths with the field-measured depths of two sets of external corrosion defects identified on two in-service natural gas pipelines.

A simulation-based methodology is proposed to evaluate the time-dependent system reliability of a segment of a pressurized pipeline containing multiple active metal-loss corrosion defects. The methodology considers three distinctive failure modes, namely small leak, large leak and rupture, and incorporates the hierarchical Bayesian power-law growth model for the depth of individual corrosion defect. Both the conventional Monte Carlo simulation and MCMC simulation techniques are employed in the methodology to evaluate the failure probability. The methodology is illustrated using a joint of an underground natural gas pipeline that is currently in service.

Keywords: Metal-loss corrosion, pipeline, ILI, growth model, measurement error, Bayesian updating, MCMC and reliability.

Dedication

To my parents, Md. Moslem Miah and Safia Khatoon

Acknowledgments

First of all, I would like to express my sincere appreciation and deep gratitude to my supervisor, Dr. Wenxing Zhou for his patient guidance, understanding, and most importantly for continuously supporting me with his profound insight, and constant encouragement throughout this study. I was fortunate enough to have the opportunity of being a member of his research group. His door was always open for me even in his busiest days. This thesis would definitely have not been possible without him.

I would also like to thank Dr. Hanping Hong, Dr. Michael Bartlett and Dr. Jeff T. Wood for being my examiners and for their constructive advice to this thesis. I would also express my gratitude to Shahani Kariyawasam and Hong Wang from TransCanada for their valuable comments and suggestions during a project related to my thesis.

I would like to thank my colleagues of our research group for making my graduate life so enjoyable and also for their encouragement and assistances. My especial thanks go to Shenwei Zhang who helped me a lot not only in my research but also the courses we took together.

Financial support provided by TransCanada and the Natural Sciences and Engineering Research Council of Canada (NSERC) and by the Faculty of Engineering at Western University is gratefully acknowledged.

Finally, I would like to thank my parents and my sisters for everything they have done for me leading up to this moment. Last but not least, I would like to thank Jannatul Fardows for her love, encouragement and support throughout my Master's program.

Table of Contents

CERTIFICATE OF EXAMINATION	ii
Abstract	iii
Dedication	v
Acknowledgments	vi
Table of Contents	vii
List of Tables	xii
List of Figures	xiii
List of Abbreviations, Symbols, Nomenclature	xv
Chapter 1 Introduction	1
1.1 Background.....	1
1.2 Objective and Research Significance.....	8
1.3 Scope of the Study	8
1.4 Thesis Format.....	10
References.....	10
Chapter 2 Bayesian Model for Calibration of ILI Tools	13
2.1 Introduction.....	13
2.2 Bayesian Methodology	16
2.2.1 Basic Formulation.....	16

2.2.2 Markov Chain Monte Carlo Simulation	18
2.3 Measurement Error Model for Corrosion Defects	20
2.4 Measurement Error of Field Measurement	22
2.5 Bayesian Calibration Model for ILI Tools	24
2.5.1 Formulation and the Likelihood Function	24
2.5.2 Prior Distributions.....	25
2.6 Case Study	27
2.6.1 General.....	27
2.6.2 Case 1.....	28
2.6.3 Case 2.....	38
2.7 Conclusion	42
References.....	43
Chapter 3 Hierarchical Bayesian Corrosion Growth Model Based on In-Line	
Inspection Data.....	46
3.1 Introduction.....	46
3.2 Hierarchical Bayesian Model.....	49
3.3 ILI Data and Measurement Uncertainties	54
3.4 Hierarchical Bayesian Corrosion Growth Model	55
3.4.1 Formulation and the Likelihood Function	55
3.4.2 Prior Distribution	57

3.4.3 Hyper-prior Distribution	58
3.5 Case Study	60
3.5.1 General.....	60
3.5.2 Case 1.....	61
3.5.3 Case 2.....	77
3.5.4 Effect of Correlation among the Random Scattering Measurement Errors	88
3.6 Comparison with Industry Practice.....	93
3.7 Conclusion	95
References.....	97

Chapter 4 Time-dependent System Reliability Analysis of a Corroding

Pipeline	101
4.1 Introduction.....	101
4.2 Limit State Functions.....	104
4.3 Burst and Rupture Pressure Models.....	107
4.4 Corrosion Growth Model.....	109
4.5 System Reliability Analysis	110
4.5.1 Basic Assumptions	110
4.5.2 Analysis Procedure.....	110
4.6 Numerical Example	113
4.6.1 General.....	113

4.6.2 Growth Mode for the Defect Depth	114
4.6.3 Probabilistic Characteristics of Input Parameters	118
4.6.4 Results.....	120
4.6.5 Sensitivity analysis.....	121
4.7 Conclusion	124
References.....	125
Chapter 5 Summary and Conclusions	128
5.1 General.....	128
5.2 Bayesian Model for Calibration of ILI Tools.....	128
5.3 Hierarchical Bayesian Corrosion Growth Model Based on In-line Inspection Data	130
5.4 Time-dependent System Reliability Analysis of a Corroding Pipeline	133
5.5 Recommendations for Future Work.....	134
References.....	135
Appendix 2A Algorithms for Performing Markov Chain Monte Carlo Simulation.....	136
2A.1 Metropolis-Hastings Algorithm	136
2A.2 Gibbs Sampler.....	139
References.....	142
Appendix 2B Grubbs' Estimator and Jaech's Estimator	144

2B.1 Grubbs' Estimator	144
2B.2 Jaech's Estimator.....	145
References.....	146
Appendix 2C Derivation of the Conditional Posterior Distributions of Parameters of Bayesian Calibration Model	147
Appendix 2D OpenBUGS code for Bayesian calibration model of Case 1.....	152
Appendix 2E OpenBUGS code for Bayesian calibration model of Case 2.....	156
Appendix 3A Derivation of the Conditional Posterior Distributions of the HBM corrosion growth model	160
Appendix 3B OpenBUGS code for HBM model of Case 1.....	166
Appendix 3C OpenBUGS code for HBM model of Case 2	171
Curriculum Vitae.....	176

List of Tables

Table 2.1 Mean values of the parameters in the calibration models for ILI tools used in Case 1	35
Table 2.2 Mean values of the correlation coefficients (ρ_{kl}) between the random scattering errors for different ILI tools used in Case 1	35
Table 2.3 Mean values of the parameters in the calibration models for ILI tools used in Case 2	39
Table 2.4 Mean values of the correlation coefficients (ρ_{kl}) between the random scattering errors for different ILI tools in Case 2	40
Table 3.1 MSEPs for the models with partially-correlated, fully-correlated and independent random scattering errors	90
Table 3.2 p -values of the null hypothesis, H_0 : $MSEP_1 = MESP_2$ ($MSEP_1 = MESP_3$) and alternative hypothesis H_a : $MSEP_1 < MESP_2$ ($MSEP_1 < MESP_3$)	92
Table 4.1 Probabilistic characteristics of the basic random variables used in the reliability analysis	119
Table 4.2 Nominal values of the input parameters used in the reliability analysis.....	120

List of Figures

Figure 1.1 Schematic of a general corrosion process	3
Figure 1.2 Corrosion mechanism on an underground metallic pipeline (Beavers and Thompson 2006)	4
Figure 1.3 Example of corrosion on a steel pipeline	4
Figure 1.4 A typical in-line inspection tool.....	6
Figure 1.5 Sensor configuration of an MFL tool (Clapham et al. 2004)	6
Figure 2.1 Comparison of defect depths measured by laser scan technology and UT	23
Figure 2.2 Manual matching of defects on a selected pipe joint	28
Figure 2.3 Trace plots of α_1 , α_2 , α_3 , and α_4	30
Figure 2.4 Trace plots of β_1 , β_2 , β_3 , and β_4	31
Figure 2.5 Trace plots of $\Sigma_{\epsilon_{11}}$, $\Sigma_{\epsilon_{12}}$ and $\Sigma_{\epsilon_{22}}$	32
Figure 2.6 Marginal posterior distributions of α_1 , α_2 , α_3 , and α_4	33
Figure 2.7 Marginal posterior distributions of β_1 , β_2 , β_3 , and β_4	33
Figure 2.8 Comparison of field-measured depths and ILI-reported depths for the recoated defects on the pipeline in Case 1	38
Figure 2.9 Comparison of field-measured depths and ILI-reported depths for the recoated defects on the pipeline in Case 2	41
Figure 3.1 Graphical representation of a typical hierarchical Bayesian model	52
Figure 3.2 Graphical representation of the full hierarchical Bayesian corrosion growth model	60
Figure 3.3 Apparent growth paths of the 62 corrosion defects indicated by the ILI data.....	62
Figure 3.4 Trace plots of a_1 , a_2 and a_3	65
Figure 3.5 Trace plots of b_1 , b_2 and b_3	66
Figure 3.6 Trace plots of t_{o1} , t_{o2} and t_{o3}	67
Figure 3.7 Box plot of the components of parameter vector \mathbf{a} of Case 1	69
Figure 3.8 Box plot of the components of parameter vector \mathbf{b} of Case 1	70
Figure 3.9 Box plot of the components of parameter vector \mathbf{t}_o of Case 1	71
Figure 3.10 Box plot of the components of parameter vector $\boldsymbol{\sigma}_\eta$ of Case 1	72
Figure 3.11 Comparison between the predicted and field- measured depths in 2010 for Case 1	74

Figure 3.12 Predicted growth paths for defects #3, #6, #7, #19 and #60 on pipeline of Case 1.....	77
Figure 3.13 Apparent growth paths of the 60 corrosion defects indicated by the ILI data.....	78
Figure 3.14 Box plot of the components of parameter vector \mathbf{a} of Case 2.....	80
Figure 3.15 Box plot of the components of parameter vector \mathbf{b} of Case 2.....	81
Figure 3.16 Box plot of the components of parameter vector \mathbf{t}_o of Case 2.....	82
Figure 3.17 Box plot of the components of parameter vector σ_η of Case 2.....	83
Figure 3.18 Comparison between the predicted and field-measured depths in 2011 for Case 2.....	84
Figure 3.19 Predicted growth paths for defect #13, #23, #35, #50 and #56 on pipeline of Case 2.....	87
Figure 3.20 Comparison of the predicted depths from the models with partially-correlated, fully-correlated and independent random scattering errors with field-measured depths in 2010 for the corrosion defects in Case 1.....	89
Figure 3.21 Comparison of the predicted depths from the models with partially-correlated, fully-correlated and independent random scattering errors with field-measured depths in 2011 for the corrosion defects in Case 2.....	89
Figure 3.22 Comparison between the predicted depths from the linear growth model and field-measured depths in 2010 for the corrosion defects in Case 1.....	94
Figure 3.23 Comparison between the predicted depths from the linear growth model and field-measured depths in 2011 for the corrosion defects in Case 2.....	95
Figure 4.1 Dimensions of a typical corrosion defect on pipeline.....	105
Figure 4.2 Predicted growth paths for defects #2, #4, #5 and #7 on the selected pipe joint.....	116
Figure 4.3 Marginal posterior probability density functions of predicted depths in 2012, 2016 and 2021 for defects #2, #4, #5 and #7.....	118
Figure 4.4 Cumulative failure probabilities of the pipe segment for three different failure modes.....	121
Figure 4.5 Impact of correlation between the model errors of the burst capacity models, e , for different defects on the system reliability.....	122
Figure 4.6 Impact of correlation between the maximum-to-average depth ratios, ζ , for different defects on the system reliability.....	123

List of Abbreviations, Symbols, Nomenclature

a_i, b_i	= parameters of the power-law growth model for defect i
D	= outside diameter of the pipeline
da_i	= actual depth of the i^{th} static defect
da_{ij}	= actual depth of the i^{th} defect at the time of the j^{th} inspection
d_{avg}	= average depth of the corrosion defect
df_i	= field-measured depth of the i^{th} static defect
df_{ij}	= field-measured depth of the i^{th} defect at the time of the j^{th} inspection
d_{max}	= maximum depth of the corrosion defect
dm_{ij}	= ILI-reported depth of the i^{th} defect obtained from the j^{th} inspection
e	= model error associated with the burst capacity model
g_1	= limit state function for the corrosion defect penetrating the pipe wall
g_2	= limit state function for plastic collapse under internal pressure at the defect
g_3	= limit state function for the unstable axial extension of the through-wall
H_a	= alternative hypothesis
H_o	= null hypothesis
HBM	= hierarchical Bayesian model
ILI	= in-line inspection
iid	= independent and identically distributed
ind	= independent
l_i	= length of corrosion defect i
l_{oi}	= length of the defect i at the time of last inspection
r_l	= length growth rate of corrosion defect
MCMC	= Markov chain Monte Carlo
MFL	= Magnetic Flux Leakage
$MSEP$	= mean squared error of prediction
M	= Folias factor or bulging factor
P_{ll}	= probability of large leak
P_{rp}	= probability of rupture

P_{sl}	= probability of small leak
p	= internal pressure of the pipeline
r_b	= burst pressure resistance of the pipe at the defect
r_{bc}	= predicted burst pressure without model error
r_i	= growth rate for defect i in the linear model
r_o	= burst pressure resistance of a defect-free pipe
r_{rp}	= pressure resistance of the pipeline at the location of the through-wall defect
SMYS	= specified minimum yield stress
SMTS	= specified minimum tensile strength
T	= total forecasting period
t_{oi}	= corrosion initiation time of defect i
t_j	= elapsed time from the installation date up to the j^{th} inspection
UT	= ultrasonic
wt	= wall thickness
α_j	= constant bias associated with j^{th} inspection tool
β_j	= non-constant bias associated with j^{th} inspection tool
$\boldsymbol{\varepsilon}_i$	= vector of random scattering errors associated with the depths reported by ILI tools for the i^{th} defect
ε_{ij}	= random scattering errors of the ILI-reported depths of the i^{th} defect at the j^{th} inspection
φ_i	= random scattering errors of the field-measured depth of the i^{th} static defect
φ_{ij}	= random scattering errors of the field-measured depth of the i^{th} defect at the j^{th} inspection
η_{ij}	= model error of the power-law growth model associated with defect i at time j
μ_a	= mean value of the prior distribution of a_i
μ_b	= mean value of the prior distribution of b_i
$\boldsymbol{\mu}_i$	= vector of mean values of ILI-reported depths at different times for defect i
$\boldsymbol{\Sigma}_\varepsilon$	= covariance matrix of random scattering error
σ_a^2	= variance of the prior distribution of a_i
σ_b^2	= variance of the prior distribution of b_i

σ_f	= flow stress of the pipe steel
σ_k	= standard deviation of the random scattering error of the ILI tool used in the k^{th} inspection
σ_y	= yield strength of the pipe steel
σ_u	= ultimate strength of the pipe steel
σ_k^2	= variance of the random scattering error of the ILI tool used in the k^{th} inspection
$\sigma_{\eta_i}^2$	= variance of the prior distribution of η_{ij} associated with defect i
ρ_{kl}	= correlation coefficient between the random scattering errors associated with the ILI tools used in the k^{th} and l^{th} inspections
τ	= time elapsed between the year of last inspection and the year for which the failure probability is forecasted
ξ	= maximum-to-average depth ratio for corrosion defects on pipeline

Chapter 1 Introduction

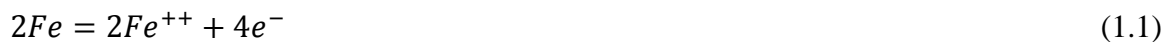
1.1 Background

Pipelines are transport large quantities of hydrocarbons (e.g. crude oil and natural gas) from the production sites to the end users. Compared with other means of transporting hydrocarbons such as rail cars and tanker trucks, pipelines are safer, more efficient and cost-effective (PHMSA 2012). There are about 500,000 km of transmission pipelines that carry natural gas, oil, and other hazardous liquids across the United States (Parfomak 2011). According to the Canadian Energy Pipeline Association, there are more than 100,000 km of oil and gas transmission pipelines in Canada. In 2010, the 71,000 km long pipelines regulated by the National Energy Board (NEB) of Canada shipped about \$85.5 billion worth of hydrocarbons at an estimated transportation cost of only \$5.5 billion (NEB 2010).

As pipelines age the protective coatings on the pipelines have the potential to lose their effectiveness and therefore leave the pipelines vulnerable to corrosion (Benmoussa et al. 2006; Jeglic 2004). In fact, corrosion is one of the most common contributors to the failure of transmission pipelines in North America and Western Europe (Bolt and Owen 1999; Eiber et al. 1995; PHMSA 2012). A comparative study of pipeline performance reported by NEB (2008) indicates that about 63% of pipeline ruptures (the most severe pipeline failure mode) that had occurred between 1991 and 2006 on the NEB-regulated pipelines in Canada were due to corrosion (metal loss and stress corrosion cracking, as defined by CSA Z662-07). The data collected by the Pipeline and Hazardous Materials

Safety Administration (PHMSA) of the United States Department of Transportation (DOT) show that approximately 25% of pipeline ruptures were caused by corrosion during this time span in the US. The PHMSA database (PHMSA 2012) indicates that corrosion was the cause for a total of 166 significant incidents¹ on the onshore gas pipelines in the US between 1992 and 2011; these incidents resulted in 13 fatalities, 4 injuries and a total property loss of worth about \$115 million (in 2011 US \$).

Corrosion is an electro-chemical process that is caused by the chemical interaction between metal and its surrounding environment, and results in degradation of metal (Davis 2000; Peabody 2001). The corrosion process involves the combination of oxidation and reduction reactions, referred to as the Redox reaction. The coupled action of losing electrons (oxidation) by the metal and consuming those electrons (reduction) by the oxidant such as oxygen is key for corrosion to occur. The typical oxidation and reduction reactions for steel are shown in Eqs. (1.1) and (1.2), respectively.



¹ A significant incident is defined by DOT as an incident that causes one or more of the following: 1) fatalities or injuries requiring hospitalization the patient; 2) property damage exceeding a certain monetary threshold; 3) product loss exceeding a certain amount and 4) release of product resulting in fire or explosion.

The mechanism of general corrosion is schematically shown in Fig. 1.1. As shown in the figure, the essential conditions for corrosion to take place are 1) existence of an anode and a cathode; 2) metallic connection between the anode and cathode (i.e. the electrode), and 3) immersion of anode and cathode in an electrically conductive medium (i.e. the electrolyte). The anode, cathode, electrode and electrolyte are all contained in the so-called corrosion cell.

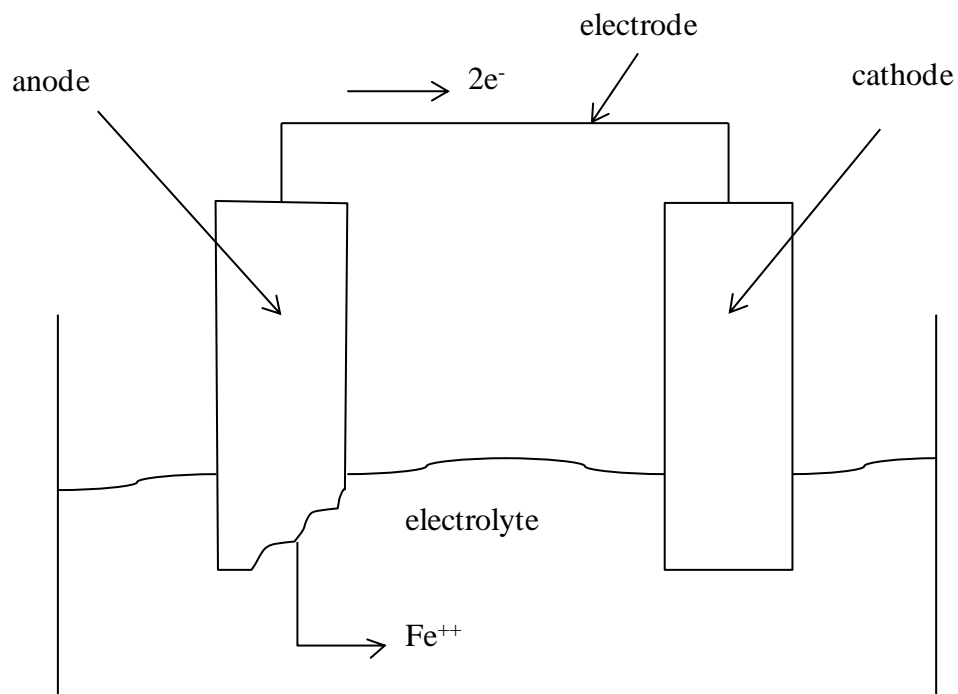


Figure 1.1 Schematic of a general corrosion process

In case of underground pipelines, the anode and cathode in the corrosion cell can form at different locations on the same pipeline due to the differences in metal grain composition, milling imperfections, scratches, threads, etc (Beavers and Thompson 2006). The pipeline itself acts as the electrode, whereas the surrounding soil works as the electrolyte. The difference in the soil resistivity, oxygen concentration, moisture content

and various ion concentrations favors the flow of free electrons. Once corrosion starts to occur, the anode portion of the pipe will corrode, resulting in metal loss and thinning of the pipe wall. The mechanism of corrosion on a pipeline is illustrated in Fig. 1.2. An entire corrosion cell can occur within a drop of water. Therefore, hundreds of corrosion defects can appear within a small portion of a pipeline. Figure 1.3 shows corrosion on an underground steel pipeline.

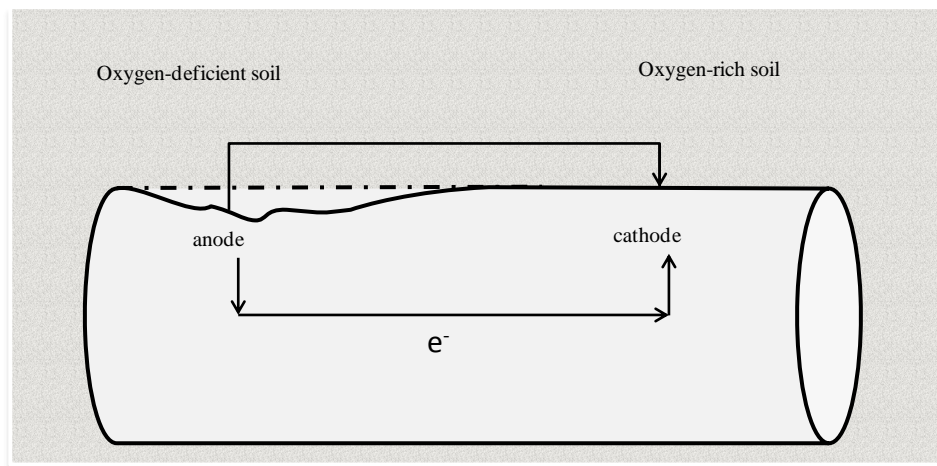


Figure 1.2 Corrosion mechanism on an underground metallic pipeline (Beavers and Thompson 2006)

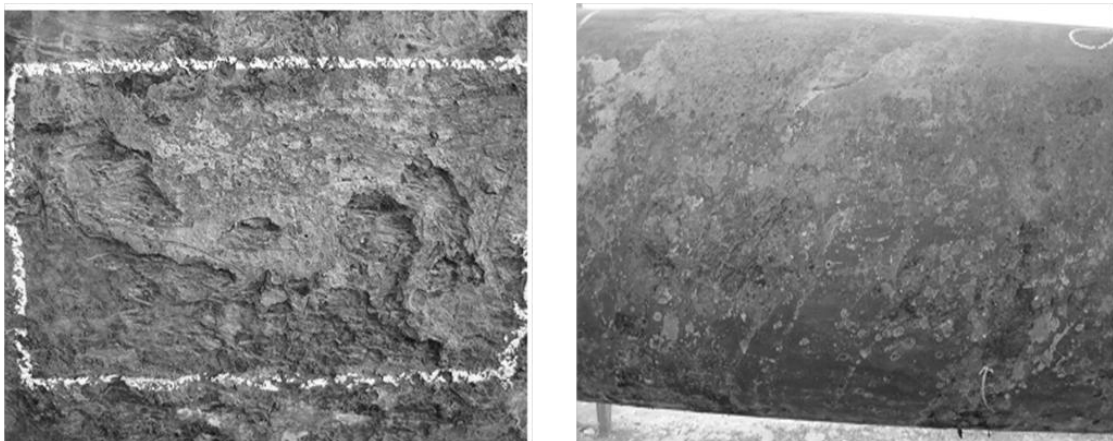


Figure 1.3 Example of corrosion on a steel pipeline

In-line inspection (ILI) tools, also known as “smart pigs”, are widely used to detect, locate and size corrosion anomalies on pipelines (Caleyo et al. 2007; Desjardins 2001; Nessim et al. 2008). There are mainly two types of ILI tools, namely the magnetic flux leakage (MFL) and ultrasonic (UT) tools. The MFL tools are commonly used to inspect gas pipelines, whereas UT tools are used in liquid pipelines. A typical high resolution MFL tool is shown in Fig. 1.4. Because the inspection data available to this study all come from MFL tools, the underlying mechanisms of the MFL tool are briefly described in the following.

During an in-line inspection, an MFL tool is propelled by the product in the pipeline and produces a magnetic flux in the pipe wall using a strong permanent magnet or direct current electromagnet. The presence of a corrosion defect causes the distortion of the flux field, i.e. the so-called leakage, which is detected by the circumferential array of the MFL detectors. Once a defect is identified, the leakage signal and position (longitudinal and circumferential) of the signal on the pipeline are recorded and stored in the data recording device of the tool. High-resolution MFL tools (commonly used nowadays) can differentiate between corrosion defects located on the external and internal surfaces of the pipe wall. The mechanism of detecting a corrosion defects on pipeline by a typical MFL tool is depicted in Fig. 1.5, which is reproduced from Clapham et al. (2004).



Figure 1.4 A typical in-line inspection tool

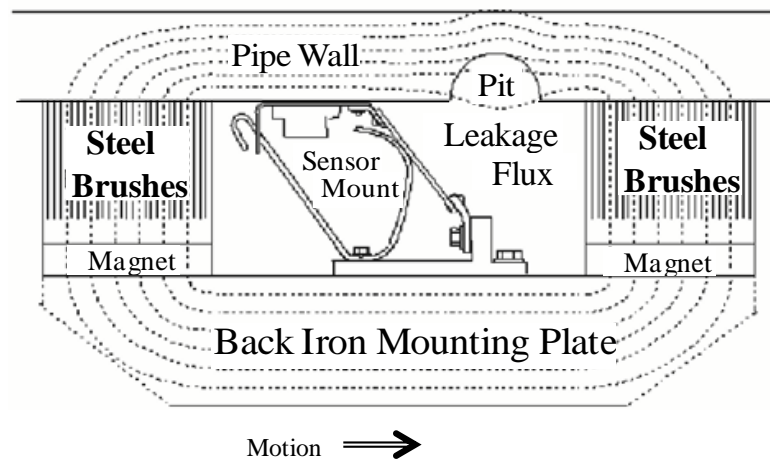


Figure 1.5 Sensor configuration of an MFL tool (Clapham et al. 2004)

The leakage signal obtained from the ILI tool represents the volumetric metal loss of the pipe wall. These signals are then converted into the defect geometry, i.e. depth (in the through pipe wall thickness direction), length (in the pipeline's longitudinal direction) and width (in the pipeline's circumferential direction), using the sizing algorithm of that particular tool. The sizing algorithm is usually developed based on the so-called pull through test (Race et al. 2007; Sutherland et al. 2010), where a section of pipeline with pre-generated defects of several depth, length and width ranges are tested by the ILI tool.

The signals obtained from the tool are calibrated against the known depths, lengths and widths of the defects to develop a sizing model. From the results of the pull through test, ILI vendors can also quantify the tool accuracy. The accuracy of an ILI tool is commonly specified as a two-sided confidence interval, e.g. the measured defect depth is accurate within $\pm 10\%$ wall thickness (wt) with a confidence level of 80%.

Pipeline operators develop and implement comprehensive integrity management programs to ensure the safe operation of pipelines. The pipeline integrity management with respect to corrosion typically consists of in-line inspection, defect assessment and mitigation (Kishawy and Gabbar 2010). Characterization of the growth of corrosion defects plays a crucial role in the pipeline integrity management. The corrosion growth rate is essential to the forecast of the failure probability of the pipelines, determination of the inspection interval and prioritization of defect mitigation and repair. On one hand, overly conservative estimates of the corrosion growth rates lead to too frequent inspections and unnecessary excavations and repairs, making the integrity management program costly. On the other hand, under-estimation of the corrosion growth may leave critical defects unmitigated and result in failure of the pipeline.

As more and more pipelines are now being inspected by ILI tools on a regular basis, the ILI data from multiple inspections naturally provide valuable information about the growth of corrosion defects on the pipeline. Therefore, there is a pressing need in the pipeline industry for developing models to predict the growth of corrosion defects based on repeated in-line inspections data (Kariyawasam and Peterson 2010). This is the main drive for the present study.

1.2 Objective and Research Significance

The study reported in this thesis is a part of a Collaborative Research and Development (CRD) program jointly funded by the Natural Sciences and Engineering Research Council (NSERC) of Canada and TransCanada Pipelines Limited. The objectives of the study were 1) to develop a probabilistic model to characterize the growth of the depths of individual metal-loss corrosion defects on energy pipelines based on data collected from multiple ILIs; and 2) to incorporate the developed corrosion growth model in the reliability analysis to evaluate the failure probability of the pipeline due to corrosion. The study was focused on the growth of the depth of metal-loss corrosion defects; the growth of length of metal-loss corrosion defects or growth of other types of corrosion defects (e.g. stress corrosion cracking) was not considered.

The growth model developed in this study accounts for both systematic and random measurement errors associated with ILI tools, and is specific to individual corrosion defects. The model will assist pipeline integrity engineers in making informed decisions about re-inspection interval and defect mitigation plan that satisfy both the safety and resource constraints. The proposed reliability analysis method provides a framework to incorporate the growth model in the pipeline corrosion reliability analysis, which will facilitate reliability- and risk- based pipeline integrity management.

1.3 Scope of the Study

This study consists of three main components that are presented in Chapters 2, 3 and 4, respectively. Chapter 2 describes a Bayesian model to calibrate the ILI tools, i.e. quantifying the measurement errors of the ILI tool, based on ILI-reported and field-

measured depths for the static defects on the pipeline. The application of the proposed model was demonstrated using the static defects on two subject pipelines currently in service in Alberta.

In Chapter 3, a hierarchical Bayesian corrosion growth model is presented to characterize the growth of the depth of individual corrosion defects based on ILI data from multiple inspections. This model takes into account the measurement errors (i.e. bias and random scattering error) associated with the ILI tools and also the potential correlation between the random scattering errors among different ILI tools. The Markov Chain Monte Carlo (MCMC) simulation technique was employed to evaluate the posterior distributions of the parameters of the growth model. Two sets of active corrosion defects detected on the two subject pipelines considered in Chapter 2 were used to illustrate and validate the proposed growth model.

Chapter 4 presents a methodology that can be used to evaluate the time-dependent system reliability of a segment of onshore natural gas pipeline containing active corrosion defects considering three distinctive failure modes, namely small leak, large leak and rupture. The hierarchical corrosion growth model described in Chapter 3 was incorporated in the reliability analysis to predict the depth of the corrosion defect at a given time. The failure probability is evaluated using random samples generated from both the simple Monte Carlo simulation and MCMC simulation. The methodology is illustrated using a pipe joint in one of the subject pipelines.

1.4 Thesis Format

This thesis is prepared in an Integrated-Article Format as specified by the School of Graduate and Postdoctoral Studies at Western University, Canada. The first chapter, Chapter 1, is the introductory section of the entire thesis with its own bibliography. The main body of the thesis contains three chapters, Chapters 2, 3 and 4. Each of these chapters is presented as a stand-alone manuscript without any abstract, but with its own references. The final chapter, Chapter 5, includes a summary of the study, main conclusion of the thesis and recommendations for future work.

The tabulated data, mathematical derivations and programming codes are provided in the appendices following the last chapter. An identification that consists of a number and a letter is given to each appendix. The identification number and letter of each appendix represent the associated chapter and the sequence of appearance of the appendix in that chapter, respectively. For instance, Appendix 2A is the first appendix associated with Chapter 2.

References

Beavers, J. A., and Thompson, N. G., 2006. External Corrosion of Oil and Natural Gas Pipelines, *ASM Handbook Volume 13C: Corrosion: Environments and Industries*, ASM International, pp. 1015-1025.

Benmoussa, A., Hadjel, M., and Traisnel, M., 2006. Corrosion behavior of API 5L X-60 pipeline steel exposed to near-neutral pH soil simulating solution. *Materials and Corrosion*, 57(10), pp. 771-777.

Bolt, R., and Owen, R. W., 1999. Recent Trends in Gas Pipeline Incidents (1970-1997): a report by the European Gas Pipeline Incidents Data Group (EGIG), *IMEchE Conference Transactions 1999-8 (C571)*, Institution of Mechanical Engineers, Newcastle upon Tyne, UK.

Caleyo, F., Alfonso, L., Espina-Hernández, J. H., and Hallen, J. M., 2007. Criteria for performance assessment and calibration of in-line inspections of oil and gas pipelines. *Measurement Science and Technology*, 18(7).

Clapham, L., Babbar, V., and Byrne, J., 2004. Detection of Mechanical Damage using the Magnetic Flux Leakage Technique. *Proceedings of International Pipeline Conference*, ASME, Calgary, Alberta, Canada.

CSA, 2007. *CSA-Z662 Oil and Gas Pipeline Systems*. Canadian Standards Associations, Rexdale, Ontario.

Davis, J. R., 2000. *Corrosion: Understanding the Basics*, ASM International, Ohio, USA.

Desjardins, G., 2001. Corrosion Rate and Severity Results from In-Line Inspection Data. *CORROSION 2001*, NACE International.

Eiber, R. J., Miele, C. R., and Wilson, P. R., 1995. An Analysis of DOT Reportable Incidents on Gas Transmission and Gathering Lines for June 1984 Through 1992, *Topical Report to Line Pipe Research Supervisory Committee of the Pipeline Research Committee of the American Gas Association*, NG-18 Report No. 213, American Gas Association.

Jeglic, F., 2004. Analysis of Ruptures and Trends on Major Canadian Pipeline Systems, National Energy Board, Calgary, Canada.

Kariyawasam, S., and Peterson, W., 2010. Effective Improvements to Reliability Based Corrosion Management. *Proceedings of 8th International Pipeline Conference*, ASME, Calgary, Alberta, Canada, pp. 603-615.

Kishawy, H., and Gabbar, H., 2010. Review of Pipeline Integrity Management Practices. *International Journal of Pressure Vessels and Piping*, 87 (7), pp. 373-380.

National Energy Board (NEB), 2008, Focus on Safety and Environment: A Comparative Analysis of Pipeline Performance 2000–2006, National Energy Board, Calgary, Alberta, Canada.

National Energy Board (NEB), 2010. Annual Report 2010 to Parliament, National Energy Board, Canada.

Nessim, M., Dawson, J., Mora, R., and Hassanein, S., 2008. Obtaining Corrosion Growth Rates From Repeat In-Line Inspection Runs and Dealing With the Measurement Uncertainties. *Proceedings of 7th International Pipeline Conference*, ASME, Calgary, Alberta, Canada, pp. 593-600.

Parfomak, P. W., 2011, Keeping America's Pipelines Safe and Secure: Key Issues for Congress, *Encyclopedia of Earth*.

Peabody, A. W., 2001. *Control of Pipeline Corrosion*. NACE International, Houston, Texas, USA.

PHMSA, 2012, Pipeline Incidents and Mileage Reports, March 2012. Pipeline & Hazardous Materials Safety Administration, <http://primis.phmsa.dot.gov/comm/reports/safety/PSI.html>.

Race, J. M., Dawson, S. J., Stanley, L. M., and Kariyasawam, S., 2007. Development of a predictive model for pipeline external corrosion rates. *Journal of Pipeline Engineering*, 6(1), pp. 15-29.

Sutherland, J., Bluck, M., Pearce, J., and Quick, E., 2010. Validation of Latest Generation MFL In-Line Inspection Technology Leads to Improved Detection and Sizing Specification for Pinholes, Pitting, Axial Grooving and Axial Slotting. *Proceedings of 8th International Pipeline Conference*, ASME, Calgary, Alberta, Canada, pp. 225-232.

Chapter 2 Bayesian Model for Calibration of ILI Tools

2.1 Introduction

Over the last few decades, the in-line inspection (ILI) technology has been widely used to identify, locate and size corrosion defects on pipelines. Despite the enormous advancement in the ILI technology, ILI data are subjected to measurement errors resulting from imperfections in the ILI tool and associated sizing algorithm (Fenyvesi and Dumalski 2005; Nessim et al. 2008). The measurement error includes the systematic error, i.e. the constant and non-constant bias of the ILI data (Caleyó et al. 2007), and random scattering error (i.e. repeatability error) of the data (Coleman and Miller 2010; Spencer et al. 2010). Moreover, the corrosion growth rate calculated from multiple ILI runs involve additional measurement errors due to differences in the magnetic strength of different ILI tools, change of the defect sizing algorithm and differences in the sizing model for defects, i.e. box or cluster, between inspections (Fenyvesi and Dumalski 2005).

The in-line inspection data can be used to quantify the growths of the depths of corrosion defects on pipelines, which is considered one of the most critical tasks for pipeline corrosion management. It is critically important to account for the measurement error of the ILI data in determining the corrosion growth rate on pipelines (Bhatia et al. 1998). Although the measurement error can be inferred from the specifications of the ILI tool, it is more appropriate to evaluate the de-facto measurement error of the ILI data for a specific pipeline. Such an analysis is referred to as calibration of the ILI tool. Knowledge of the de-facto measurement error will also help the ILI vendors to improve

the measurement technology and sizing algorithm for corrosion defects on a given pipeline.

The measurement errors of the ILI data reported by a given ILI tool are typically evaluated by comparing the field-measured and ILI-reported depths for a set of corrosion defects. The field-measured depths are obtained from the dig sites using field-measuring instruments, such as the pit gauge, ultrasonic thickness (UT) measuring device and the laser profilometer. Bhatia et al. (1998) used the well-established Grubbs (Grubbs 1948) and Jaech (Jaech 1985) estimators to quantify the measurement errors associated with the ILI tool and the field-measuring instrument, and found that Grubbs' method sometimes result in negative values for the variance of the measurement error, which is unrealistic. Jaech's method can overcome such a drawback in Grubbs' method and ensures that the variance of the measurement error to be positive. Furthermore, both Grubbs' method and Jaech's method assume that the measurement is unbiased; that is, the measurement error only includes the random scattering error. This assumption may be unrealistic for ILI tools.

Caleyo et al. (2007) developed a statistical method to calibrate the ILI tools using the ILI-reported data and corresponding field measurements. The so-called V-Wald and V-Jaech methods were introduced to quantify the bias of the ILI data and variances of the scattering errors of both the ILI data and field measurements, respectively. However, the potential correlations between the measurement errors associated with different ILI tools that are based on the same inspection technology (e.g. MFL) and used to inspect the same pipeline at different times cannot be evaluated from their reported model.

The objective of the study reported in this chapter was to develop a model to calibrate the ILI tool and quantify the measurement error, including the constant and non-constant bias as well as the random scattering error, of the ILI data. The potential correlations between the scattering errors associated with different ILI tools were also considered in the proposed model. The calibration was carried out using the Bayesian methodology based on comparing the ILI data with the corresponding field measurements.

This chapter is organized as follows. Section 2.2 describes the statistical methodologies (i.e. Bayesian method and Markov Chain Monte Carlo simulation) employed in this study to calibrate the ILI tools. The basic assumptions associated with the calibration model are presented in Section 2.3. Section 2.4 describes the measurement errors associated with the field-measuring devices. Section 2.5 includes the Bayesian formulation of the calibration model as well as the prior distributions for the parameters of the calibration model. Section 2.6 illustrates the application of the calibration model in two case studies that involve real ILI and field measurement data on two pipelines currently in service. The conclusions of the chapter are summarized in Section 2.7.

2.2 Bayesian Methodology

2.2.1 Basic Formulation

The Bayesian approach is an advanced tool to fit a probability model to a set of observations by evaluating the unknown parameters of the model in a probabilistic way (Gelman 2004). The Bayesian method treats the unknown parameters of a physical process as random variables rather than as deterministic values. It incorporates the prior knowledge about the parameters, which may arise from the results of previous studies or experience. The prior knowledge is then updated based on the observed data to obtain the revised opinion about the parameters. The updated belief can be further considered as the prior distribution for future updating when new data are available. Therefore through this iterative process the uncertainty in the parameters is minimized.

Given a set of n observations, $\mathbf{X} = (x_1, x_2, \dots, x_n)$, and a collection of k unknown parameters, $\boldsymbol{\theta} = (\theta_1, \theta_2, \dots, \theta_k)$ that characterize the physical process underlying the observed data, one can specify the Bayesian model for the parameters. The objective of the Bayesian analysis is to find the updated opinion about the unknown parameters $\boldsymbol{\theta}$ based on Bayes' theorem given by (Bayes and Price 1763)

$$p(\boldsymbol{\theta}|\mathbf{X}) = \frac{p(\boldsymbol{\theta}) \times p(\mathbf{X}|\boldsymbol{\theta})}{p(\mathbf{X})} \quad (2.1)$$

where $p(\bullet)$ denotes the probability density function of \bullet . Here $p(\boldsymbol{\theta})$, which is called the *prior distribution* of the parameters, characterizes the belief regarding the unknown parameters $\boldsymbol{\theta}$ prior to any modeling. The information contained in the data is introduced via the so-called *likelihood* for the data, $p(\mathbf{X}|\boldsymbol{\theta})$, which is the value of the probability

density function associated with the data conditional on the parameters θ . The entity $p(\theta|\mathbf{X})$ is known as the *posterior distribution*, which reflects the combined information from the data and prior distribution. The quantity $p(\mathbf{X})$ is a normalizing constant that ensures the left hand side of Eq. (2.1) to be a probability distribution; that is, $p(\theta|\mathbf{X})$ integrates to unity, and $p(\mathbf{X})$ is known as the *marginal likelihood* and can be obtained by integrating the numerator on the right hand side of Eq. (2.1) with respect to the unknown parameters θ . Thus,

$$p(\mathbf{X}) = \int p(\mathbf{X}|\theta) p(\theta) d\theta \quad (2.2)$$

Taking into consideration the normalizing constant, one can write Eq. (2.1) as

$$p(\theta|\mathbf{X}) \propto p(\mathbf{X}|\theta) \times p(\theta) \quad (2.3)$$

where the symbol “ \propto ” indicates proportionality.

Consider an example to illustrate the Bayesian method. Assume that $\mathbf{y} = (y_1, y_2, \dots, y_n)$ represents a set of n data that follow a Poisson distribution with an unknown rate parameter λ . Further assume that the prior distribution of λ follows a gamma distribution with known shape parameter κ and scale parameter θ . Therefore, the likelihood and prior distribution can be written as,

$$\text{Likelihood: } p(\mathbf{y}|\lambda) = \prod_{i=1}^n \frac{e^{-\lambda} \lambda^{y_i}}{y_i!} = \frac{e^{-n\lambda} \lambda^{\sum_{i=1}^n y_i}}{\prod_{i=1}^n y_i!}; i = 1, 2, \dots, n$$

$$\text{Prior distribution: } p(\lambda) = \frac{\theta^\kappa}{\Gamma(\kappa)} \lambda^{\kappa-1} e^{-\theta\lambda}$$

where $\Gamma(\bullet)$ denotes the gamma function.

The posterior distribution of λ can be evaluated from Eq. (2.3) as follows:

$$p(\lambda|\mathbf{y}, \kappa, \beta) \propto p(\mathbf{y}|\lambda)p(\lambda) \propto \frac{e^{-n\lambda} \lambda^{\sum_{i=1}^n y_i}}{\prod_{i=1}^n y_i!} \times \frac{\theta^\kappa}{\Gamma(\kappa)} \lambda^{\kappa-1} e^{-\theta\lambda} \propto e^{-(n+\theta)\lambda} \lambda^{n\bar{y}+\kappa-1} \quad (2.4)$$

where $\bar{y} = \frac{1}{n} \sum_{i=1}^n y_i$ is the mean value of the observations. Note that the terms that are independent of λ (such as $\Gamma(\kappa)$ and θ^κ) in Eq. (2.4) are omitted in the last step because they are part of the proportionality constant. Based on Eq. (2.4), it can be concluded that the posterior distribution of λ follows a gamma distribution with shape parameter and scale parameters equal to $n\bar{y}+\kappa$ and $n+\theta$, respectively.

2.2.2 Markov Chain Monte Carlo Simulation

The main purpose of the Bayesian analysis is to evaluate the probabilistic characteristics (e.g. mean, variance and quantiles) of the posterior distribution of the unknown model parameters. Therefore, it is necessary to obtain the marginal posterior distribution of each parameter. The marginal distribution of a parameter θ_i of the parameter vector $\boldsymbol{\theta}$, $p(\theta_i|\mathbf{X})$, and the mean value of θ_i , $E(\theta_i|\mathbf{X})$, can be evaluated as follows:

$$p(\theta_i|\mathbf{X}) = \iint \dots \int p(\boldsymbol{\theta}|\mathbf{X}) d\boldsymbol{\theta}_{(-i)} \quad (2.5)$$

$$E(\theta_i|\mathbf{X}) = \int \theta_i p(\theta_i|\mathbf{X}) d\theta_i \quad (2.6)$$

where $\boldsymbol{\theta}_{(-i)}$ denotes the vector of θ 's excluding θ_i .

In some cases, closed-form solutions of the integrals in Eqs. (2.5) and (2.6) are available, or they can be easily computed using numerical methods. But in most applications analytic or direct numerical evaluation of these integrals is very difficult, if not impossible, due to the complexity and high dimensionality of the Bayesian model. To overcome this difficulty, the Markov Chain Monte Carlo (MCMC) simulation technique has been widely used in the Bayesian analysis (Gilks et al. 1996).

MCMC works by sequentially generating random samples of uncertain parameters to form a Markov process whose stationary distribution is the joint posterior distribution of the parameters. The difference between MCMC and the conventional Monte Carlo simulation is that the sample generated in a given sequence in MCMC depends on the sample generated in the previous sequence, whereas the samples generated in different trials of the conventional Monte Carlo simulation are independent.

The MCMC simulation starts by assigning an arbitrary initial value to each of the parameters considered. After an initial set of sequences, i.e. the so-called burn-in period, the subsequent sequences are considered to converge to the joint posterior distribution of the parameters. The samples generated in different sequences in MCMC are typically autocorrelated. To reduce the autocorrelation, the so-called “thinning” technique is employed, where only samples from every k^{th} ($k > 1$) iteration are stored for the output analysis (Congdon 2006; Link and Eaton 2012). The generated sequences can be approximated as independent samples by choosing the thinning interval (also known as sampling lag) appropriately. The samples generated after the burn-in period using a suitable thinning interval can be used to evaluate the probabilistic characteristics of the

joint posterior distribution or the marginal distribution of a given parameter, just like the conventional Monte Carlo simulation.

There are several standard sampling algorithms to generate MCMC samples from the joint posterior distributions. The most commonly used algorithms are the Metropolis-Hastings algorithm and the Gibbs sampling. These two algorithms are briefly described in Appendix 2A.

2.3 Measurement Error Model for Corrosion Defects

Consider that a set of corrosion defects on a given pipeline have been measured by multiple ILI tools and field-measuring instruments at different times. The defect depths reported by the ILI tools and field-measuring instrument are assumed to be related to the actual depth as follows (Fuller 1987; Jaech 1985):

$$dm_{ij} = \alpha_j + \beta_j da_{ij} + \varepsilon_{ij} \quad (2.7a)$$

$$df_{ij} = da_{ij} + \varphi_{ij} \quad (2.7b)$$

where dm_{ij} is the ILI-reported depth of the i^{th} defect obtained from the j^{th} inspection; α_j and β_j are the calibration parameters of the ILI tool employed in the j^{th} inspection, which characterize the bias of the tool (i.e. if $\alpha_j = 0$ and $\beta_j = 0$ the tool is unbiased; if $\alpha_j \neq 0$ and $\beta_j = 0$ the tool has a constant bias, and if $\alpha_j \neq 0$ and $\beta_j \neq 0$ the tool has both constant and non-constant bias); da_{ij} and df_{ij} denote the actual and field-measured depths of the i^{th} defect at the time of the j^{th} inspection, respectively; ε_{ij} and φ_{ij} represent the random scattering errors of the ILI-reported and field-measured depths of the i^{th} defect at the j^{th}

inspection, respectively; and α_j , β_j , ε_{ij} and φ_{ij} are all uncertain. The main assumptions of the measurement error model are as follows:

- α_j (or β_j), $j = 1, 2, \dots$, are independent of each other;
- the field measurement is unbiased and includes the random scattering error only (Bhatia et al. 1998; Caleyó et al. 2007);
- ε_{ij} has a mean value of zero; at a given inspection time j , ε_{ij} are mutually independent for $i = 1, 2, \dots$; for a given defect i , ε_{ij} ($j = 1, 2, \dots$) are correlated (due to the fact that the ILI tools used at different times in general have the same underlying inspection technology such as MFL) and follow a multivariate normal distribution with a mean of zero and a covariance matrix of Σ_ε ;
- φ_{ij} are independent and identically distributed (*iid*) random variables for $i, j = 1, 2, \dots$, and follow a normal distribution with zero mean and variance of σ_φ^2 , and
- ε_{ij} and φ_{ij} are independent (Bhatia et al. 1998; Morrison et al. 2000).

In practice, an excavated pipeline segment will be fully recoated before being re-buried; the recoating essentially arrests the growth of all the corrosion defects on the segment and makes it highly unlikely that the segment will be re-excavated for corrosion mitigation in the future. This implies that 1) only one field measurement is usually available for a given defect and 2) the defect for which the field measurement is available will become static (or cease growing) after the field measurement. Given this observation, Eq. (2.7) can be rewritten for a set of static defects as follows:

$$dm_{ij} = \alpha_j + \beta_j da_i + \varepsilon_{ij} \quad (2.8a)$$

$$df_i = da_i + \varphi_i \quad (2.8b)$$

where da_i is the actual depth of the i^{th} static defect.

2.4 Measurement Error of Field Measurement

Consider that two different field-measuring tools are used to measure the depths of the same defects at the dig site. Following Eq. (2.8b), we have

$$df_{i1} = da_i + \varphi_{i1} \quad (2.9a)$$

$$df_{i2} = da_i + \varphi_{i2} \quad (2.9b)$$

where φ_{i1} and φ_{i2} are the measurement errors associated with the two field-measuring tools, respectively. Further assume that φ_{i1} and φ_{i2} are normally distributed random variables with zero means and variances of $\sigma_{\varphi_1}^2$ and $\sigma_{\varphi_2}^2$, respectively. The parameters $\sigma_{\varphi_1}^2$ and $\sigma_{\varphi_2}^2$ can be evaluated using Grubbs' or Jaech's method (Fuller 1987; Jaech 1985). The procedures of estimating the measurement error variances using Grubbs' and Jaech's method are outlined in Appendix 2B.

McNealy et al. (2010) calibrated various field instruments, such as laser scanner and ultrasonic thickness device, that are commonly used to measure the depth of the corrosion defect at dig sites. The standard deviations of the measurement errors associated with the laser scanner and ultrasonic pen probe were reported to be 0.94% and 1.56% wall thickness (wt), respectively, for a pipeline with a wall thickness of 6.35 mm (0.25 inch).

In the present work, a similar study was conducted to evaluate the measurement errors associated with a laser scanner and an ultrasonic thickness device based on the measured depths of 80 corrosion defects on a natural gas pipeline located in Alberta, Canada. Using Jaech's method (Jaech 1985), it was found that the standard deviations of the measurement errors associated with the laser scanner and UT device are $1.01\%wt$ and $0.92\%wt$, respectively. The unity plot for the UT and laser scanner is shown in Fig. 2.1. These findings suggest that the measurement errors associated with the field-measuring tools are sufficiently small to be ignored in calibrating the ILI tools. Therefore, Eq. (2.8a) becomes

$$dm_{ij} = \alpha_j + \beta_j df_i + \varepsilon_{ij} \quad (2.10)$$

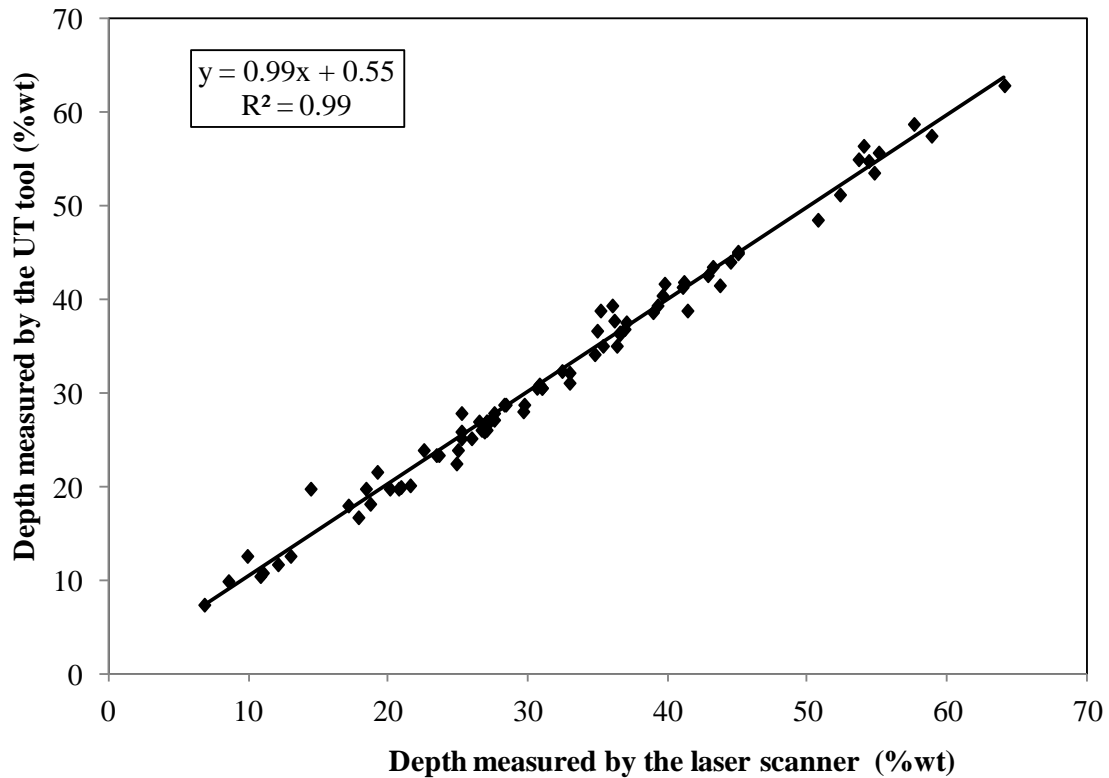


Figure 2.1 Comparison of defect depths measured by laser scan technology and UT

2.5 Bayesian Calibration Model for ILI Tools

2.5.1 Formulation and the Likelihood Function

Consider that the depths of m static defects, df_i ($i = 1, 2, \dots, m$), have been obtained through field measurement. The depths of these defects are further measured by ILI tools at n different inspections carried out after the field measurement (i.e. $j = 1, 2, \dots, n$). Let \mathbf{dm}_i denote $(dm_{i1}, dm_{i2}, \dots, dm_{in})^T$ for given df_i , where “T” represents transposition. It follows from the description in Section 2.4 that \mathbf{dm}_i follows a multi-normal distribution with a mean vector of $\boldsymbol{\mu}_i = \boldsymbol{\alpha} + \boldsymbol{\beta}df_i$ and a covariance matrix of $\boldsymbol{\Sigma}_\varepsilon$, where $\boldsymbol{\alpha} = (\alpha_1, \alpha_2, \dots, \alpha_n)^T$, $\boldsymbol{\beta} = (\beta_1, \beta_2, \dots, \beta_n)^T$, and $\boldsymbol{\Sigma}_\varepsilon$ is an $n \times n$ matrix. The elements of $\boldsymbol{\Sigma}_\varepsilon$ are denoted by $\rho_{kl}\sigma_k\sigma_l$ for $k, l = 1, 2, \dots, n$, where ρ_{kl} represents the correlation between the scattering errors associated with the ILI tools used in the k^{th} and l^{th} inspections; if $k = l$, $\rho_{kl} = 1$ and $\rho_{kl}\sigma_k\sigma_l$ then equals σ_k^2 , which is the variance of the scattering error of the ILI tool used in the k^{th} inspection. It is assumed that \mathbf{dm}_i ($i = 1, 2, \dots, m$) are mutually independent given df_i , $\boldsymbol{\alpha}$, $\boldsymbol{\beta}$ and $\boldsymbol{\Sigma}_\varepsilon$; in other words, the order of measurements is of no significance and exchangeability (Bernardo and Smith 2007) is considered appropriate. The distribution function for \mathbf{dm}_i can be written as,

$$\mathbf{dm}_i \underset{\sim}{\overset{ind}{\sim}} MVN(\boldsymbol{\mu}_i, \boldsymbol{\Sigma}_\varepsilon), i = 1, 2, \dots, m \quad (2.11a)$$

$$\boldsymbol{\mu}_i = \boldsymbol{\alpha} + \boldsymbol{\beta}df_i \quad (2.11b)$$

where “ \sim ” indicates the assignment of a probability distribution to a given random variable; “ ind ” denotes independency between \mathbf{dm}_i and \mathbf{dm}_k (for $i \neq k$), and $MVN(\boldsymbol{\mu}_i, \boldsymbol{\Sigma}_\varepsilon)$ denotes a multivariate normal distribution with a mean vector of $\boldsymbol{\mu}_i$ and a covariance

matrix of Σ_ε . Note that Eq. (2.11a) defines the likelihood function for $d\mathbf{m}_i$ given df_i , α , β and Σ_ε .

2.5.2 Prior Distributions

The constant biases associated with the ILI tools, i.e. α_j ($j = 1, 2, \dots, n$), can be positive or negative. For this reason, the normal distribution was considered appropriate as the prior distribution for α_j . On the other hand, the non-constant biases, β_j , is considered positive for the ILI tools. Therefore, the Beta distribution was adopted as the prior distribution for β_j . It is also assumed that the biases for different ILI tools are independent and identically distributed (*iid*). Given the above, the prior distributions for α_j and β_j are specified as follows:

$$\alpha_1, \alpha_2, \dots, \alpha_n \stackrel{iid}{\sim} N(a, b^2) \quad (2.12)$$

$$\beta_1, \beta_2, \dots, \beta_n \stackrel{iid}{\sim} Be(c, d, l, u) \quad (2.13)$$

where $N(a, b^2)$ denotes a normal distribution with a mean value of a and a variance of b^2 ; $Be(c, d, l, u)$ denotes a Beta distribution with shape parameters c and d , a mean value of $\frac{cu+dl}{c+d}$, a variance of $\frac{cd(u-l)^2}{(c+d)^2(c+d+1)}$, a lower bound of l and an upper bound of u .

The gamma distribution is widely used as the prior distribution of the inverse of the (uncertain) variance of a univariate random variable, because the gamma distribution is defined for positive values only and can be conveniently set to be non-informative (Congdon 2010; Gelman 2004). Note that the inverse of the variance of a distribution is

also known as the precision parameter in the literature (Lunn et al. 2009). The multivariate generalization of the gamma distribution, known as the Wishart distribution (Wishart 1928), is the most commonly used prior distribution for the inverse of a covariance matrix. Therefore, the prior distribution for Σ_ε was assigned as follows:

$$\Sigma_\varepsilon^{-1} \sim W(\mathbf{R}, k) \quad (2.14)$$

where $W(\mathbf{R}, k)$ denotes the Wishart distribution with a scale matrix parameter \mathbf{R} ($n \times n$) and a degree-of-freedom parameter k ($k \geq n$). The parameter k is typically chosen as small as possible (i.e. n or the rank of \mathbf{R}) to represent non-informative prior knowledge for the Wishart distribution (Lunn et al. 2009; O'Hagan et al. 2001).

In Eqs. (2.12) through (2.14), the quantities $a, b, c, d, l, u, \mathbf{R}$ and k are called the *hyper-parameters* of the Bayesian model and were assumed to be known in this study. Given df_i and \mathbf{dm}_i ($i = 1, 2, \dots, m$), the full conditional posterior distributions for α_j, β_j ($j = 1, 2, \dots, n$) and Σ_ε that are used to generate the MCMC samples were derived and are given in Appendix 2C. Given the MCMC samples, statistical inference (e.g. mean and standard deviation) can be made for each of the parameters. The mean values of the elements of the covariance matrix Σ_ε can be used to evaluate the correlation coefficients among the scattering errors associated with the ILI tools. The correlation coefficient ρ_{kl} between the k^{th} and l^{th} tool is estimated as

$$\rho_{kl} = \frac{E(\Sigma_\varepsilon[k,l])}{\sqrt{E(\Sigma_\varepsilon[k,k])} \sqrt{E(\Sigma_\varepsilon[l,l])}} \quad (2.15)$$

where $E(\bullet)$ represents the mean or expectation, and $\mathbf{Z} [x, y]$ indicates the element of matrix \mathbf{Z} with the row index x and the column index y .

2.6 Case Study

2.6.1 General

Two case studies, involving real ILI data and field measurements for corrosion defects on two subject pipelines, were carried out to demonstrate the calibration model presented in the previous section. Each pipeline was inspected multiple times by high resolution Magnetic Flux Leakage (MFL) tools. A set of defects that were excavated and recoated were identified on each pipeline, and then manually matched with the corresponding defects identified by in-line inspections conducted after the recoating. An example of the defect matching is shown in Fig. 2.2. The matching was done based on the relative distance and clock position of the defects on the pipeline provided in the ILI report. The clock position of the defects on the pipeline is illustrated at the right top corner of Fig. 2.2. The field-measured and ILI-reported depths that were found to be matched were employed in the analysis. A Bayesian updating software called OpenBUGS (Version 3.2.1) (Lunn et al. 2009) was used to make statistical inferences of the parameters (i.e. α_j , β_j and Σ_ϵ) in the calibration model for each ILI tool based on the matched dataset and the Bayesian formulations given by Eqs. (2.11) through (2.14).

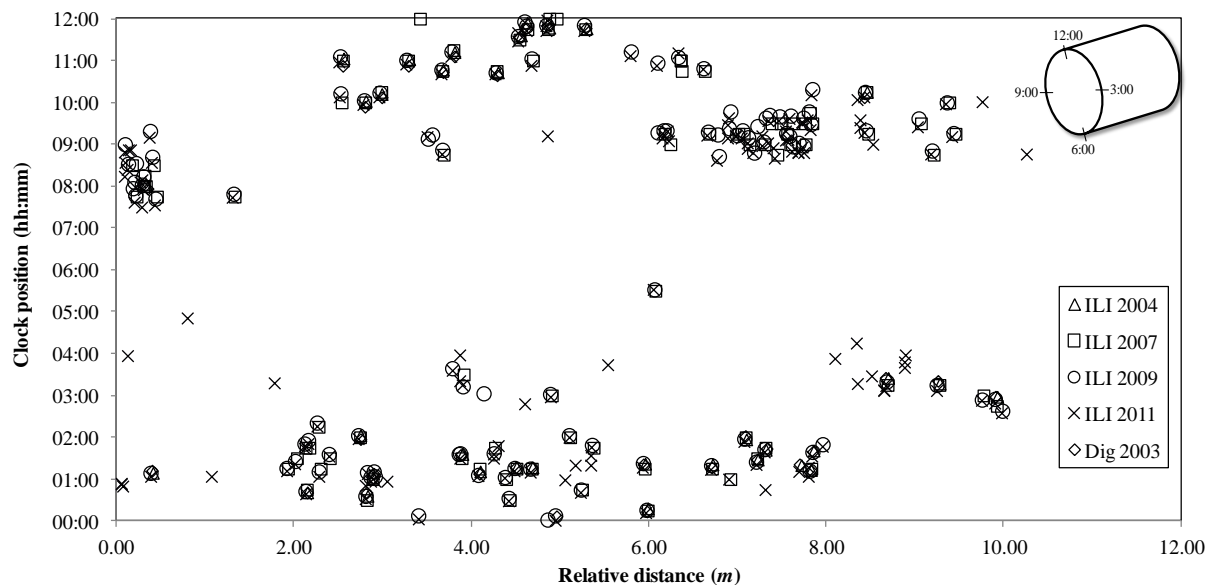


Figure 2.2 Manual matching of defects on a selected pipe joint

2.6.2 Case 1

A 137 km long natural gas pipeline was inspected by high-resolution MFL tools in 2000, 2004, 2007, 2009 and 2011. These inspections were conducted by two different vendors. The ILI tools used in 2000, 2004 and 2011 are from Vendor A, whereas the ILI tools used in 2007 and 2009 are from Vendor B. The defects that were excavated and recoated prior to the 2004 ILI were employed to calibrate the ILI tools used in 2004, 2007, 2009 and 2011. The ILI tool of 2000 was not calibrated because the defects that were field-measured and recoated prior to the inspection in 2000 were not available to the present study. It is assumed that the recoated defects become static immediately after recoating and remain static thereafter. A total of 128 recoated defects were manually compared with the defect listings reported by the 2004, 2007, 2009 and 2011 ILIs to identify the defects in each ILI that match the recoated defects.

The mean and standard deviation (i.e. a and b) of the prior distribution of the constant biases (i.e. $\alpha_1, \alpha_2, \dots, \alpha_n$) were set to be 0%wt and 100%wt, respectively, to represent non-informative prior knowledge about $\alpha_1, \alpha_2, \dots, \alpha_n$. Previous studies reported in the literature (Fuller 1987) indicated that the non-constant biases (i.e. $\beta_1, \beta_2, \dots, \beta_n$) of the calibration model given by Eq. (2.11) are generally less than 2. Therefore, the lower bound l and the upper bound u in Eq. (2.13) were set equal to 0 and 2, respectively. The shape parameters c and d were both assigned a value of 5, which makes the prior distribution symmetric about the mean value of unity. A non-informative prior distribution was assigned to Σ_ε^{-1} : the degree of freedom parameter k in Eq. (2.14) was chosen to be the smallest possible value, 4 (i.e. the total number of inspections) (Lunn et al. 2009), and the scale parameter matrix \mathbf{R} was specified as a 4×4 diagonal matrix with all the diagonal elements having a value of $0.001((\%wt)^{-2})$ (Have and Uttal 1994; Lunn et al. 2009). The OpenBUGS code developed for the analysis is included in Appendix 2D.

To check for the convergence of the samples toward the target distributions, two distinct MCMC chains with different sets of initial values were run. A total of 25,000 iterations were performed for each of the chains. A thinning interval of 5 was used to reduce the autocorrelation in the generated samples. The trace plots (i.e. plot of iterations versus the generated values) of α_j, β_j and three elements of Σ_ε are shown in Figs. 2.3 through 2.5, respectively. As shown in these figures, the samples in both chains mix well and move along a steady line without any increasing or decreasing tendencies except at the very beginning of the simulation. This indicates a very good convergence of the samples toward the posterior distributions. A burn-in period of 5000 was considered for each chain. The samples generated after the burn-in period were used to evaluate the

posterior distributions. The marginal posterior distribution plots as obtained from the OpenBUGS software for α_j and β_j ($j = 1, 2, 3$ and 4) are shown in Figs. 2.6 and 2.7, respectively.

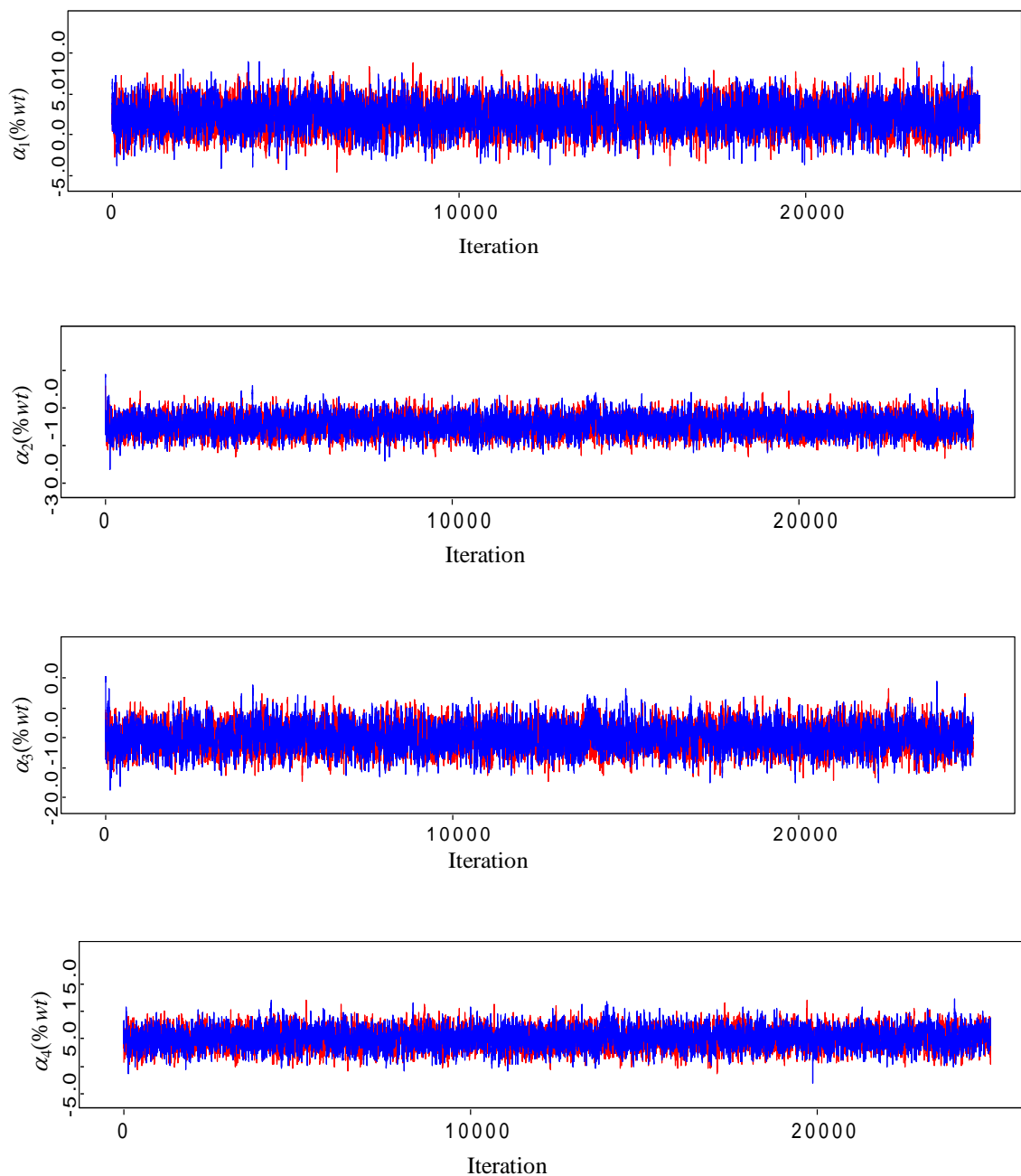


Figure 2.3 Trace plots of α_1 , α_2 , α_3 , and α_4

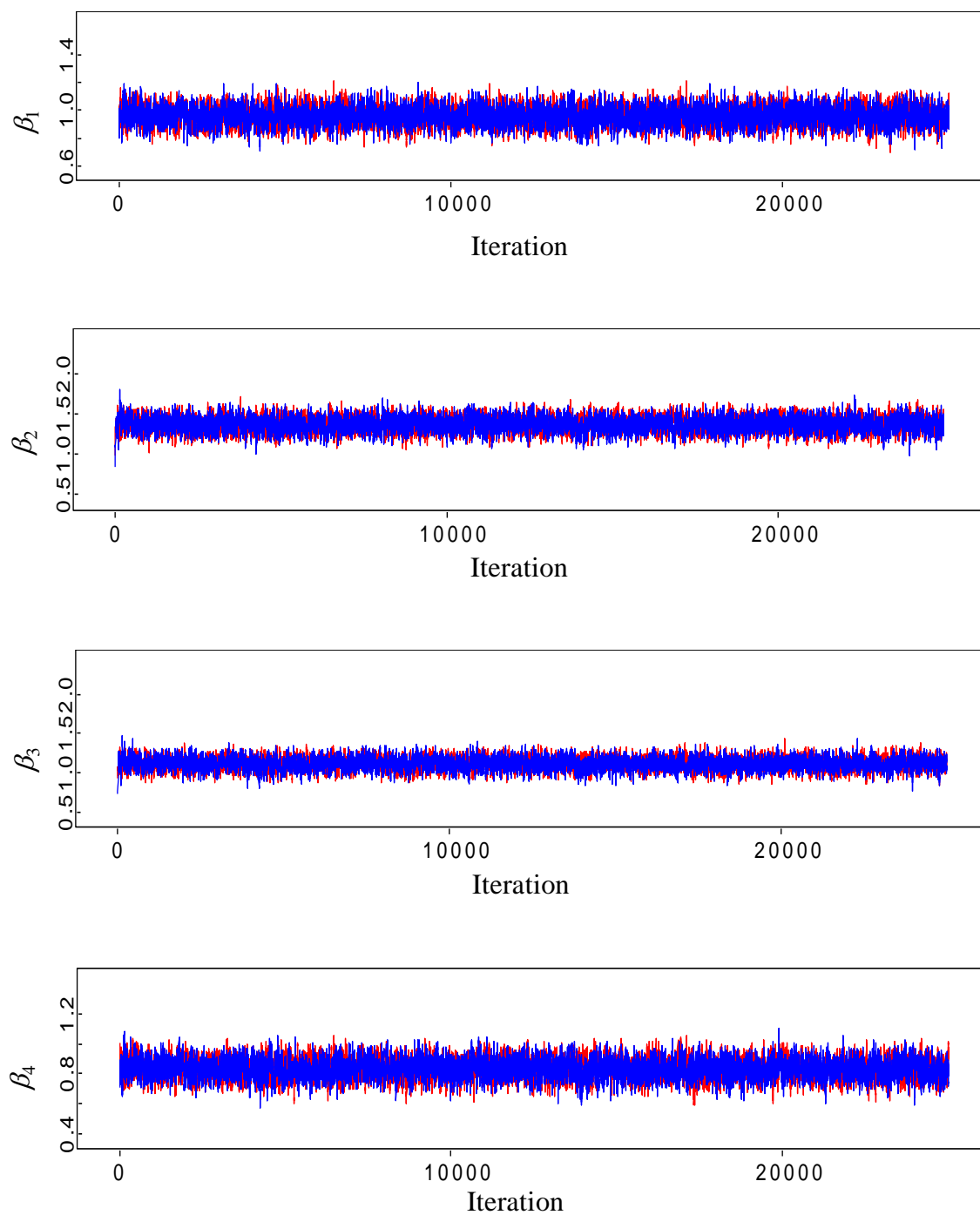


Figure 2.4 Trace plots of β_1 , β_2 , β_3 , and β_4

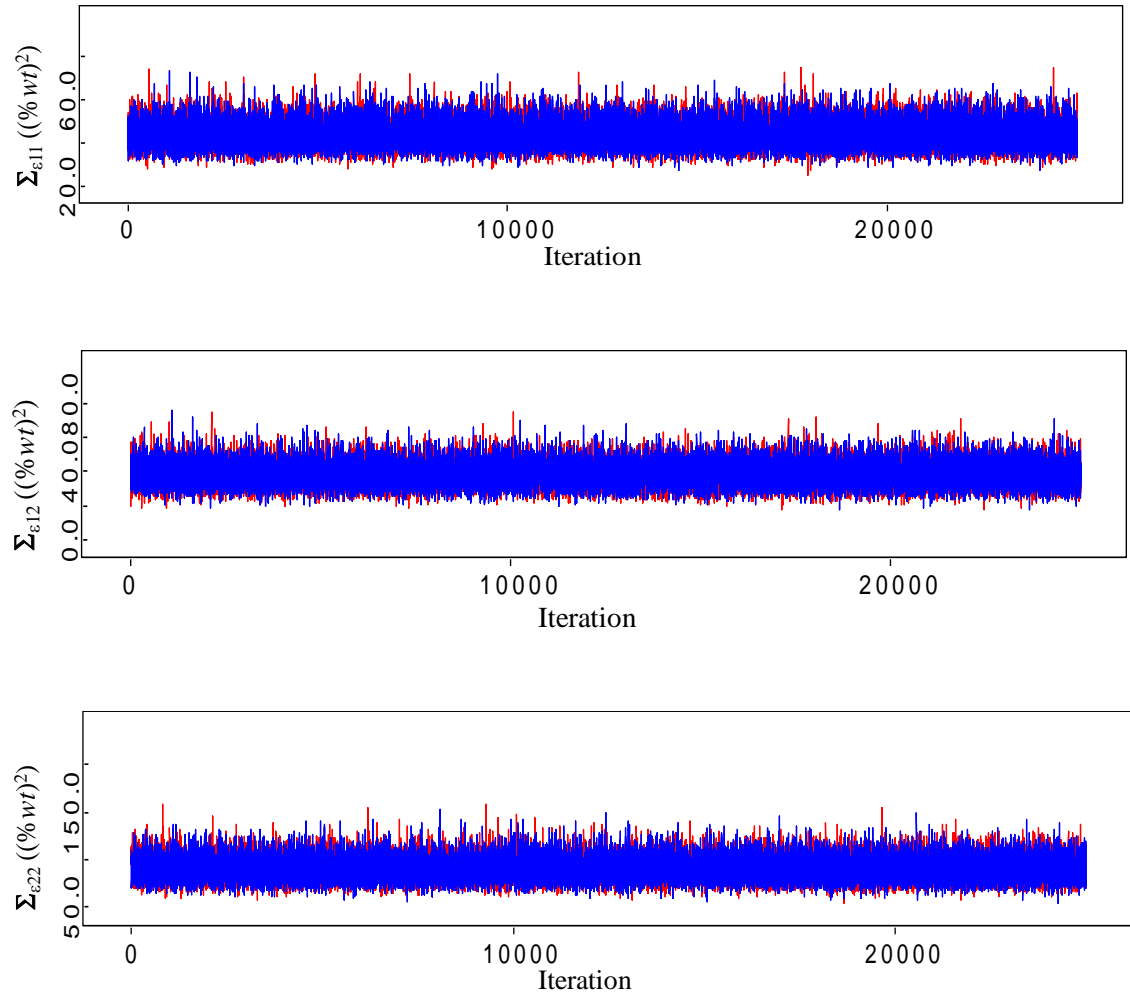


Figure 2.5 Trace plots of $\Sigma_{\epsilon_{11}}$, $\Sigma_{\epsilon_{12}}$ and $\Sigma_{\epsilon_{22}}$

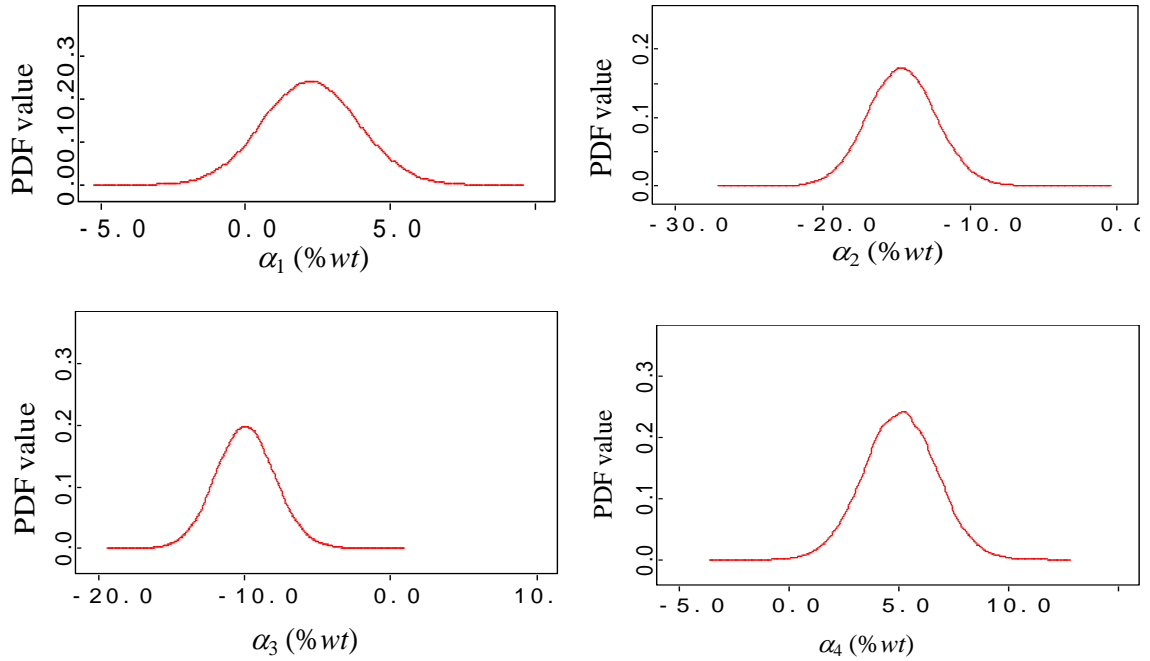


Figure 2.6 Marginal posterior distributions of α_1 , α_2 , α_3 , and α_4

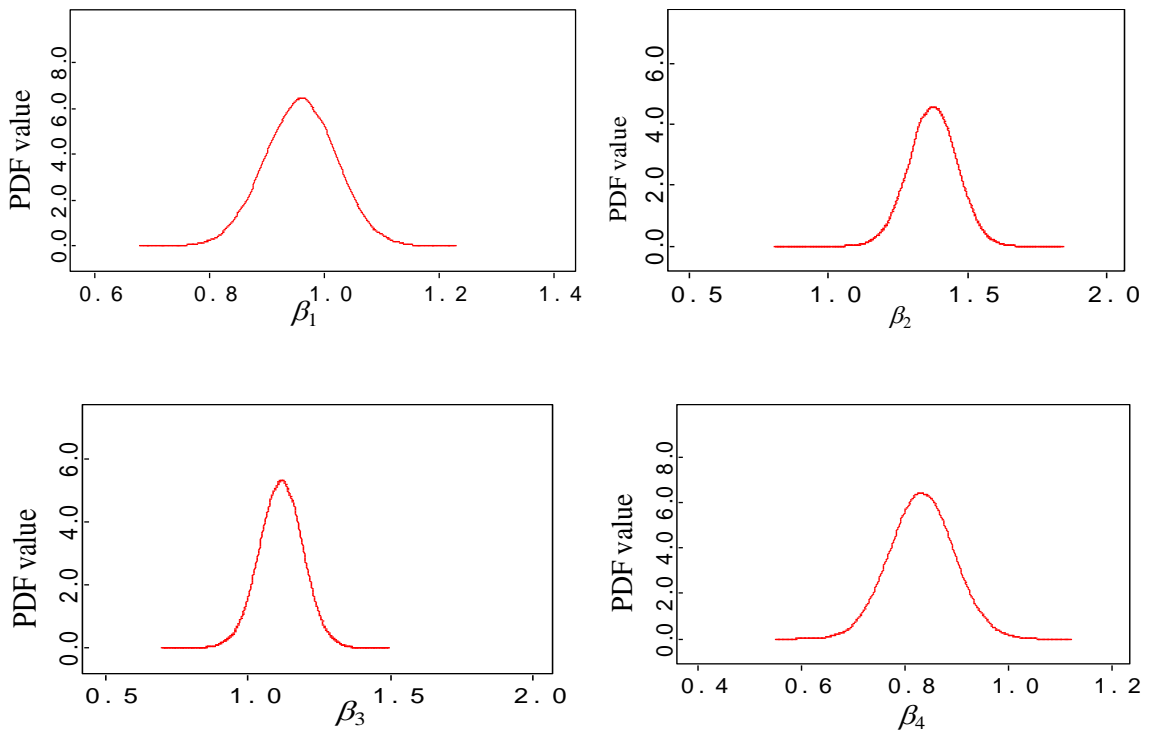


Figure 2.7 Marginal posterior distributions of β_1 , β_2 , β_3 , and β_4

The mean values of the marginal posterior distributions of the parameters are shown in Table 2.1, where σ_1 , σ_2 , σ_3 and σ_4 denote the standard deviations of the scattering errors associated with the ILI tools in 2004, 2007, 2009 and 2011, respectively. The results in Table 2.1 suggest that the 2004 ILI tool is the most accurate among the four ILI tools considered because the mean values of α_1 and β_1 are closer to zero and unity respectively than those of the other tools, and because the mean value of σ_1 is the second lowest of σ_1 , σ_2 , σ_3 and σ_4 , and in fact only slightly higher than the lowest value, σ_4 . On the other hand, the 2007 and 2009 ILI tools are associated with relatively large measurement errors because the mean values of α_2 and α_3 are markedly different from zero and because the mean values of σ_2 and σ_3 are the largest of all four tools.

The estimated mean values of the correlation coefficients (i.e. ρ_{kl} as defined in the model) between the scattering errors associated with the four ILI tools are summarized in Table 2.2. These values suggest that the scattering errors associated with different ILI tools are relatively highly correlated. The correlation coefficients are all greater than or equal to 0.70, even in the case where the corresponding ILI tools are from different vendors. Note that the correlation coefficients between the 2007 and 2009 tools ($\rho_{23} = 0.78$) and between the 2004 and 2011 tools ($\rho_{14} = 0.82$), are higher than the other correlation coefficients. This is expected because the 2007 and 2009 tools are both from the same vendor (Vendor B), and the 2004 and 2011 are also from the same vendor (Vendor A).

Table 2.1 Mean values of the parameters in the calibration models for ILI tools used in Case 1

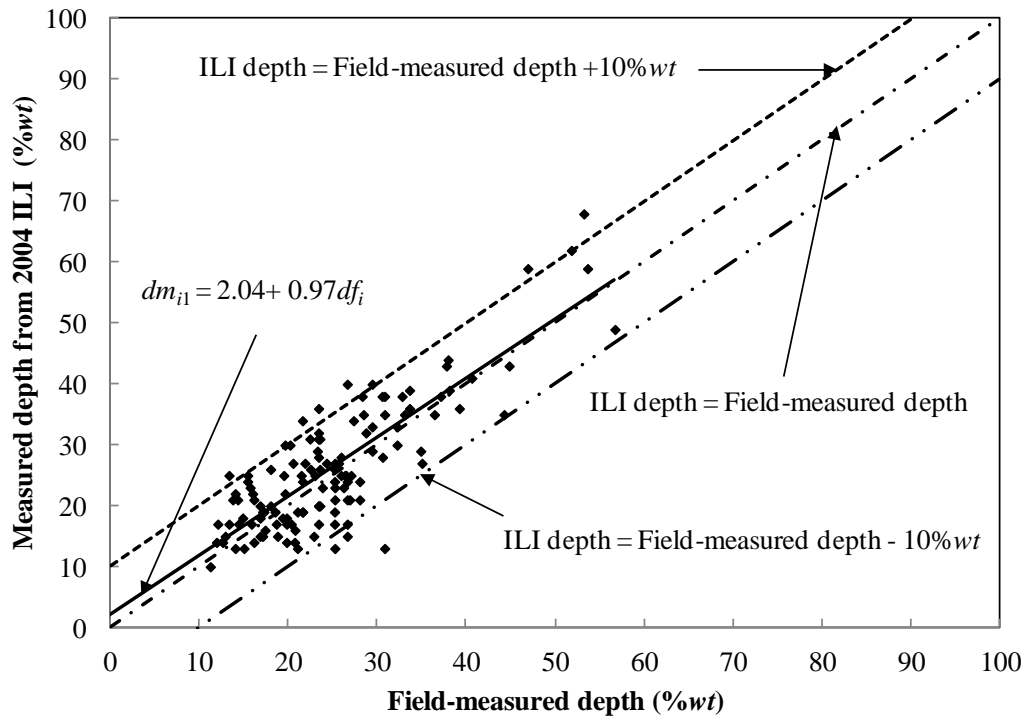
ILI 2004 (Vendor A)			ILI 2007 (Vendor B)			ILI 2009 (Vendor B)			ILI 2011 (Vendor A)		
α_1 (%wt)	β_1	σ_1 (%wt)	α_2 (%wt)	β_2	σ_2 (%wt)	α_3 (%wt)	β_3	σ_3 (%wt)	α_4 (%wt)	β_4	σ_4 (%wt)
2.04	0.97	5.97	-15.28	1.40	9.05	-10.38	1.13	7.62	4.84	0.84	5.94

Table 2.2 Mean values of the correlation coefficients (ρ_{kl}) between the random scattering errors for different ILI tools used in Case 1

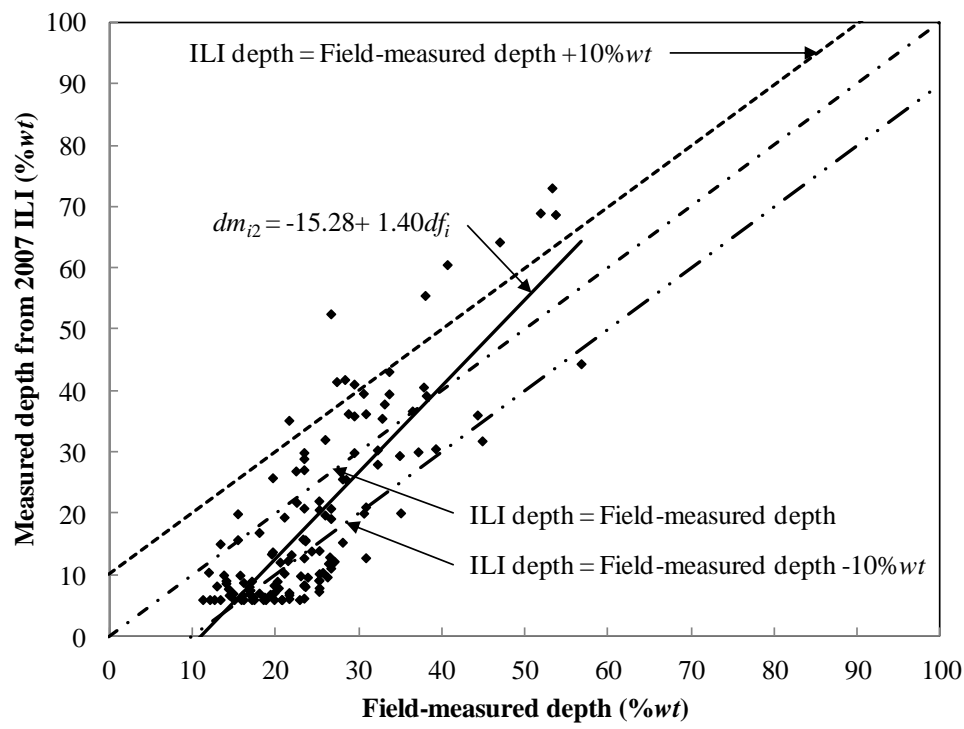
	ILI 2007 (Vendor B)	ILI 2009 (Vendor B)	ILI 2011 (Vendor A)
ILI 2004 (Vendor A)	$\rho_{12} = 0.70$	$\rho_{13} = 0.72$	$\rho_{14} = 0.82$
ILI 2007 (Vendor B)	-	$\rho_{23} = 0.78$	$\rho_{24} = 0.71$
ILI 2009 (Vendor B)	-	-	$\rho_{34} = 0.74$

To visualize the measurement errors associated with the four ILI tools, the depths reported by the ILI tools are compared with the field-measured depths of the 128 recoated defects in Figs. 2.8(a) through 2.8(d). Also shown in these figures are the unity line (i.e. 1:1 line), the bounds representing the field-measured depth $\pm 10\%$ wall thickness (*wt*), which are often used by the vendor as the confidence bounds for the tool accuracy, and the calibration line characterized by $dm_{ij} = \bar{\alpha}_j + \bar{\beta}_j df_i$ for each of the tools, where $\bar{\alpha}_j$ and $\bar{\beta}_j$ denote the mean values of α_j and β_j respectively obtained from the Bayesian analysis. Figure 2.8(a) and Fig. 2.8(d) indicate that the measurement errors associated with 2004 and 2011 ILI tools are relatively small and most of the ILI-reported defect depths fall

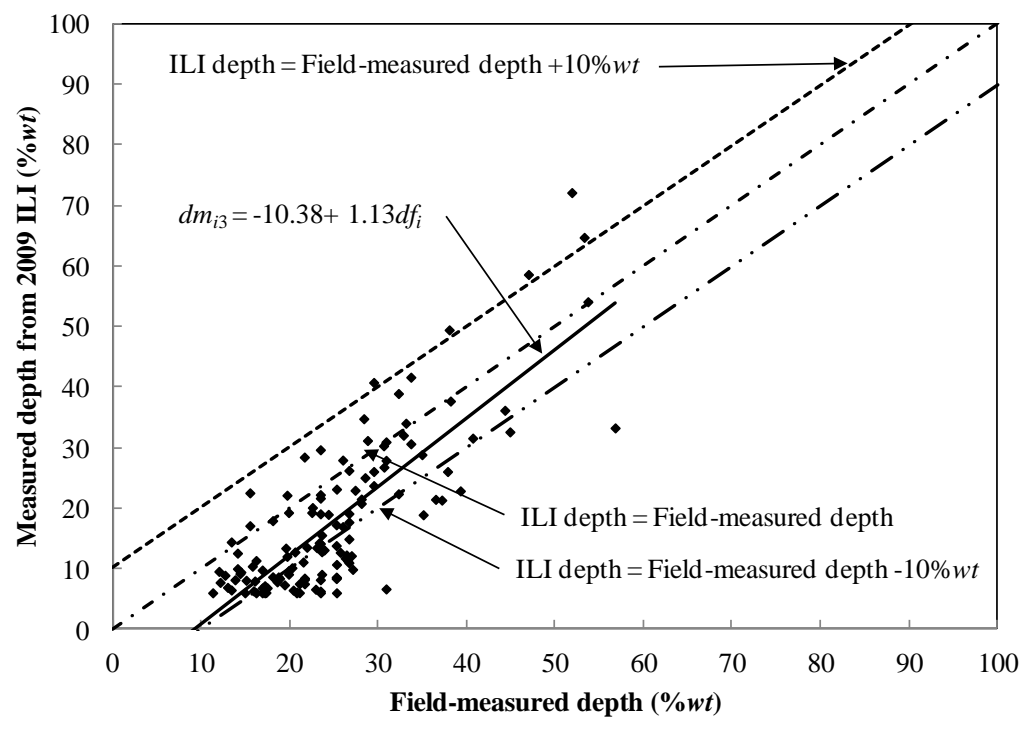
within the vendor's claimed confidence bounds. On the other hand, Fig. 2.8(b) and Fig. 2.8(c) show that both the 2007 and 2009 ILI tools tend to undersize shallow defects (say, defects with depths less than 30% *wt*) and oversize deep defects (say, depths greater than 40% *wt*).



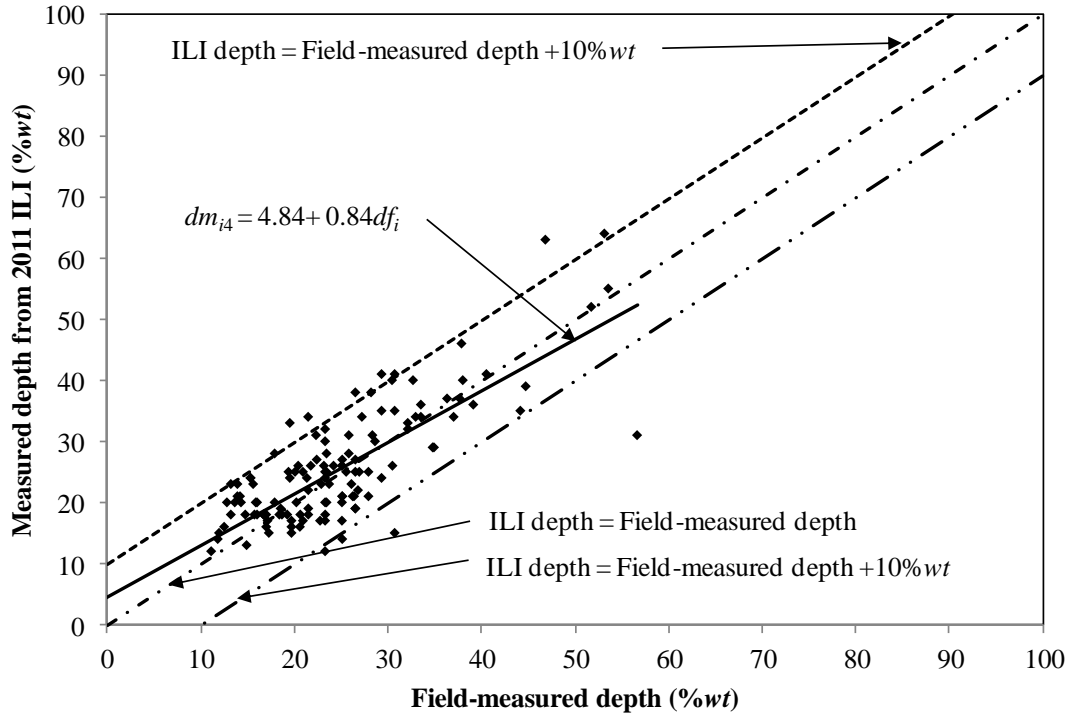
a) 2004 ILI data



b) 2007 ILI data



c) 2009 ILI data



d) 2011 ILI data

Figure 2.8 Comparison of field-measured depths and ILI-reported depths for the recoated defects on the pipeline in Case 1

2.6.3 Case 2

This case involves the calibration of three ILI tools that were used to inspect a 78.4 km long gas pipeline in 2004, 2007 and 2009 respectively. The ILI tools used in 2004 and 2009 are from vendor A, whereas the ILI tool used in 2007 is from vendor B. Corrosion defects that were recoated prior to 2004 were used to calibrate the ILI tools. A total of 128 recoated defects were matched with the ILI-reported defect listings in 2004, 2007 and 2009.

The Bayesian model described in Section 2.5 was used to evaluate the measurement errors of the three ILI tools. The same values mentioned in Section 2.6.2 were assigned

to the hyper-parameters, a , b , c , d , l and u of the prior distributions in this case. The parameter k was assigned a value of 3, whereas \mathbf{R} was selected to be a 3×3 diagonal matrix with the diagonal elements equal to $0.001 ((wt)^{-2})$. The corresponding OpenBUGS code used in the analysis is given in Appendix 2E. The estimated mean values of the calibration parameters are shown in Table 2.3. The results in Table 2.3 indicate that the ILI tool used in 2009 has the smallest bias compared with the tools used in 2004 and 2007. However, the mean value of the standard deviation of the scattering error associated with the tool in 2009 is also larger than those associated with the tools in 2004 and 2007. The estimated mean values of the correlation coefficients between the scattering errors associated with the three ILI tools are summarized in Table 2.4. Consistent with Table 2.2, Table 2.4 suggests that the scattering errors associated with different ILI tools are relatively highly correlated as the correlation coefficients are all greater than 0.70 and that the correlation coefficient is slightly higher for the tools from the same vendor (i.e. the 2004 and 2009 tools) than those of the tools from different vendors.

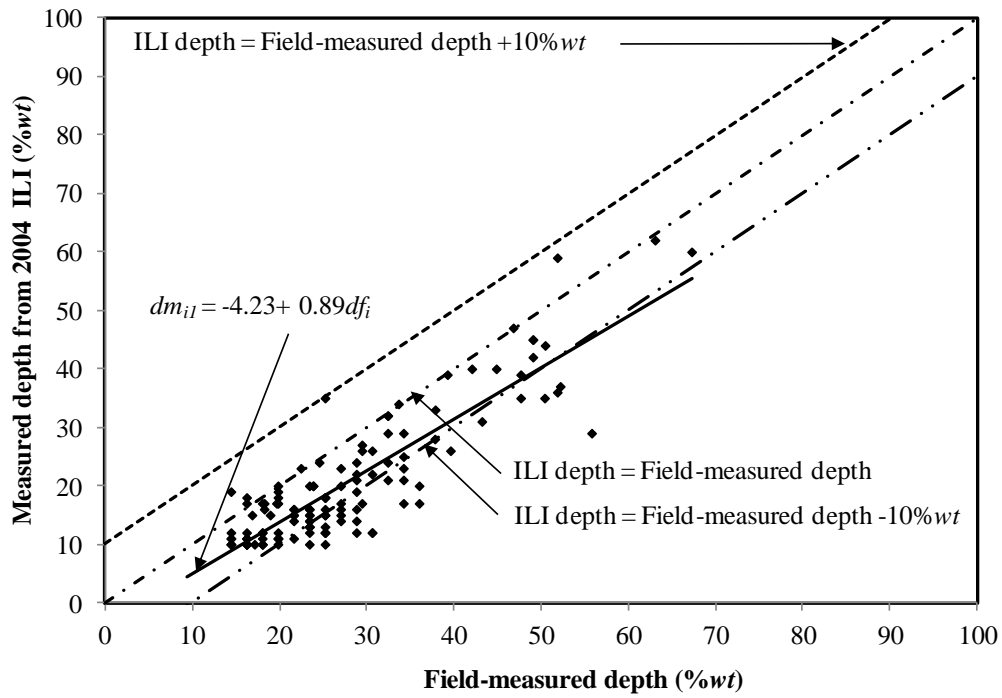
Table 2.3 Mean values of the parameters in the calibration models for ILI tools used in Case 2

ILI 2004 (Vendor A)			ILI 2007 (Vendor B)			ILI 2009 (Vendor A)		
α_1 (%wt)	β_1	σ_1 (%wt)	α_2 (%wt)	β_2	σ_2 (%wt)	α_3 (%wt)	β_3	σ_3 (%wt)
-4.23	0.89	5.32	-9.50	0.91	7.12	-3.54	1.00	7.66

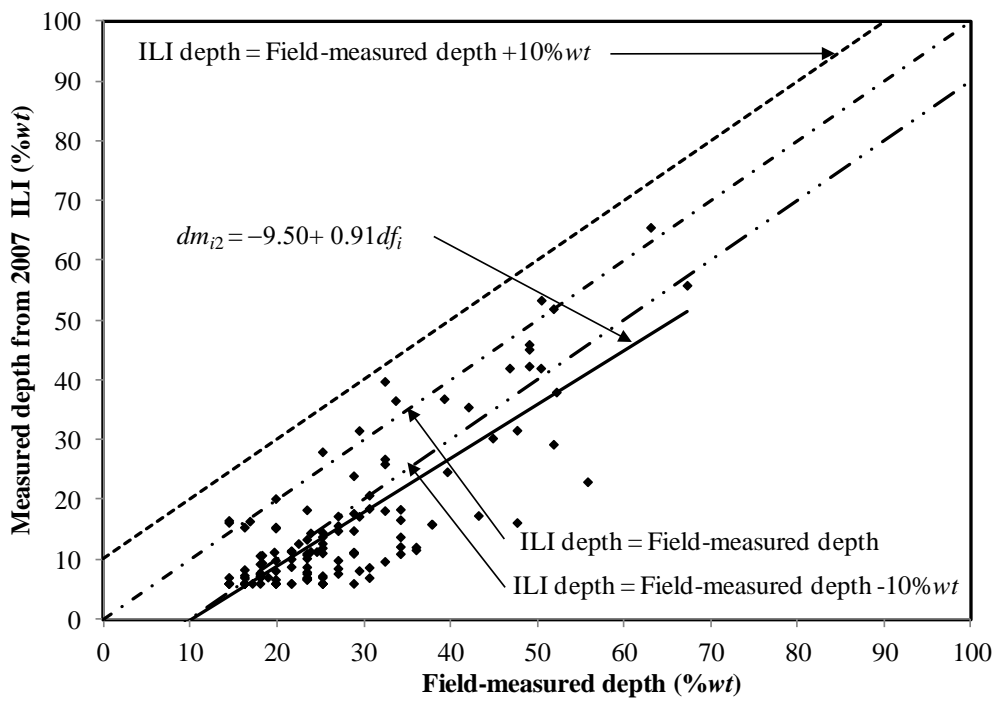
Table 2.4 Mean values of the correlation coefficients (ρ_{kl}) between the random scattering errors for different ILI tools in Case 2

	ILI 2007 (Vendor B)	ILI 2009 (Vendor A)
ILI 2004 (Vendor A)	$\rho_{12} = 0.76$	$\rho_{13} = 0.77$
ILI 2007 (Vendor B)	-	$\rho_{23} = 0.71$

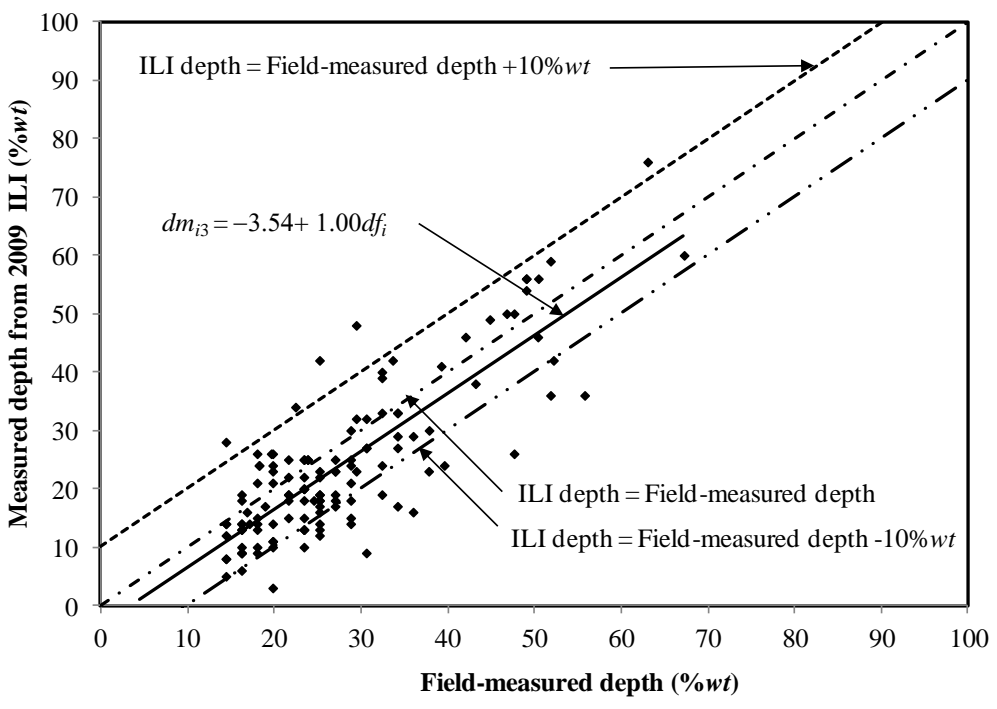
The comparison of the ILI-reported depths with the field-measured depths of the 128 recoated defects is depicted in Figs. 2.9(a) through 2.9(c). These figures suggest that the three ILI tools considered in this case study tend to undersize the depths of the corrosion defects.



a) 2004 ILI data



b) 2007 ILI data



c) 2009 ILI data

Figure 2.9 Comparison of field-measured depths and ILI-reported depths for the recoated defects on the pipeline in Case 2

2.7 Conclusion

The Bayesian method was applied to calibrate the accuracy of the ILI tools for sizing metal-loss corrosion defects on pipelines. The calibration is based on comparing the field-measured depths and ILI-reported depths for a set of defects that have been repaired and ceased growing. Jaech's method was employed first to calibrate the accuracy of the field-measuring tool by comparing the depths reported by two different field-measuring devices for a set of defects. The results suggest that the field-measured depth contains negligibly small measurement error and can be assumed to equal the actual depth. The defect depth reported by ILI was assumed to equal a linear function of the field-measured depth plus a random scattering error. The intercept and slope of the linear function, i.e. the constant and non-constant biases, as well as the random scattering error were then quantified using the Bayesian methodology. The calibration model further allows the correlation coefficients between scattering errors of different ILI tools to be quantified. The Markov Chain Monte Carlo (MCMC) simulation approach was adopted to carry out the Bayesian updating.

The application of the calibration model was illustrated through two case studies where ILI tools were used to inspect two subject pipelines at different times. The results of the calibration indicate that the measurement errors of different ILI tools vary substantially. For example, the constant and non-constant biases of the ILI tool used on the subject pipeline of Case 1 in 2004 equal $2.04\%wt$ and 0.97 , respectively, and the standard deviation of the scattering error equals $5.97\%wt$. On the other hand, the constant and non-constant biases of the ILI tool used on the same pipeline in 2007 equal -

15.28%wt and 1.40, respectively, and the standard deviation of the scattering error equals 9.05%wt. Furthermore, it was observed that the random scattering errors associated with different ILI tools are relatively highly correlated. The correlation coefficient between the scattering errors is consistently greater than or equal to 0.70, even in the case where the corresponding ILI tools are from different vendors. The calibration model reported in this chapter can be used to calibrate any number of ILI tools simultaneously and quantify the potential correlation between the measurement errors of different ILI tools. The calibration results can assist ILI vendors in improving the accuracy of the ILI data for a particular pipeline (e.g. by improving the sizing algorithm for the pipeline) and facilitate the development of a reliable corrosion growth model based on data from multiple ILI runs.

References

Bayes, M., and Price, M., 1763. An Essay towards Solving a Problem in the Doctrine of Chances. By the Late Rev. Mr. Bayes, F. R. S. Communicated by Mr. Price, in a Letter to John Canton, A. M. F. R. S. *Philosophical Transactions*, 53, pp. 370-418.

Bernardo, J., and Smith, A. F. M., 2007. *Bayesian Theory*. John Wiley & Sons Inc, New York, NY, USA.

Bhatia, A., Mangat, N. S., and Morrision, T., 1998. Estimation of Measurement Errors. *Proceedings of International Pipeline Conference*, ASME, Calgary, Alberta, Canada, p. 315.

Caleyo, F., Alfonso, L., Espina-Hernández, J. H., and Hallen, J. M., 2007. Criteria for performance assessment and calibration of in-line inspections of oil and gas pipelines. *Measurement Science and Technology*, 18(7).

Coleman, G. A., and Miller, S. J., 2010. ILI Tool Tolerance and Repeatability Effect on Corrosion Growth Rates. *Proceedings of 8th International Pipeline Conference*, ASME, Calgary, Alberta, Canada, pp. 549-556.

Congdon, P., 2006. *Bayesian Statistical Modelling*. John Wiley & Sons Ltd, Chichester, West Sussex, England.

Congdon, P. D., 2010. *Applied Bayesian Hierarchical Methods*. CRC Press, London, UK.

Fenyvesi, L., and Dumalski, S., 2005. Determining Corrosion Growth Accurately and Reliably. *Corrosion2005*, NACE International.

Fuller, W. A., 1987. *Measurement error models*. Jhon Wiley & Sons, Inc., New York, NY, USA.

Gelman, A., Carlin, J. B., Stern, H. S., Rubin, D. B., 2004. *Bayesian data analysis*. Chapman & Hall/CRC, Boca Raton, Florida, USA.

Gilks, W. R., Richardson, S., and Spiegelhalter, D. J., 1996. *Markov Chain Monte Carlo in Practice*. Chapman & Hall.

Grubbs, F. E., 1948. On Estimating Precision of Measuring Instruments and Product Variability. *Journal of the American Statistical Association*, 43(242), pp. 243-264.

Have, T. R. T., and Uttal, D. H., 1994. Subject-Specific and Population-Averaged Continuation Ratio Logit Models for Multiple Discrete Time Survival Profiles. *Journal of the Royal Statistical Society. Series C (Applied Statistics)*, 43(2), pp. 371-384.

Jaech, J. L., 1985. *Statistical analysis of measurement errors*. Jhon Wiley & Sons, Inc., New York, NY, USA.

Link, W., and Eaton, M., 2012. On thinning of chains in MCMC. *Methods in Ecology and Evolution*, 3(1), pp. 112-115.

Lunn, D., Spiegelhalter, D., Thomas, A., and Best, N., 2009. The BUGS project: Evolution, critique and future directions. *Statistics in Medicine*, 28(25), pp. 3049-3067.

McNealy, R., McCann, R., Van Hook, M., Stiff, A., and Kania, R., 2010. In-Line Inspection Performance III: Effect of In-Ditch Errors in Determining ILI Performance. *Proceedings of 8th International Pipeline Conference*, ASME, Calgary, Alberta, Canada, pp. 469-473.

Morrison, T., Mangat, N., Desjardins, G., and Bhatia, A., 2000. Validation of an In-line Inspection Metal Loss Tool. *Proceedings of International Pipeline Conference*, ASME, Calgary, Alberta, Canada, pp. 839-844.

Nessim, M., Dawson, J., Mora, R., and Hassanein, S., 2008. Obtaining Corrosion Growth Rates From Repeat In-Line Inspection Runs and Dealing With the Measurement Uncertainties. *Proceedings of 7th International Pipeline Conference*, ASME, Calgary, Alberta, Canada, pp. 593-600.

O'Hagan, A., Stevens, J. W., and Montmartin, J., 2001. Bayesian cost-effectiveness analysis from clinical trial data. *Statistics in Medicine*, 20(5), pp. 733-753.

Spencer, K., Kariyawasam, S., Tetreault, C., and Wharf, J., 2010. A Practical Application to Calculating Corrosion Growth Rates by Comparing Successive ILI Runs From Different ILI Vendors. *Proceedings of 8th International Pipeline Conference*, ASME, Calgary, Alberta, Canada, pp. 467-473.

Wishart, J., 1928. The Generalised Product Moment Distribution in Samples from a Normal Multivariate Population. *Biometrika*, 20A(1-2), pp. 32-52.

Chapter 3 Hierarchical Bayesian Corrosion Growth Model Based on In-line Inspection Data

3.1 Introduction

External metal-loss corrosion is a major threat to the structural integrity of pipelines (Kiefner et al. 2001). Quantifying the growth of corrosion over time is critically important for the risk and reliability analysis of pipelines, planning for corrosion mitigation and repair, and determination of time intervals for corrosion inspections. On one hand, underestimation of the growth of corrosion defects may lead to critical defects being missed by mitigation actions - failure of these defects can have serious consequences in terms of human safety, environmental damages, and economic loss. On the other hand, overly conservative estimation of the growth can lead to unnecessary inspections and defect mitigations that result in significant cost penalties to pipeline operators. Hence it is vital to develop a model that can characterize the growth of individual corrosion defects on pipelines with a high level of accuracy (Kariyawasam and Peterson 2010).

In-line inspection (ILI) tools are being widely used to detect and size corrosion defects on pipelines. Over the last decade, researchers have been devoting a great deal of efforts to characterizing the growth of corrosion defects based on the ILI data. Because the depth (i.e. in the through pipe wall thickness direction) of a corrosion defect on a pipeline is the most critical dimension that impacts the structural integrity of the pipeline, the growth of the defect depth has been the main focus of the research. Worthingham et

al. (2000) used the data from three consecutive ILIs to develop a corrosion growth model and evaluated the accuracy of the proposed model by comparing the predicted depths five years after the last ILI with the corresponding field-measured depths. Desjardins (2001) reported a study to determine the corrosion growth rate and severity of the corrosion on pipelines based on the data obtained from a single ILI run as well as multiple ILI runs. The data from a single ILI run together with the information about the condition of the pipeline during construction and age of the pipeline were used to calculate the bulk growth rate of the corrosion defects on a pipeline. Achterbosch and Grzelak (2006) developed a linear growth model for depths of corrosion defects on a pipeline in the Netherlands based on the data from four consecutive ILI runs. The so-called constrained maximum likelihood method was used to estimate the parameters of the proposed linear growth model by incorporating the bias and measurement uncertainty of the ILI tools. Nessim et al. (2008) developed an approach to probabilistically characterize the defect-specific as well as segment-specific corrosion growth rates using the data from two successive ILI runs. The probability distribution of the average growth rate within the time interval between the two inspections was defined as a function of the ratio between the apparent growth rate evaluated using the ILI data and the measurement error of the estimated growth rate. This approach is only applicable for two ILI data sets.

Several researchers carried out experiments to investigate the corrosion process on metals buried in soil and reported that the growth of metal-loss corrosion is more appropriately characterized by non-linear functions of time than by linear functions (Soares and Garbatov 1999). Romanoff (1989) proposed a power-law growth model for the depths of the corrosion defects on buried metals based on data collected from 128 test

locations throughout the United States between 1910 and 1955. Caleyó et al. (2009) suggested a power-law model for the depth of pitting corrosion on underground pipelines and used various properties of the pipe material and surrounding soils to evaluate the parameters of the model. A time-dependent growth model for corrosion defects on underground pipelines was proposed by Maes et al. (2009), whereby the growth of the defect depth was assumed to follow a non-homogenous gamma process with a time-dependent shape parameter and a time-independent scale parameter. The hierarchical Bayesian method (Banerjee et al. 2004) as well as a simple equivalent log-likelihood method was employed to evaluate the model parameters based on the ILI data. Their model took into account the random scattering error in the ILI data, but did not consider the bias of the ILI data. The corrosion initiation time was also ignored in the model.

The objective of the study reported in this chapter was to develop a defect-specific growth model for the depths of corrosion defects on energy pipelines based on data obtained from multiple in-line inspections. The model incorporates the measurement errors associated with the ILI tools, which include both the bias (constant and non-constant) and random scattering error. The defect depth was assumed to follow a power-law function of time. The parameters of the growth model were assumed to be time-invariant. The hierarchical Bayesian methodology was employed to evaluate the parameters of the growth model.

The organization of this chapter is as follows. Section 3.2 includes a brief description of the hierarchical Bayesian methodology. This is followed by the description of the ILI data and associated measurement uncertainties in Section 3.3. The formulation of the

hierarchical Bayesian corrosion growth model as well as the specification of the prior and hyper-prior distributions is presented in Section 3.4. In Section 3.5, two case studies that involve two real pipelines currently in service are used to illustrate the application of the proposed model. The effect of correlations among the random scattering measurement errors on the model prediction is also examined in this section. In Section 3.6, the predictions made by the proposed model are compared with those of the linear growth model commonly used in the pipeline industry. The conclusions of this chapter are summarized in Section 3.7.

3.2 Hierarchical Bayesian Model

The Bayesian method treats the unknown parameters of a physical process as random variables rather than deterministic values. The method allows the prior knowledge about the parameters, which can be obtained from previous studies or experience, to be updated based on the observed data to obtain the updated opinion about the parameters. The updated belief can be further considered as the prior distribution for future updating when new data are available. Therefore through this iterative process the uncertainty about the parameters is minimized. The hierarchical Bayesian model (HBM) (Banerjee et al. 2004; Gelman et al. 2004) is a special case of the Bayesian model in which the prior distribution is decomposed in conditional distributions in a sequential order (Robert 2007). Hierarchical Bayesian models are powerful tools to make statistical inferences of parameters of a model that have complex interactions between them, and are particularly suitable to characterize population models in which the parameters characterizing the

model for an individual in the population are considered to be related to the parameters for the other individuals from the same population (Demichelis 2006).

Consider a population of n random variables, Y_i ($i = 1, 2, \dots, n$) that characterize similar physical processes. Suppose that a set of unknown parameters, θ_i , define the probability distribution of random variable Y_i . One can assign a prior distribution, $p(\theta_i|\lambda)$, to θ_i , where $p(\theta_i|\lambda)$ represents the probability density function of θ_i conditional on the known parameters λ , which are assumed to be common to the population of Y_i . Further let y_i represent a set of observed data for Y_i . By combining the observed data and prior distribution, the updated opinion about θ_i can be evaluated based on Bayes' theorem given by (Bayes and Price 1763)

$$p(\theta_i|y_i) = \frac{p(y_i|\theta_i) \times p(\theta_i|\lambda)}{p(y_i)} \quad (3.1)$$

where $p(\theta_i|y_i)$ is the *posterior distribution* of θ_i ; $p(y_i|\theta_i)$ is the so-called *likelihood* function, and $p(y_i)$ is a normalizing constant, which ensures that $p(\theta_i|y_i)$ integrates to unity. The value of $p(y_i)$ can be obtained by integrating the product of the likelihood and prior distribution with respect to θ_i . Thus,

$$p(y_i) = \int p(y_i|\theta_i) \times p(\theta_i|\lambda) d\theta_i \quad (3.2)$$

Taking into consideration the normalizing constant, one can write Eq. (3.1) as,

$$p(\theta_i|y_i) \propto p(y_i|\theta_i) \times p(\theta_i|\lambda) \quad (3.3)$$

where the symbol “ \propto ” indicates proportionality.

Note that until this point the above formulation is a standard Bayesian setup where a prior distribution is assigned to parameters θ_i that govern the distribution of Y_i . This model can be extended by assuming that parameters λ that govern the distribution of θ_i are also random variables and by assigning a prior distribution, $p(\lambda/\gamma)$, to λ . Here, $p(\lambda/\gamma)$ and γ are referred to as the *hyper-prior* and *hyper-parameters*, respectively (Banerjee et al. 2004). The parameters γ characterize the prior beliefs about λ and are typically assumed to be known quantities, although in theory one can also treat λ as random variables and proceed to another layer of hierarchy. The hierarchical structure of such a Bayesian model is depicted in Fig. 3.1 where square nodes represent deterministic (known) quantities and oval nodes represent stochastic component of the model. This model can be summarized as follows:

Likelihood of data: $p(\mathbf{y}_i|\theta_i)$

First stage prior: $p(\theta_i/\lambda)$

Second stage prior: $p(\lambda/\gamma)$

Posterior distribution of θ_i : $p(\theta|\bullet) \propto p(\mathbf{y}_i|\theta_i) p(\theta_i/\lambda)$

Posterior distribution of λ : $p(\lambda|\bullet) \propto p(\theta_1, \theta_2, \dots, \theta_i, \dots, \theta_n|\lambda) p(\lambda/\gamma)$

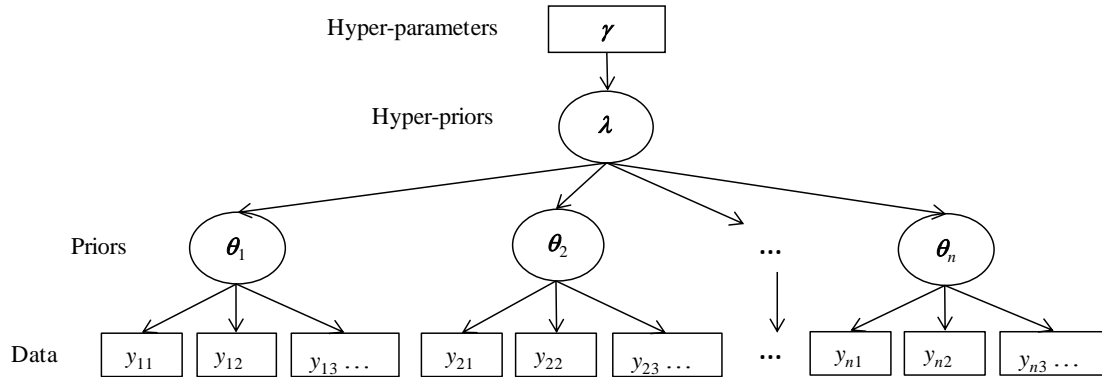


Figure 3.1 Graphical representation of a typical hierarchical Bayesian model

The main advantages of HBM compared to other statistical models are as follows:

- In the hierarchical model the parameters of a specific group or individual can borrow information from the corresponding parameters of other groups or individuals with similar characteristics (Ntzoufras 2011). Therefore, the individual level inference can be made accurately and robustly even if the sample size of the observed data for a given individual is small. This is particularly advantageous for characterizing the growth of individual corrosion defects on a pipeline as the number of inspections is usually limited for a given defect.
- HBM can account for uncertainties from different sources through the hierarchical prior assignment. It provides robust estimates of the parameters because the posterior results are averaged across different prior choices (Robert 2007).

- The decomposition of priors in a hierarchical structure facilitates assigning conjugate priors to some of the parameters so that the corresponding conditional posterior distributions can be derived in closed form, and therefore simplifies the computation of the model by permitting the simple Gibbs-based sampling scheme to be used in updating the parameters (Robert 2007).

The probabilistic characteristics (e.g. mean, variance and percentiles) of the random variables involved in the Bayesian model can be evaluated by integrating the corresponding marginal posterior distributions. But in most cases, the close-formed solution for the posterior distribution is not available due to the complexity and high dimensionality of the Bayesian model. This difficulty was overcome in the early 1990s with the development of the Markov Chain Monte Carlo (MCMC) techniques. The MCMC techniques involve the construction of a Markov chain that starts from the assumed initial values of the parameters and eventually converges to the target distribution (i.e. the so-called stationary distribution), which, in our case, is the joint posterior distribution. The effect of initial values is minimized by discarding the samples drawn at the beginning of iterations known as the “burn-in” period. The samples generated after the burn-in period are then used to make statistical inferences of the parameters. Two types of algorithm are frequently used to conduct the MCMC sampling, namely the Metropolis-Hastings algorithm and Gibbs sampler (Gelman et al. 2004). A brief description of these two sampling algorithms is given in Appendix 2A.

3.3 ILI Data and Measurement Uncertainties

To quantify the growth of the depths of corrosion defects based on the data obtained from multiple ILI runs, the measurement errors of the ILI data must be taken into account (Fenyvesi and Dumalski 2005). The two main components of the measurement error are the systematic error, i.e. constant and non-constant bias of the ILI tool (Caleyo et al. 2007) and the repeatability error associated with the tool (Coleman and Miller 2010; Huyse and Roodselaar 2010; Spencer et al. 2010).

The measurement bias (constant and/or non-constant) associated with an ILI tool represents the ability of the tool to measure the true depth of a corrosion defect accurately, on average (Caleyo et al. 2007). The repeatability error, also referred to as the random scattering error, results from the inherent variability associated with the ILI tool. This component of the measurement error is typically assumed to follow a normal distribution with a zero mean and a certain standard deviation. Furthermore, the random scattering errors among different ILI tools that are based on the same technology (e.g. Magnetic Flux Leakage or ultrasonic) can be relatively highly correlated (see Chapter 2). A Bayesian method for quantifying the constant bias, non-constant bias and random scattering error of the ILI tool, as well as the correlation between the random scattering errors associated with different tools is described in Chapter 2.

3.4 Hierarchical Bayesian Corrosion Growth Model

3.4.1 Formulation and the Likelihood Function

Consider that m corrosion defects on a given pipeline have been detected and sized by ILI tools at n different inspection times. The defect depths reported by ILI tools are assumed to be related to the corresponding actual depths as follows (Fuller 1987; Jaech 1985):

$$dm_{ij} = \alpha_j + \beta_j da_{ij} + \varepsilon_{ij} \quad (3.4)$$

where dm_{ij} and da_{ij} denote the ILI-reported and actual depths of the i^{th} defect ($i = 1, 2, \dots, m$) obtained from the j^{th} inspection ($j = 1, 2, \dots, n$), respectively; α_j and β_j are the calibration parameters of the j^{th} ILI tool, which characterize the bias of the tool, and ε_{ij} represents the random scattering error of the ILI-reported depth of the i^{th} defect at the j^{th} inspection.

Let $\boldsymbol{\varepsilon}_i = [\varepsilon_{i1}, \varepsilon_{i2}, \dots, \varepsilon_{in}]^T$ denote the vector of random scattering errors associated with the depths reported by n ILI tools for the i^{th} defect, where “T” denotes transposition. It is assumed that $\boldsymbol{\varepsilon}_i$ follows a multivariate normal distribution, $MVN(\mathbf{0}, \boldsymbol{\Sigma}_\varepsilon)$, with a mean vector of zeros and a covariance matrix of $\boldsymbol{\Sigma}_\varepsilon$.

$$\boldsymbol{\varepsilon}_i \sim MVN(\mathbf{0}, \boldsymbol{\Sigma}_\varepsilon), i = 1, 2, \dots, m \quad (3.5)$$

where “ \sim ” indicates the assignment of probability distribution to a given random variable.

The values of α_j , β_j and Σ_ε for different ILI tools can be evaluated using a Bayesian approach by comparing the ILI-reported depths with the corresponding field-measured depths for a given set of defects (see Chapter 2). These parameters were treated as deterministic (i.e. known) values in the corrosion growth model. By combining Eqs. (3.4) and (3.5), the distribution function of \mathbf{dm}_i can be written as,

$$\mathbf{dm}_i \stackrel{ind}{\sim} MVN(\boldsymbol{\mu}_i, \boldsymbol{\Sigma}_\varepsilon), i = 1, 2, \dots, m \quad (3.6a)$$

$$\boldsymbol{\mu}_i = \boldsymbol{\alpha} + \boldsymbol{\beta} \mathbf{da}_i \quad (3.6b)$$

where “*ind*” denotes independency between \mathbf{dm}_i and \mathbf{dm}_k ($i \neq k$); $\mathbf{dm}_i = [dm_{i1}, dm_{i2}, \dots, dm_{in}]^T$, $\boldsymbol{\mu}_i = [\mu_{i1}, \mu_{i2}, \dots, \mu_{in}]^T$, $\boldsymbol{\alpha} = [\alpha_1, \alpha_2, \dots, \alpha_n]^T$, $\boldsymbol{\beta}$ is an n -by- n diagonal matrix with diagonal elements equal to β_j ($j = 1, 2, \dots, n$), and $\mathbf{da}_i = [da_{i1}, da_{i2}, \dots, da_{ij}, \dots, da_{in}]^T$. The exchangeability condition (Bernardo and Smith 2007) was assumed to be applicable to \mathbf{dm}_i ($i = 1, 2, \dots, m$); in other words, \mathbf{dm}_i were assumed to be mutually independent given $\boldsymbol{\alpha}$, $\boldsymbol{\beta}$, $\boldsymbol{\Sigma}_\varepsilon$ and \mathbf{da}_i .

In this study, the growth of the (actual) depth of a corrosion defect was assumed to follow a power-law function of time. It is further assumed that the parameters of the power-law growth model are invariant with respect to time, and specific to each individual defect. Finally, defects were assumed to be spatially independent. Based on the power-law model, the depth of defect i at the j^{th} inspection is given by

$$da_{ij} = a_i(t_j - t_{oi})^{b_i} + \eta_{ij} \quad (3.7)$$

where t_j (years) is the elapsed time from the installation date up to the j^{th} inspection; η_{ij} represents the model error of the power-law growth model associated with defect i at time t_j , and a_i , b_i and t_{oi} are the parameters of the growth model for defect i . The parameter a_i ($a_i > 0$) is indicative of the growth of the defect depth within one year from the defect initiation; b_i ($b_i > 0$) defines the rate of change of the growth path; that is, $b_i = 1$, $b_i > 1$ and $0 < b_i < 1$ characterize a linear, an accelerating and a decelerating growth path respectively, and t_{oi} (years) represents the corrosion initiation time, i.e. the elapsed time (years) from the time of installation up to the time at which defect i starts to grow.

3.4.2 Prior Distribution

In practice, the number of inspections is usually limited for a given defect. Therefore, hierarchical prior distributions were assumed for the parameters a_i and b_i , so that the information borrowed from other defects through the hierarchy of priors can facilitate the evaluation of the posterior distributions of these parameters. The truncated normal distribution was assigned as the prior distributions for a_i and b_i , because the parameters must be positive ($a_i, b_i > 0$). Furthermore, the choice of the normal distribution improves the computational stability and efficiency of the model. Because of the specific prior knowledge about the corrosion initiation time, i.e. between zero and the time elapsed from installation up to the first inspection (t_1), the prior distribution of t_{oi} was assumed to have only one level of hierarchy and be uniformly distributed between zero and t_1 . The model error η_{ij} for defect i was assumed to follow a normal distribution with a mean value of zero (i.e. the power-law model is considered on average unbiased for each

defect) and a defect-specific variance. The prior distributions of a_i , b_i , t_{oi} and η_{ij} ($i = 1, 2, \dots, m; j = 1, 2, \dots, n$) are summarized as follows:

$$a_i \underset{\sim}{\overset{iid}{N}}(\mu_a, \sigma_a^2); a_i > 0 \quad (3.8a)$$

$$b_i \underset{\sim}{\overset{iid}{N}}(\mu_b, \sigma_b^2); b_i > 0 \quad (3.8b)$$

$$t_{oi} \underset{\sim}{\overset{iid}{U}}(0, t_1) \quad (3.8c)$$

$$\eta_{ij} \sim N(0, \sigma_{\eta_i}^2) \quad (3.8d)$$

where *iid* denotes independent and identically distributed; $N(x, y^2)$ denotes a normal distribution with a mean value of x and a variance of y^2 , and $U(lb, ub)$ represents a uniform distribution with a lower bound of lb and an upper bound of ub . For a given defect i , η_{ij} were assumed to be independent and identically distributed at different times, and at a given time t_j , η_{ij} were assumed to be independent for different defects.

3.4.3 Hyper-prior Distribution

The parameters of the prior distributions of a_i , b_i and η_{ij} were considered random variables and assigned another level of priors that are known as hyper-priors of the model. The normal and inverse-gamma distributions were assumed as the prior distributions of μ_a (μ_b) and σ_a^2 ($\sigma_b^2, \sigma_{\eta_i}^2$), respectively, because these are well known conjugate priors of a normal distribution, and the use of the conjugate prior allows posterior distributions to be evaluated efficiently (Carlin and Louis 2000). If a random variable Z follows an inverse-gamma distribution, $IG(\lambda, \gamma)$, with a shape parameter λ and

a scale parameter γ , then $1/Z$ follows a gamma distribution, $G(\lambda, 1/\gamma)$, with a shape parameter λ , a scale parameter $1/\gamma$ and the corresponding probability density function is given by $\frac{1}{\Gamma(\lambda)} \left(\frac{1}{\gamma}\right)^\lambda \left(\frac{1}{Z}\right)^{\lambda-1} e^{-\frac{1}{\gamma Z}}$ (Gelman et al. 2004). Given the above, the prior distributions of μ_a , μ_b , $1/\sigma_a^2$, $1/\sigma_b^2$ and $1/\sigma_{\eta_i}^2$ are specified as follows:

$$\mu_a \sim N(c, d^2) \quad (3.9a)$$

$$1/\sigma_a^2 \sim G(e, f) \quad (3.9b)$$

$$\mu_b \sim N(g, h^2) \quad (3.9c)$$

$$1/\sigma_b^2 \sim G(k, l) \quad (3.9d)$$

$$1/\sigma_{\eta_i}^2 \stackrel{iid}{\sim} G(o, p) \quad (3.9e)$$

where c , d , e , f , g , h , k , l , o and p are called the hyper-parameters of the model and are assumed to be known quantities.

The full hierarchical Bayesian model structured with the aforementioned prior and hyper-prior distributions is depicted in Fig. 3.2. In this figure, rectangular nodes refer to known constants and oval nodes represent the stochastic (uncertain) components of the model. The logistic (i.e. deterministic) relationship and the stochastic relationship (i.e. relationship established through probability distributions) between different parameters are indicated by the double-edged arrows and single-edged arrows, respectively. Iterative structures, such as loop from $i = 1$ to $i = m$, are indicated by the plates. Such a representation of the model is called *directed acyclic graph* (DAG) (Lunn et al. 2009;

Spiegelhalter 1998). The full conditional posterior distributions of all the parameters are derived in Appendix 3A.

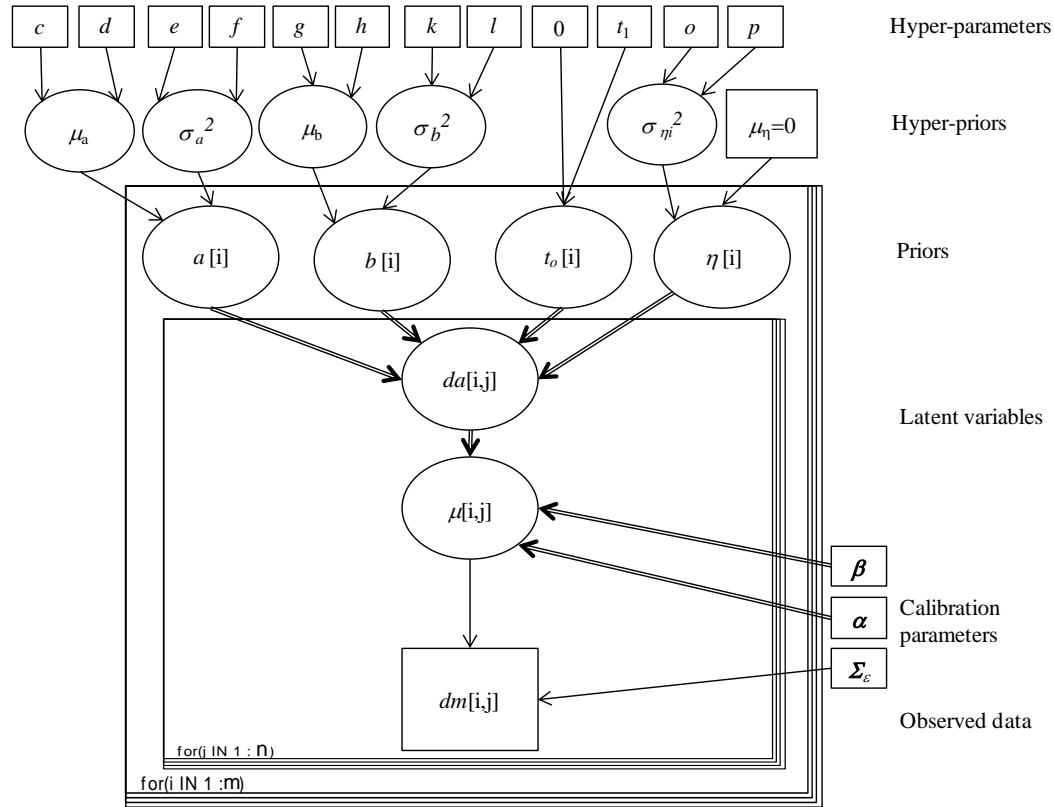


Figure 3.2 Graphical representation of the full hierarchical Bayesian corrosion growth model

3.5 Case Study

3.5.1 General

The application of the proposed corrosion growth model is illustrated by carrying out two case studies that involve two underground natural gas pipelines. The pipelines, which are currently in service, were inspected multiple times by high-resolution MFL tools over the last decade. For the purpose of model validation, two sets of external

corrosion defects that were measured at the dig sites were considered in the case studies. These defects were identified and manually matched with the corresponding defect listings reported by the ILIs prior to the defects being excavated and field measured. The matched ILI data were used to evaluate the parameters of the growth models (i.e. a_i , b_i , t_{oi} and η_{ij}) using the Bayesian updating software OpenBUGS (Lunn et al. 2009). The estimated parameters of the growth models were then used to predict the depths of the defects. The predicted depths at the time of field measurement were compared with the corresponding field-measured depths for model validation.

3.5.2 Case 1

The corrosion defects on the subject pipeline described in Case 1 of Chapter 2 were used to develop the hierarchical Bayesian corrosion growth model in this case. The pipeline was installed in 1972. Several joints of this pipeline were excavated in 2010, and the depths of the corrosion defects on the excavated pipe joints were measured using the ultrasonic (UT) thickness device at the dig sites. A total of 62 such defects was identified and matched with the corresponding defects reported by the ILI tools in 2000, 2004 and 2007. Note that the former two ILI tools are from Vendor A and the latter one is from Vendor B. As the measurement error associated with the UT tool has been found to be very small (see Chapter 2), the field-measured depth was assumed to equal the actual depth of the defect; therefore, the actual depths of the 62 defects in 2010 are known. The ILI data of 2000, 2004 and 2007 were used to develop the model; and the predicted depths were compared with the corresponding field-measured depth in 2010. Although an ILI was also carried out for the pipeline in 2009, the corresponding data

were not used in developing the model so that the prediction is for a forecasting period that is not too short (i.e. 3 years, from 2007 to 2010). The apparent growths of the 62 defects from 2000 to 2007 as indicated by the ILI data are shown in Fig. 3.3. This figure illustrates the randomness of the growth pattern of the corrosion defects on the pipeline. Furthermore, the depths of some defects as reported by the ILI tools decrease from 2000 to 2004 and/or from 2004 to 2007. Because the actual depth of a corrosion defect cannot decrease, this observation suggests that the measurement errors of the ILI tools have a large impact on the apparent growth of the defects.

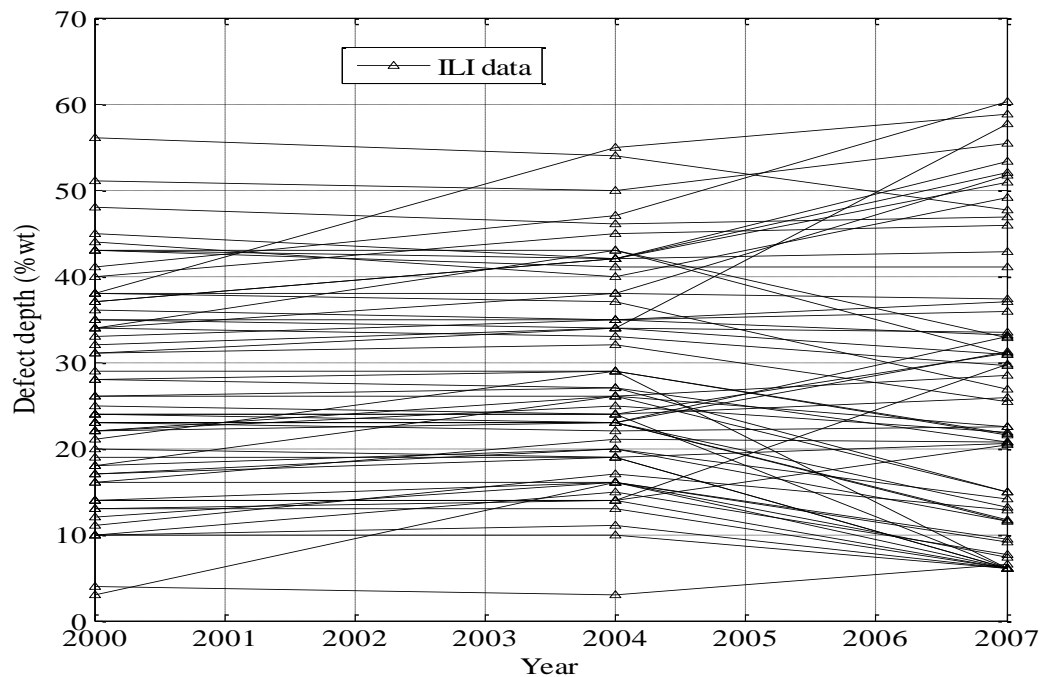


Figure 3.3 Apparent growth paths of the 62 corrosion defects indicated by the ILI data

The measurement errors of the ILI tools as reported in Chapter 2 (see results for Case 1) were used in this study. Because the measurement error of the ILI tool used in 2000 was not quantified due to a lack of relevant information, it was assumed that the constant and non-constant biases (i.e. α and β) associated with the ILI tool used in 2000 are the

same as those for the ILI tool used in 2004. This is based on the fact that the two ILI tools are from the same vendor (Vendor A) and employ the same sizing algorithm. It was further assumed that the correlation coefficient between the random scattering errors of the 2000 and 2004 ILI tools is the same as that between the ILI tools used in 2004 and 2011, given that the 2011 tool is also from Vendor A (see Chapter 2). The correlation coefficient between the scattering errors of the 2000 and 2007 tools were assumed to be the same as that between the 2004 and 2007 ILI tools. The biases (constant and non-constant) and standard deviations of the random scattering errors of the ILI tools, as well as the correlation coefficients between the scattering errors associated with different ILI tools were assumed to equal the mean values of the posterior distributions of these parameters obtained from the Bayesian-based calibration of the ILI tool as described in Chapter 2. The specific values of these parameters are as follows (see Tables 2.1 and 2.2 in Chapter 2): $\alpha_1 = \alpha_2 = 2.04$ (%wt), $\alpha_3 = -15.28$ (%wt), $\beta_1 = \beta_2 = 0.97$, $\beta_3 = 1.40$, $\sigma_1 = \sigma_2 = 5.97$ (%wt), $\sigma_3 = 9.05$ (%wt), $\rho_{12} = 0.82$, $\rho_{13} = \rho_{23} = 0.7$, where the subscripts “1”, “2” and “3” indicate the ILI tools used in 2000, 2004 and 2007, respectively, and *wt* denotes the pipe wall thickness.

The time interval between the installation of the pipeline (1972) and time of the first inspection (2000) is 28 years. Therefore the upper bound of the prior distribution of t_{oi} in Eq. (3.8c) was set at 28 years. Due to a lack of prior knowledge about the potential values of a_i and b_i , non-informative distributions (Gelman et al. 2004) were generally assigned to the hyper-priors for a_i , b_i and $\sigma_{\eta_i}^2$. A non-informative normal distribution is commonly assumed to have a mean and variance of 0 and 10000, respectively, in the literature (Hoff 2009; Lunn et al. 2009); therefore, c (g) and d (h) in Eqs. (3.9a) and

(3.9c) were set to be 0 and 100, respectively. The shape parameter o and scale parameter p in Eq. (3.9e) both were set equal to 0.001, which result in a mean value of unity and a variance of 1000 for the prior distribution of $1/\sigma_{\eta_i}^2$. To facilitate the convergence of $1/\sigma_a^2$ and $1/\sigma_b^2$ toward their posterior marginal distributions, e (k) and f (l) were set equal to 0.01 and 100, respectively in Eqs. (3.9b) and (3.9d). Note that the hyper-parameters $c, d, e, f, g, h, k, l, o$ and p of the hyper-prior distributions in Eqs. (3.9a) through (3.9d) were considered to be dimensionless because they were used to generate random numerical values for the parameters ($\mu_a, \sigma_a^2, \mu_b, \sigma_b^2$ and $\sigma_{\eta_i}^2$) of the prior distributions only. Once the values were generated, the corresponding units were assigned; for example, μ_a and σ_a were assigned the same units as a_i , which is %wt/yr^{bi}. Further note that the prior distributions of a_i ($i = 1, 2, \dots, m$) are independent and identical with a mean of μ_a and a standard deviation of σ_a ; therefore μ_a (σ_a) has the same numerical values for all a_i but different units for different defects.

The ILI data and the calibration parameters along with the hyper-parameters were input in OpenBUGS to evaluate the marginal posterior distributions of the parameters of the growth model using the MCMC simulation. The OpenBUGS code developed for the analysis is included in Appendix 3B.

Two MCMC chains of samples with two different sets of initial values were run, and a total of 35,000 samples were stored after applying a thinning interval of 20 in each chain for the model parameters. The generated sequences of parameters (i.e. a, b and t_o) associated with three selected defects (defects #1, #2 and #3) are shown in Figs. 3.4 through 3.6. The trace plots in these figures indicate a very good convergence of the

samples toward the marginal posterior distributions of the respective parameters. A burn-in period of 10,000 was selected and the remaining 50,000 (25,000 from each chain) samples were used to make statistical inferences of the model parameters.

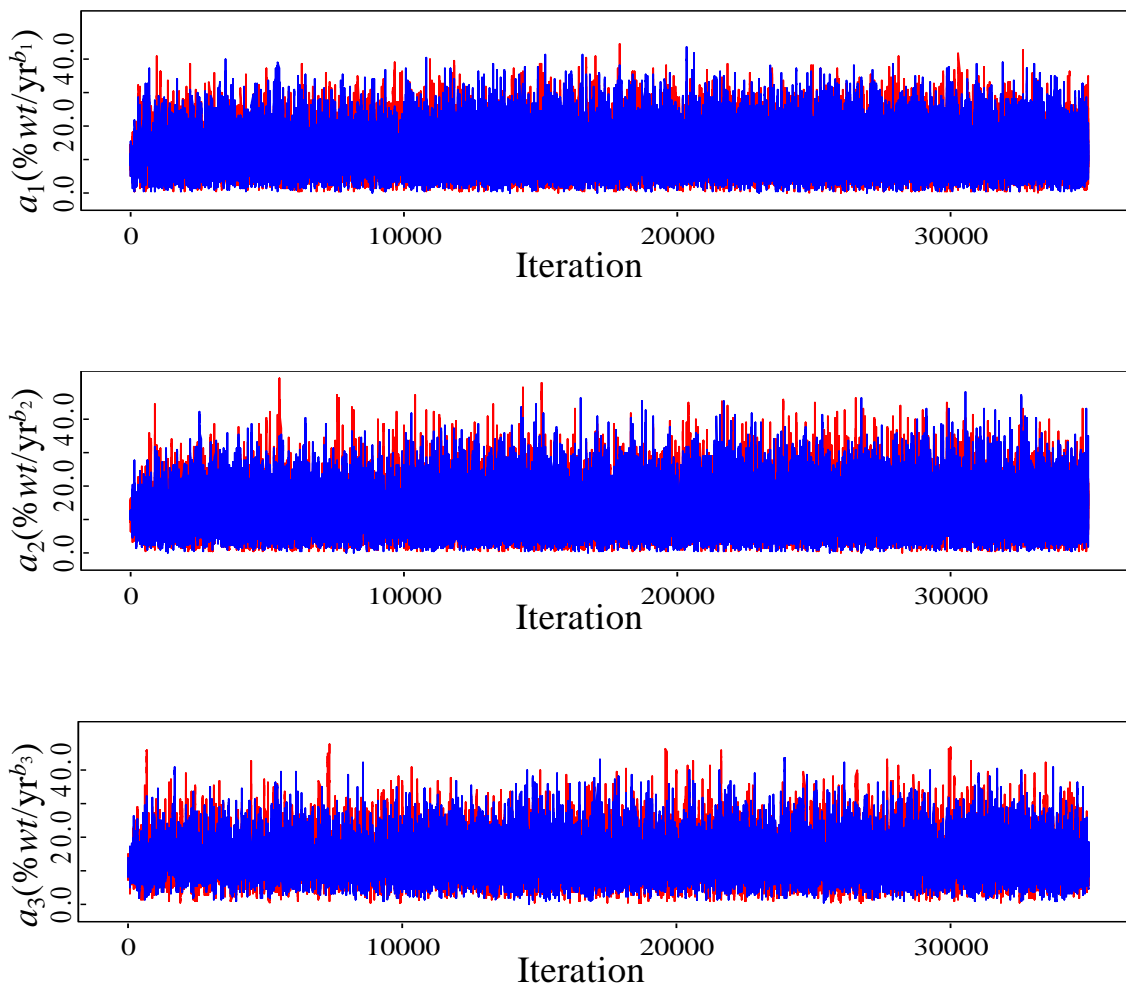


Figure 3.4 Trace plots of a_1 , a_2 and a_3

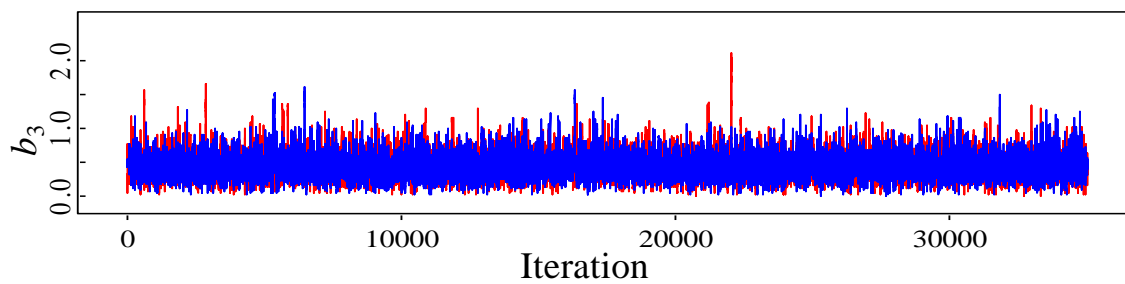
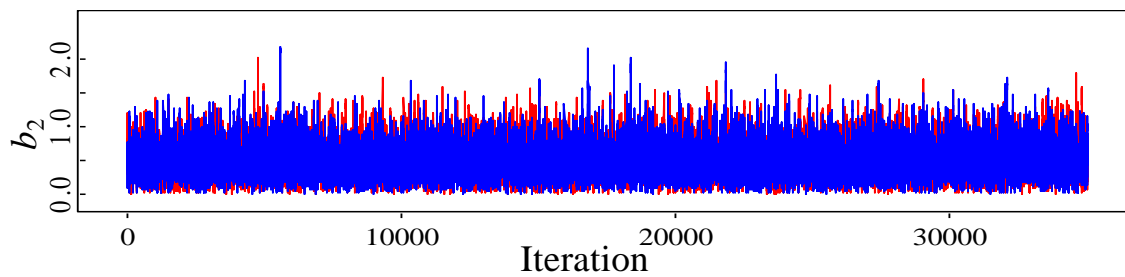
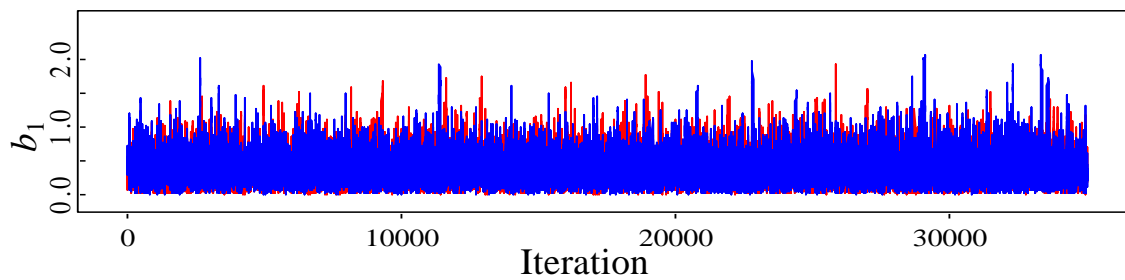
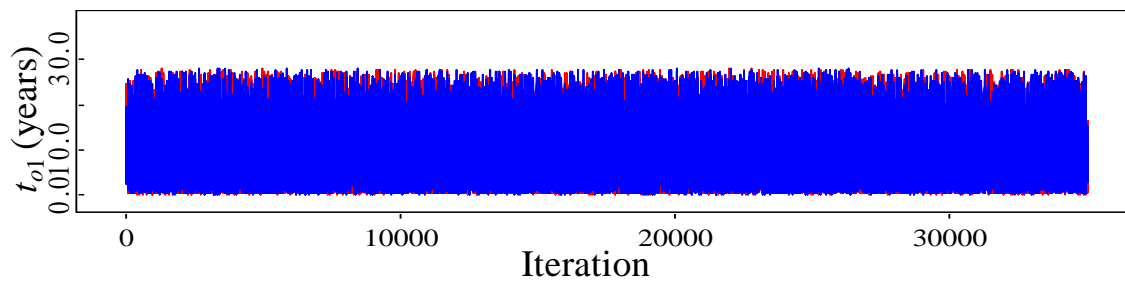


Figure 3.5 Trace plots of b_1 , b_2 and b_3



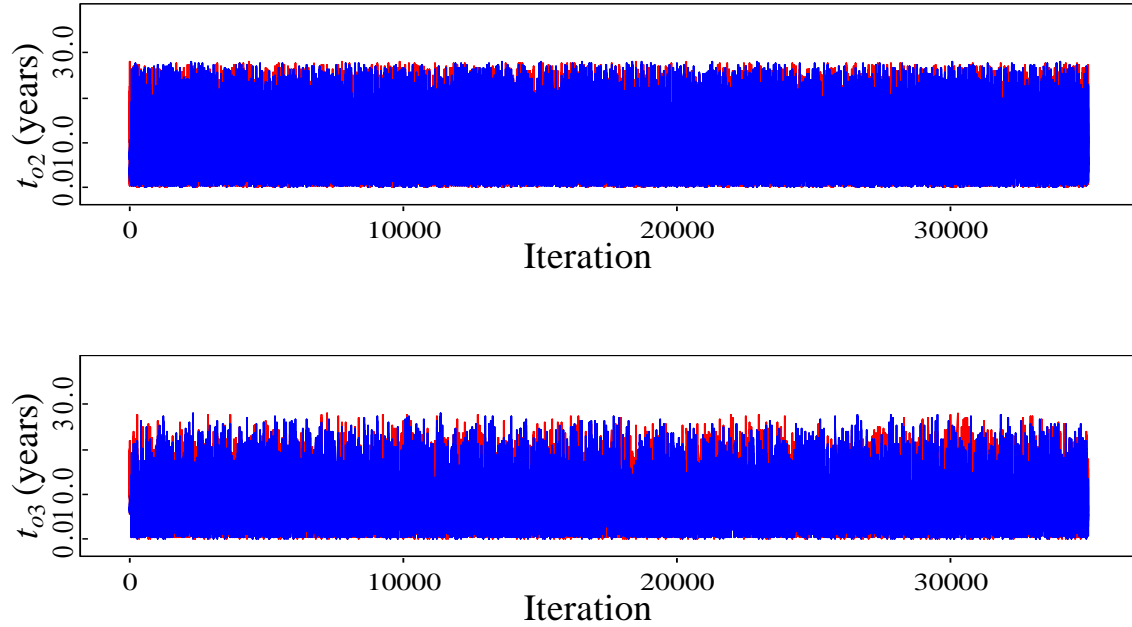


Figure 3.6 Trace plots of t_{o1} , t_{o2} and t_{o3}

The marginal posterior distributions of a , b , t_o and σ_η of all 62 defects are summarized using the so-called box plots shown in Figs. 3.7 through 3.10. The limits of each box represent the posterior quartiles (i.e. 25- and 75-percentile values) and the middle bar in the box represents the posterior median value. The two ends of the whisker lines indicate the 2.5 and 97.5 posterior percentiles. The continuous solid line indicates the overall mean of a given parameter (i.e. a , b , t_o and σ_η) for all 62 defects. The numbers beside each whisker line represents the defect ID. These figures indicate that the marginal posterior distributions of model parameters for most of the defects are skewed; therefore, the median values of the marginal posterior distributions were selected as the point estimates of the model parameters. Figure 3.8 suggests that the growths of these defects tend to follow the decelerating path because the 75-percentile values of all

b 's are less than unity. Figure 3.9 indicates that the overall mean of t_o for all 62 defects equals 13.1 years. This appears to support a commonly used assumption in the pipeline industry: the initiation time of a defect is half way between the time of installation and the time of the defect being first detected. However, it is unclear whether this mean value (13.1 years) was governed by the ILI data or by the prior information because the mean value of the prior distribution of t_{oi} is 14 years.

Although the prior distributions of a_i , b_i and t_{oi} for a given defect were assumed to be mutually independent, the analysis results indicate that the posterior distributions of these parameters are correlated. Based on the posterior samples it was found that for a given defect i , the model parameters a_i and b_i are negatively correlated with the corresponding correlation coefficient ranging from -0.75 to -0.85 for different defects; the parameters a_i and t_{oi} are weakly correlated with the corresponding correlation coefficient ranging from 0.1 to 0.3 for different defects, and there is negligible correlation between b_i and t_{oi} . Finally, it was observed that there is negligible correlation between $\sigma_{\eta_i}^2$ and a_i , b_i or t_{oi} ,

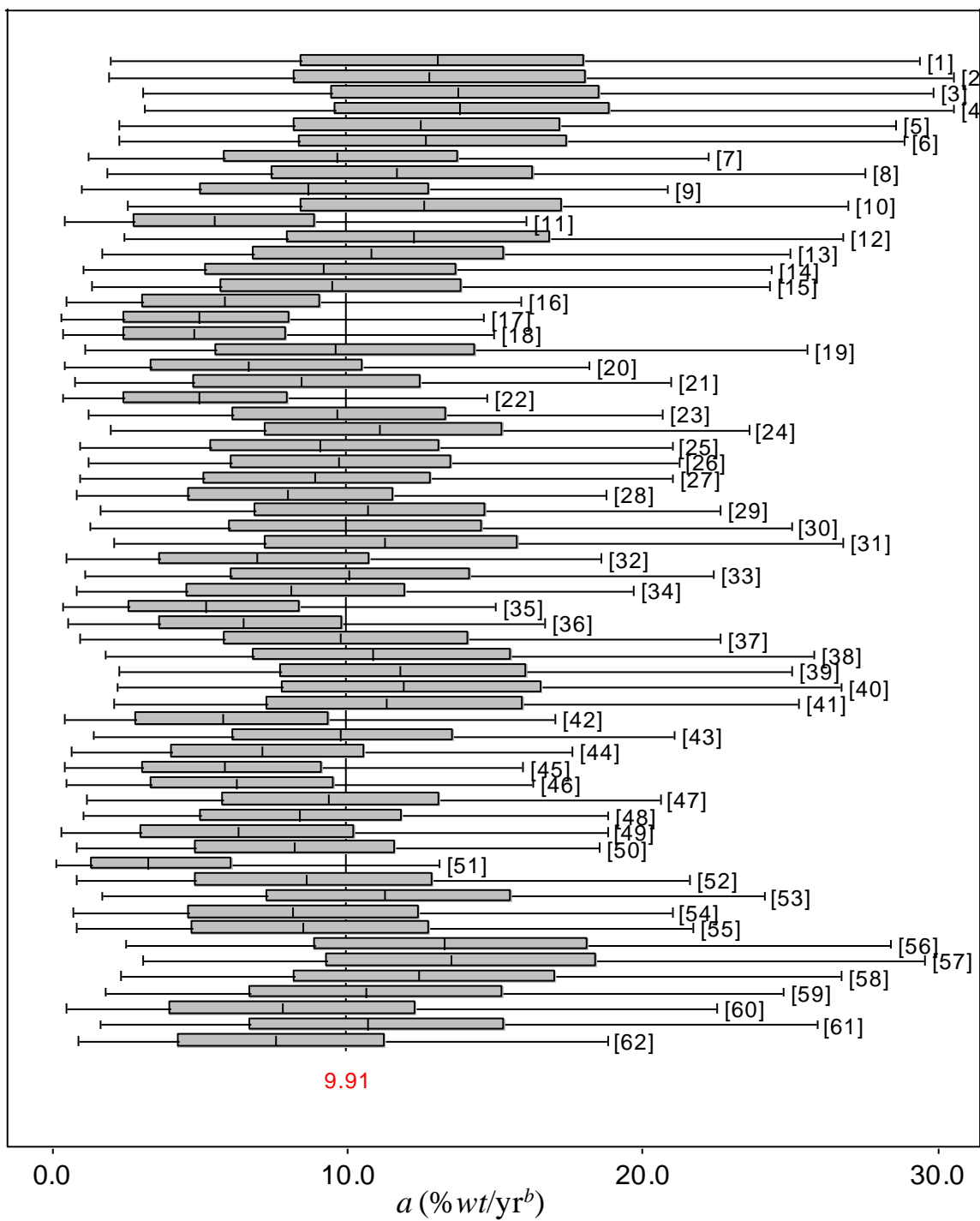


Figure 3.7 Box plot of the components of parameter vector a of Case 1

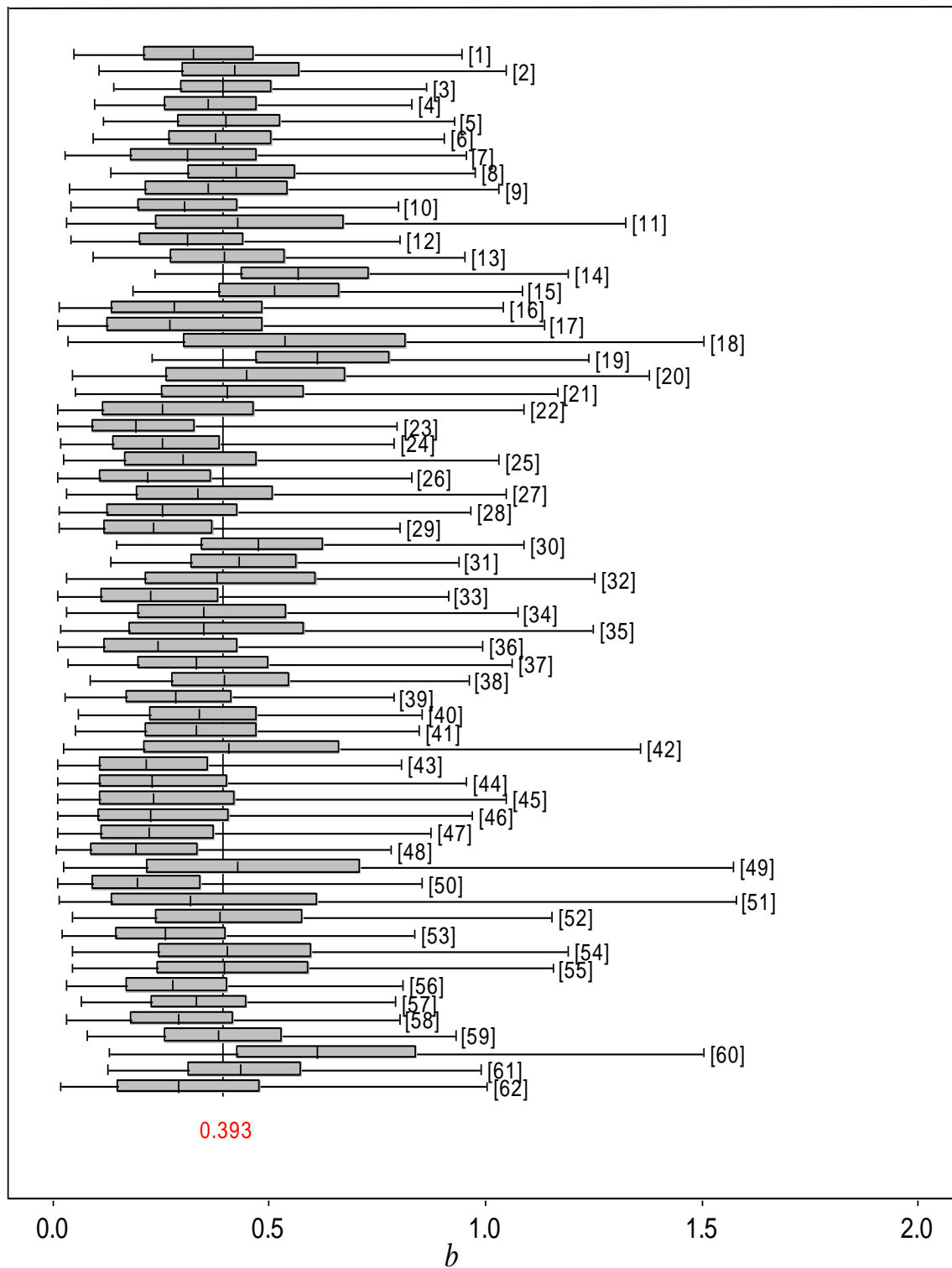


Figure 3.8 Box plot of the components of parameter vector b of Case 1

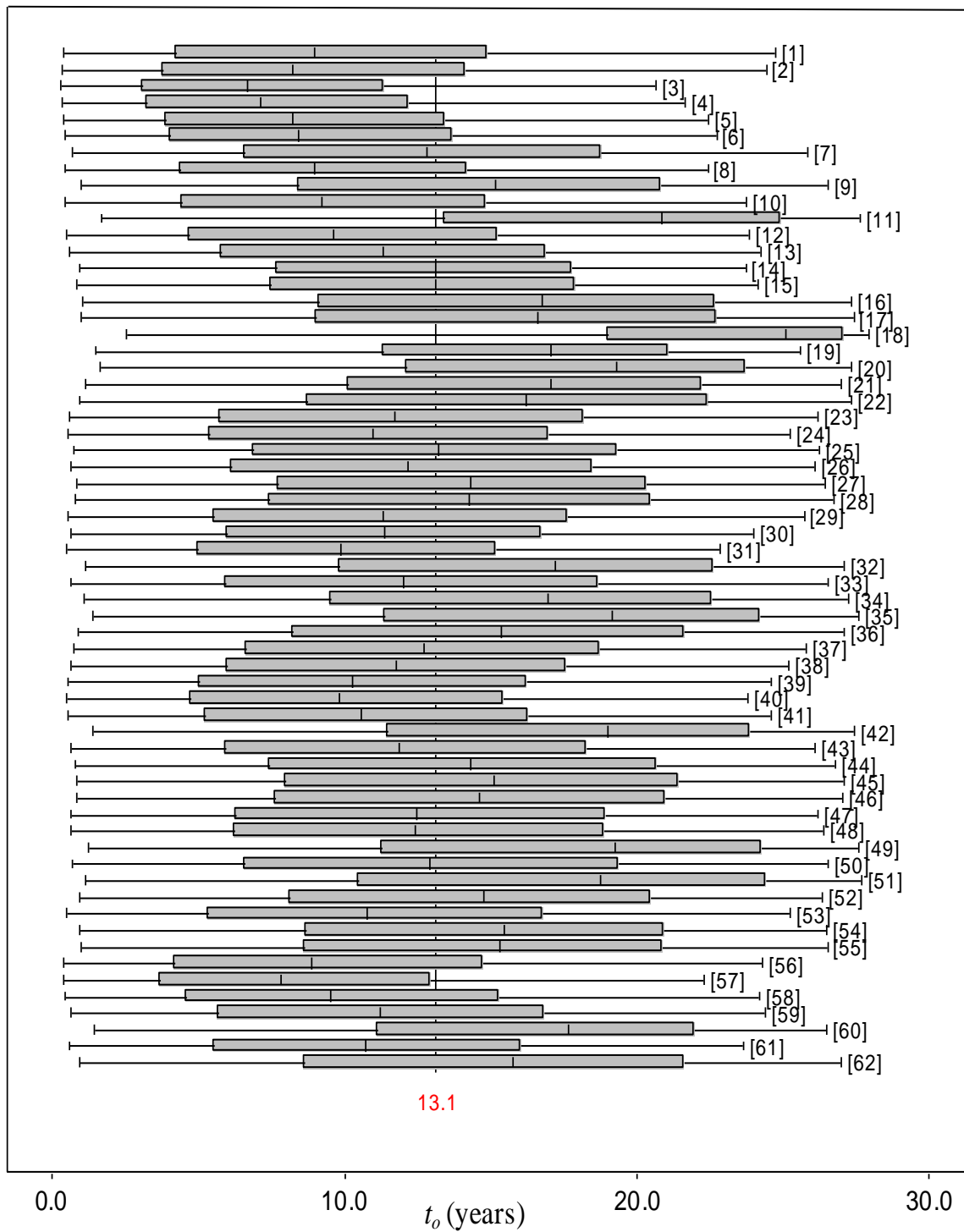


Figure 3.9 Box plot of the components of parameter vector t_o of Case 1

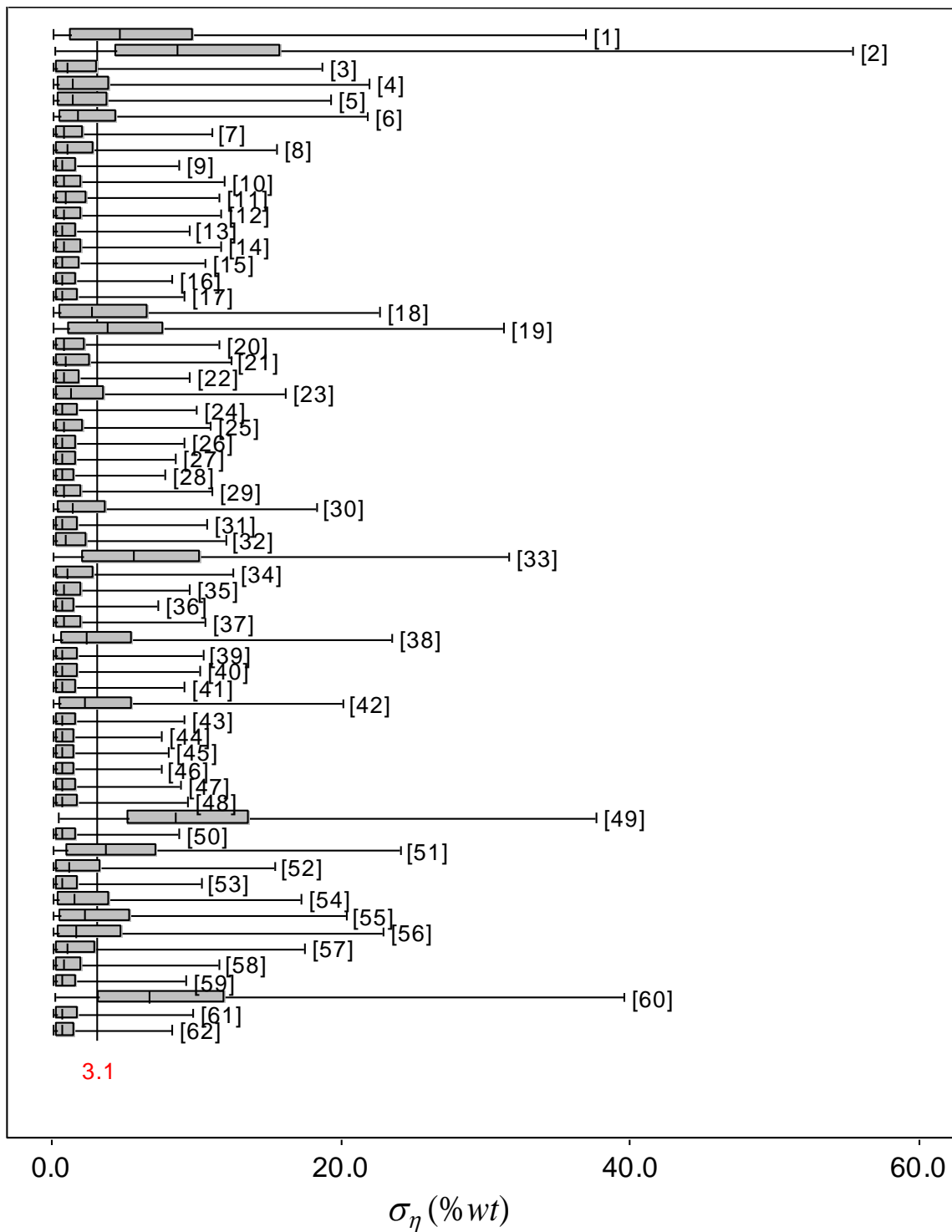


Figure 3.10 Box plot of the components of parameter vector σ_η of Case 1

The actual depths of the defects at different times were predicted by substituting the median values of the marginal posterior distributions of parameters a_i , b_i and t_{oi} into Eq. (3.7) and setting the model error to zero. The predicted depths in 2010 were compared with the actual depths obtained from field measurement. The comparison is shown in Fig. 3.11. Also shown in this figure are the 1:1 line (i.e. the line on which the predicted depth equals the field-measured depth) and the two bounding lines representing the predicted depth = field-measured depth $\pm 10\%$ wt. Figure 3.11 suggests that the proposed growth model can predict the actual depths of the defects reasonably well: approximately 89% (55) of the predicted depths fall within the two bounding lines.

The predicted growth paths from 2000 to 2010 for five arbitrarily selected defects, defects #3, #6, #7, #19 and #60, are depicted in Fig. 3.12. The growth path denoted by “prediction from medians” in Fig. 3.12 is obtained in the same way as the predicted depth shown in Fig. 3.11. The 10-, 50- and 90-percentile values as well as the mean values of the predicted depths, the ILLI-reported depths in 2000, 2004 and 2007, and the field-measured depths in 2010 are also shown in this figure. The three percentiles and mean of the predicted depths were obtained from samples of da_{ij} generated by substituting the MCMC samples of a_i , b_i and t_{oi} , and random samples of η_{ij} into Eq. (3.7). Note that the random samples of η_{ij} were generated from a normal distribution with a zero mean and a variance of $\sigma_{\eta_i}^2$, with the values of $\sigma_{\eta_i}^2$ obtained from MCMC.

Figure 3.12 indicates that the model predicts the actual depths of defects #3, #6, #19 and #60 fairly well. However, the predicted depth for defect #7 shows a substantial deviation from the actual depth. Further investigation revealed that defect #7 and several

other defects for which there are significant differences, say, greater than 10% *wt*, between the model predictions and actual depths in 2010 are either pinholes¹ or circumferential grooving² defects (Pipeline Operators Forum (POF) 2009). Consistent with the observation by Maes et al. (2008), it was observed that the ILI data tend to have large errors for these types of defects, which result in poor predictions given by the growth model.

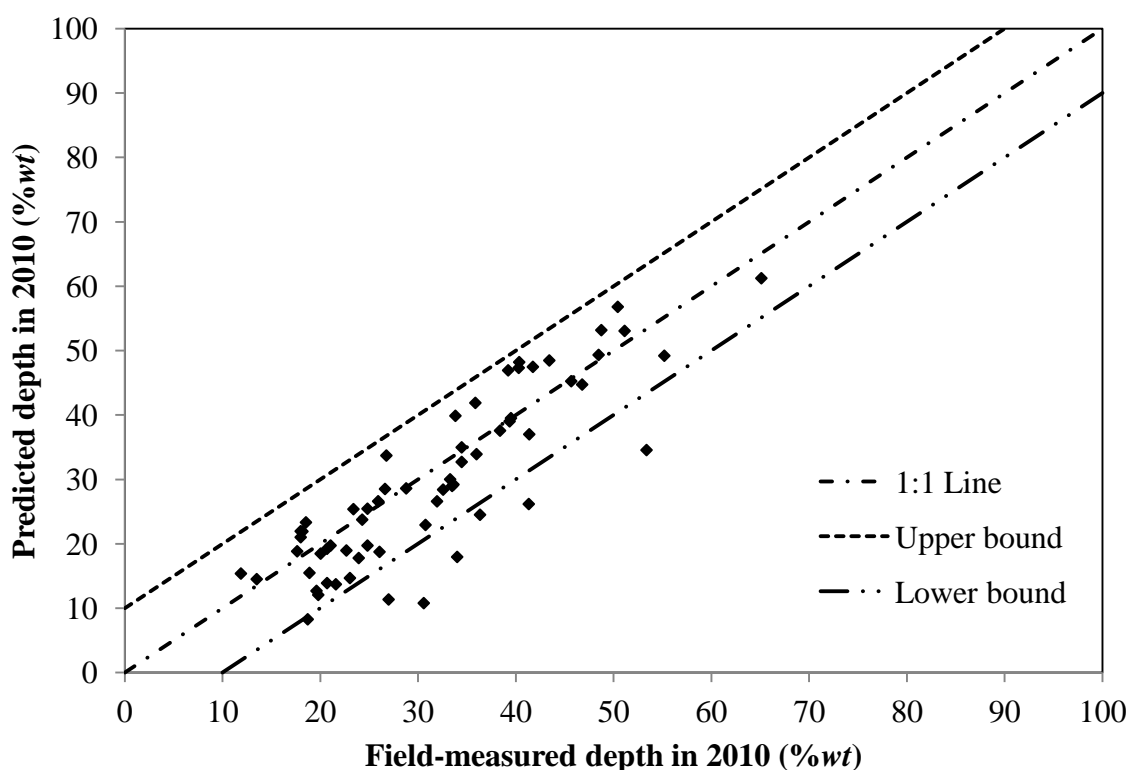
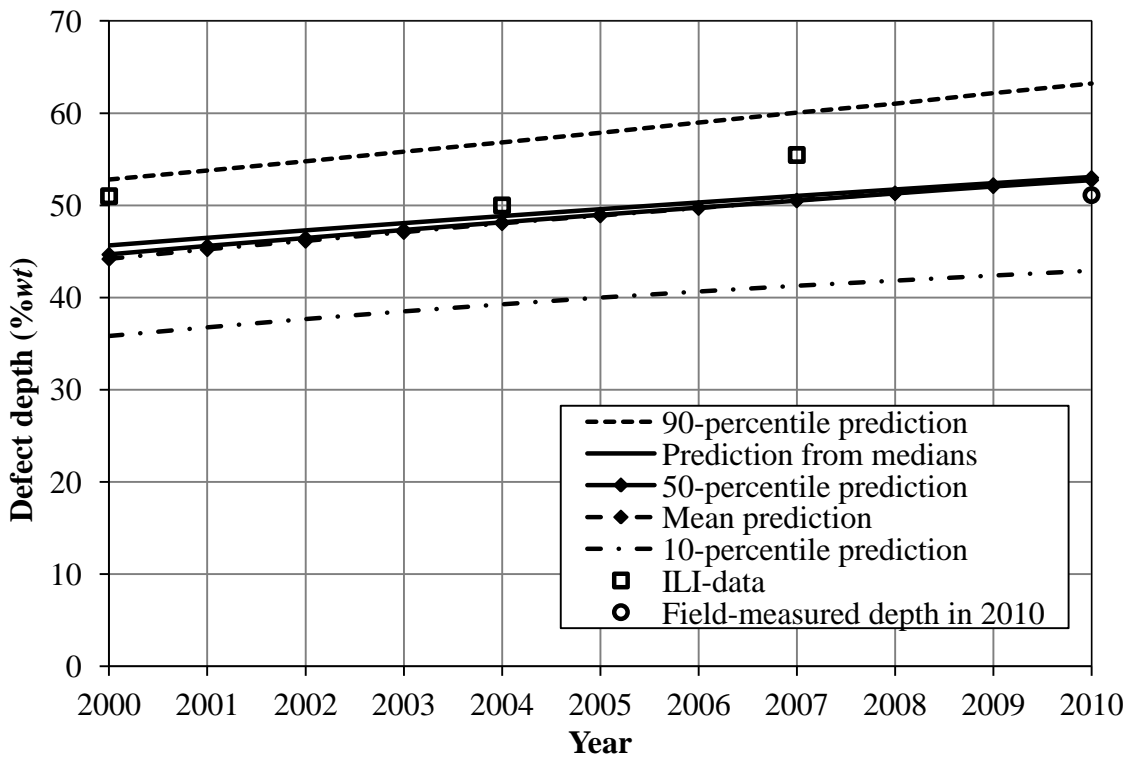


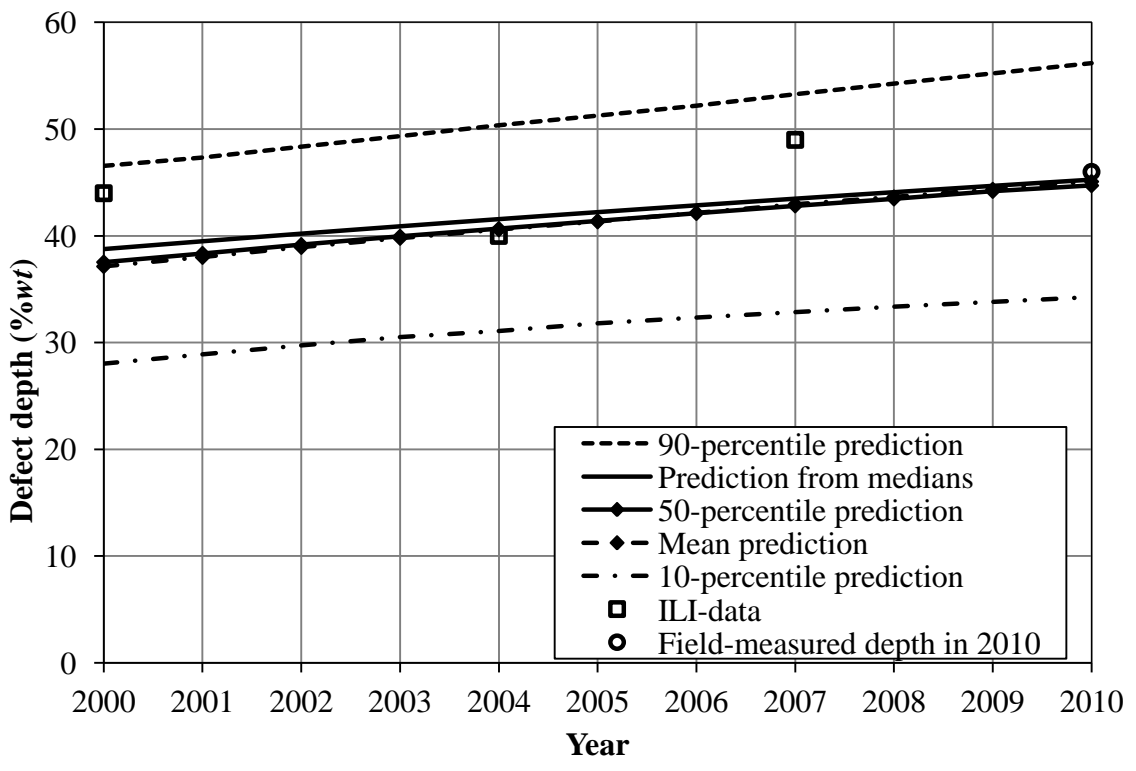
Figure 3.11 Comparison between the predicted and field-measured depths in 2010 for Case 1

¹ A pinhole is a corrosion defect with both length (in the longitudinal direction of pipeline) and width (in the circumferential direction of pipeline) less than A , where $A=10$ mm and wt for $wt < 10$ mm and $wt \geq 10$ mm, respectively.

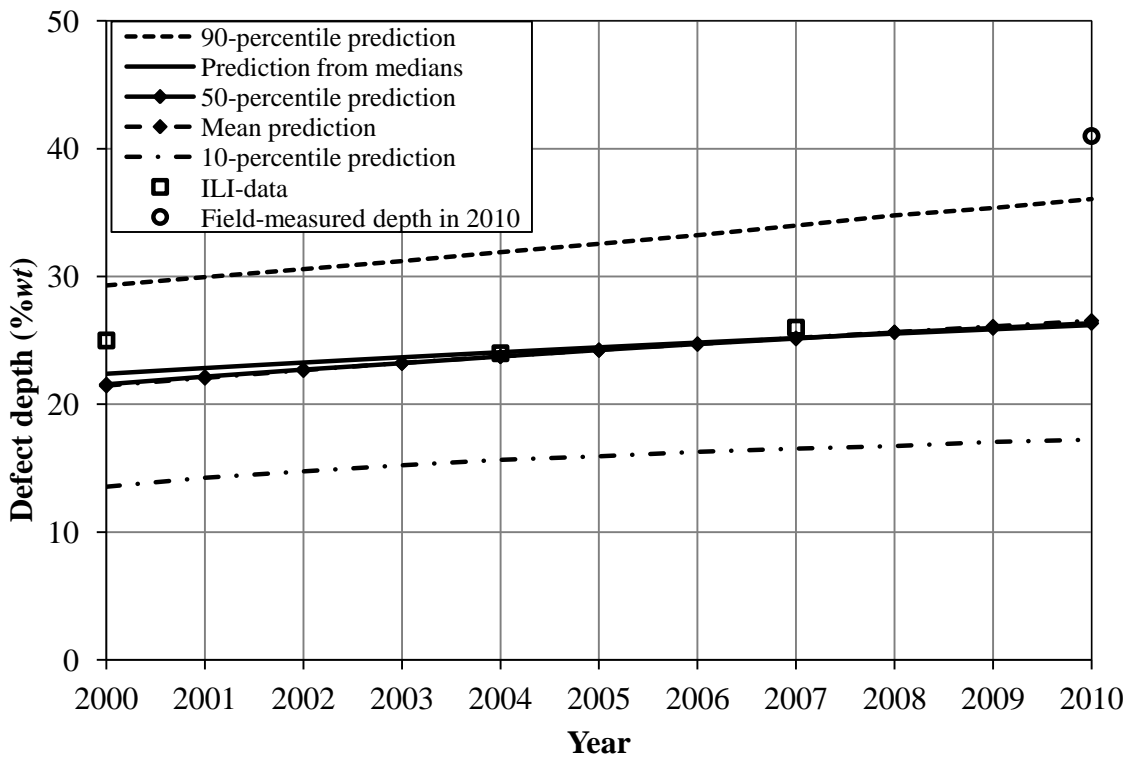
² A circumferential grooving defect has a length greater than or equal to A but less than $3A$ and a length-to-width ratio less than or equal to 0.5.



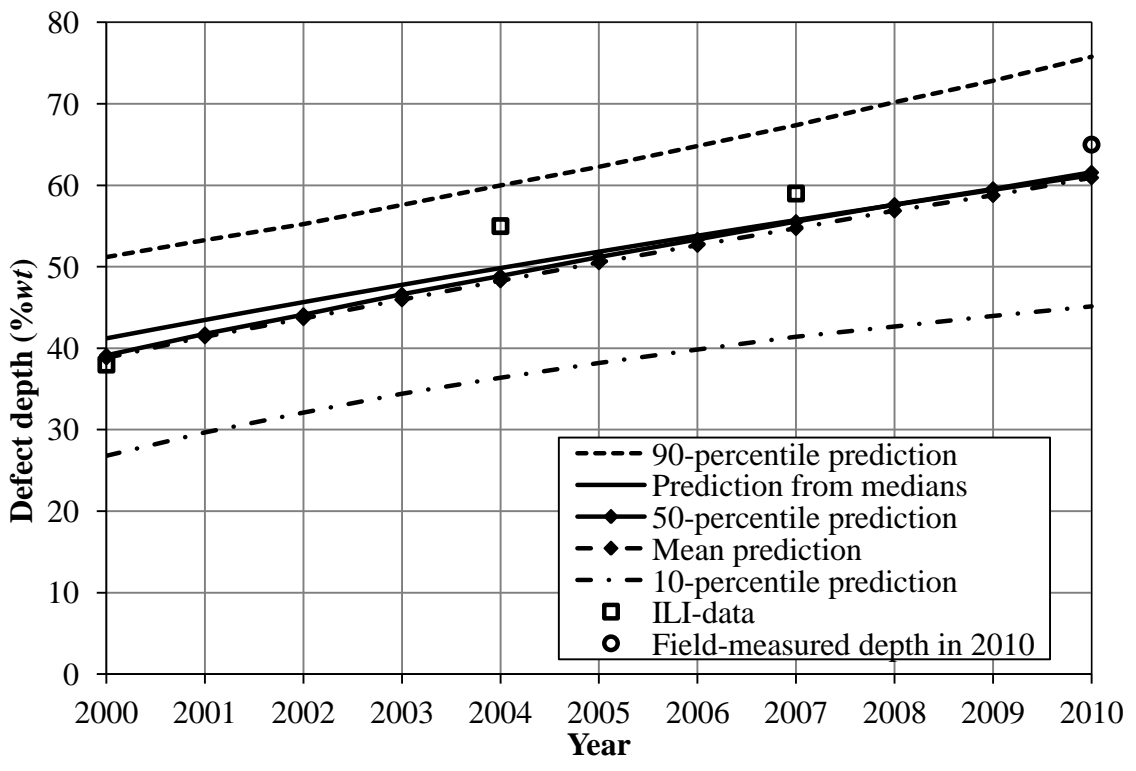
a) Defect #3



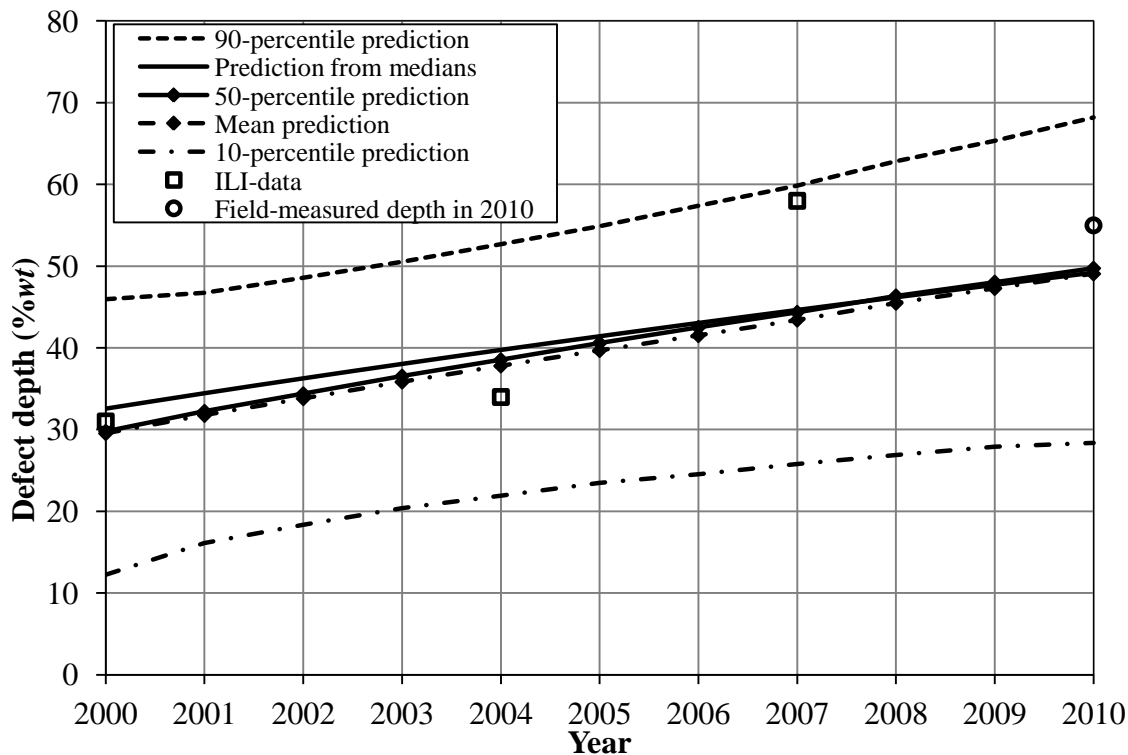
b) Defect #6



c) Defect #7



d) Defect #19



e) Defect #60

Figure 3.12 Predicted growth paths for defects #3, #6, #7, #19 and #60 on pipeline of Case 1

3.5.3 Case 2

In this case the proposed growth model was applied to the corrosion defects on the subject pipeline considered in Case 2 of Chapter 2. The corrosion defects on some pipe joints in this pipeline were excavated and field-measured in 2011. A total of 60 defects that were measured by the UT tool in the dig sites was identified in this study. Consistent with Case 1, the field-measured depths were assumed to be free of measurement error. These 60 defects were then manually matched with the corresponding defects included in the defect listings reported by ILIs conducted in 2004, 2007 and 2009. The apparent

growth pattern of these 60 defects as indicated by the ILI data is shown in Fig. 3.13. The ILI data were used to make statistical inferences of the parameters in the growth model. The actual depths of these defects in 2011 were predicted using the growth model, and then compared with the field-measured depths. Although an ILI was carried out on the pipeline in 2000, the corresponding data were not included in the analysis because only clustered defects were reported by the 2000 ILI tool, which cannot be matched with the individual defects identified by the dig report in 2011 or by the ILI tools used in 2004, 2007 and 2009. The calibration parameters of the ILI tools in 2004, 2007 and 2009 are as follows (see Tables 2.3 and 2.4 in Chapter 2): $\alpha_1 = -4.23$ (%wt), $\alpha_2 = -9.50$ (%wt), $\alpha_3 = -3.54$ (%wt), $\beta_1 = 0.89$, $\beta_2 = 0.91$, $\beta_3 = 1.0$, $\sigma_1 = 5.32$ (%wt), $\sigma_2 = 7.12$ (%wt), $\sigma_3 = 7.66$ (%wt), $\rho_{12} = 0.76$, $\rho_{13} = 0.77$ and $\rho_{23} = 0.71$, where the subscripts “1”, “2” and “3” indicate the ILI tools used in 2004, 2007 and 2009, respectively.

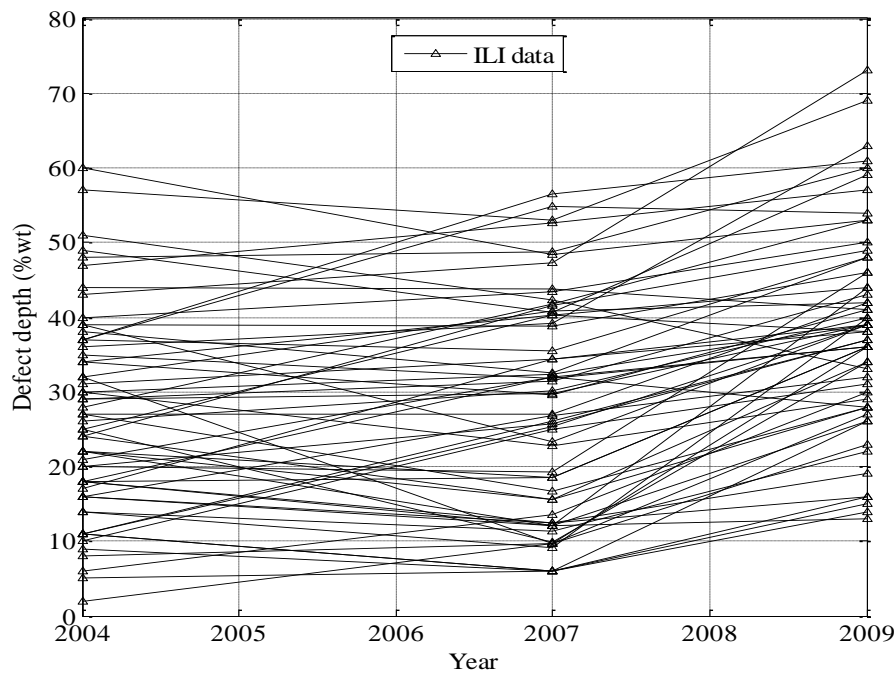


Figure 3.13 Apparent growth paths of the 60 corrosion defects indicated by the ILI data

The hyper-parameters (i.e. $c, d, e, f, g, h, k, l, o$ and p) of the prior distributions in this case were assigned the same values as those of the hyper-parameters in Case 1. Similar to Case 1, two chains were run simultaneously. A total of 35,000 samples was stored in each chain after applying the thinning interval of 20. After a burn-in period of 10,000, the remaining 25,000 samples from each chain (i.e. total sample size 50,000) were used to numerically evaluate the marginal posterior distributions of the parameters of the growth model. The corresponding OpenBUGS code used in the analysis is given in Appendix 3C.

The box plot of the marginal posterior distributions of a_i, b_i, t_{oi} and σ_{η_i} are shown in Figs. 3.14 through 3.17. Figure 3.15 indicates that the defects tend to grow at a decelerating rate in that the 75-percentile values of b for most of the defects are less than unity. Furthermore, Fig. 3.16 indicates that the overall mean of t_o for the 60 defects considered equals 14.9 years, which is close to the mean value of the prior distribution of t_o , i.e. the mid-point between the year of installation (1972) and the year at which the defects were first detected (2000). The median values of the marginal posterior distributions were considered as the point estimates of the parameters.

The MCMC samples indicated that for a given defect i , the posterior distributions of a_i and b_i are strongly correlated with the corresponding correlation coefficient ranging from -0.7 to -0.9 for different defects; a_i and t_{oi} are weakly correlated with the corresponding correlation coefficient ranging from 0.1 to 0.4 for different defects, and there is negligible correlation between b_i and t_{oi} for most of the defects. However, b_i and t_{oi} are somewhat correlated for a number of defects; for example, the correlation

coefficients between b and t_o for defects #6 and #9 were found to be 0.30 and 0.38, respectively. Finally, $\sigma_{\eta_i}^2$ is negligibly correlated with a_i , b_i or t_{oi} .

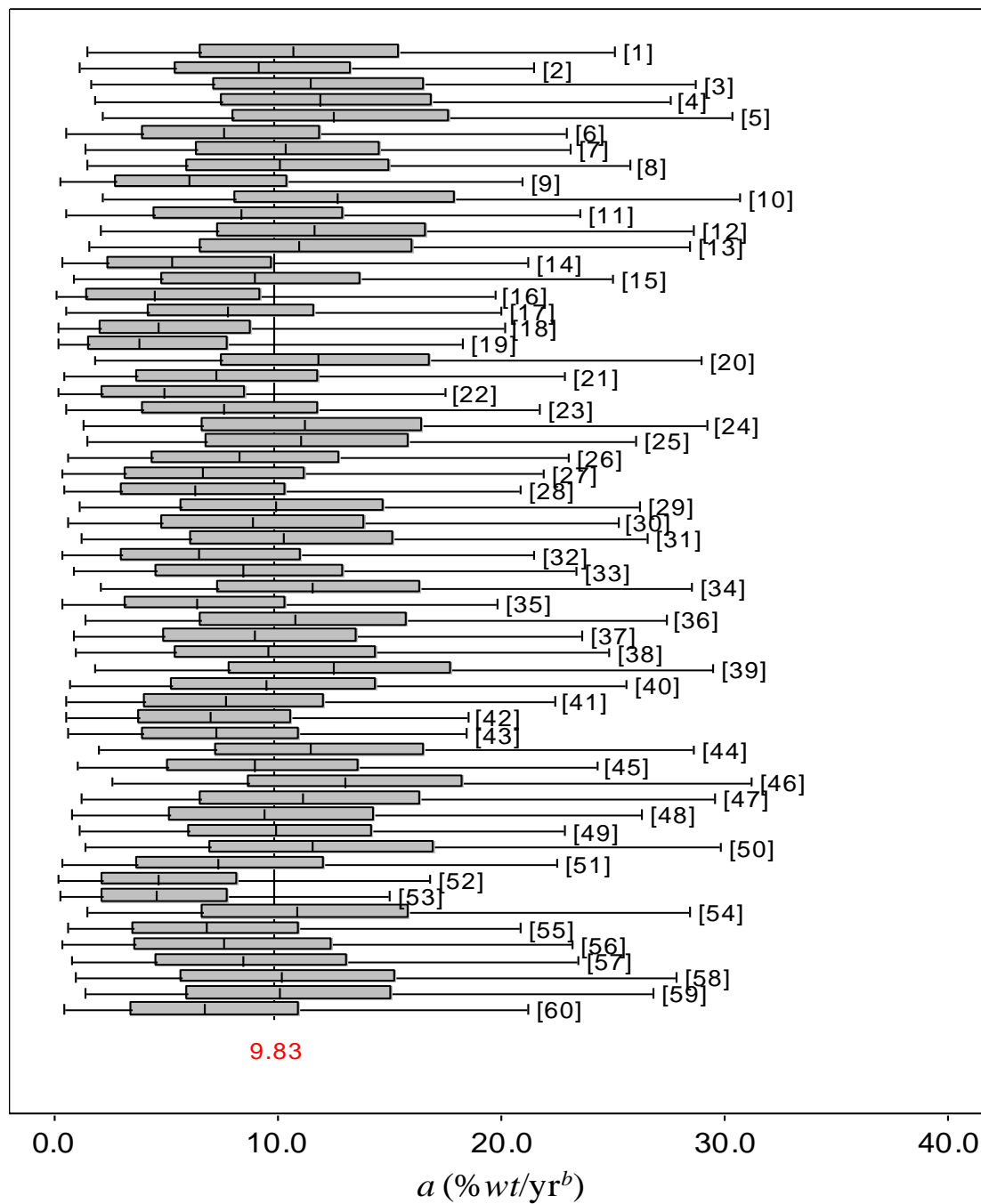


Figure 3.14 Box plot of the components of parameter vector a of Case 2

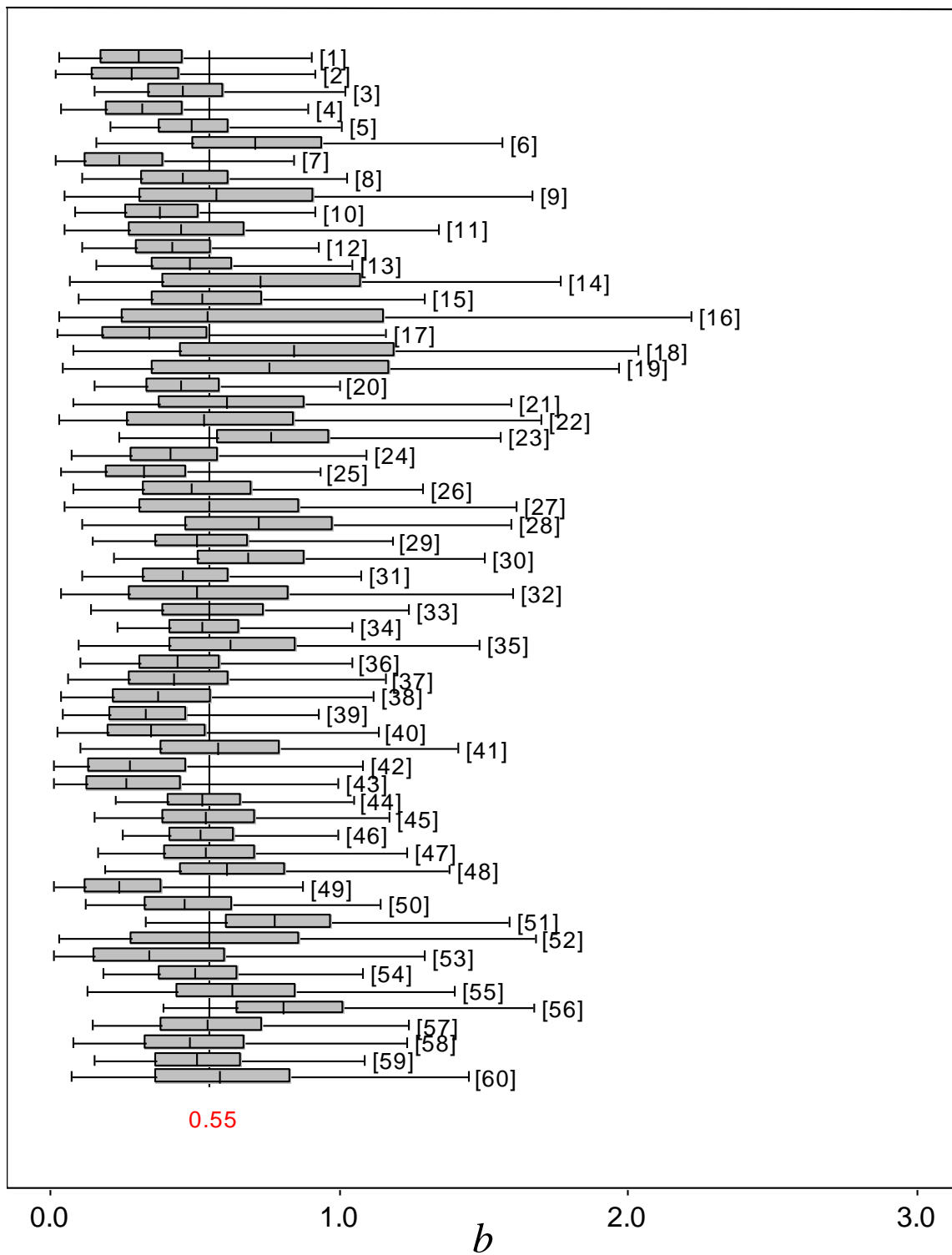


Figure 3.15 Box plot of the components of parameter vector \mathbf{b} of Case 2

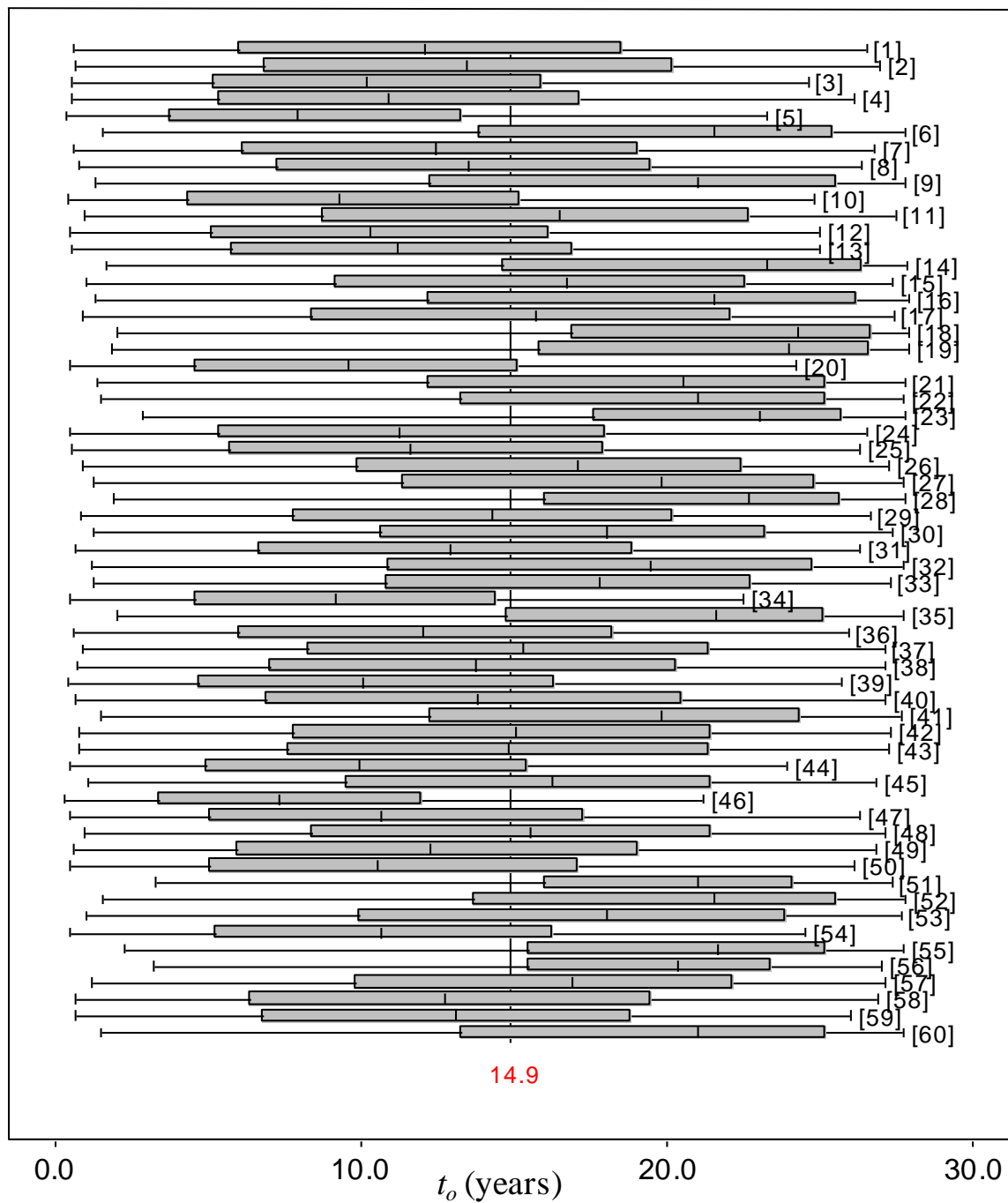


Figure 3.16 Box plot of the components of parameter vector t_o of Case 2

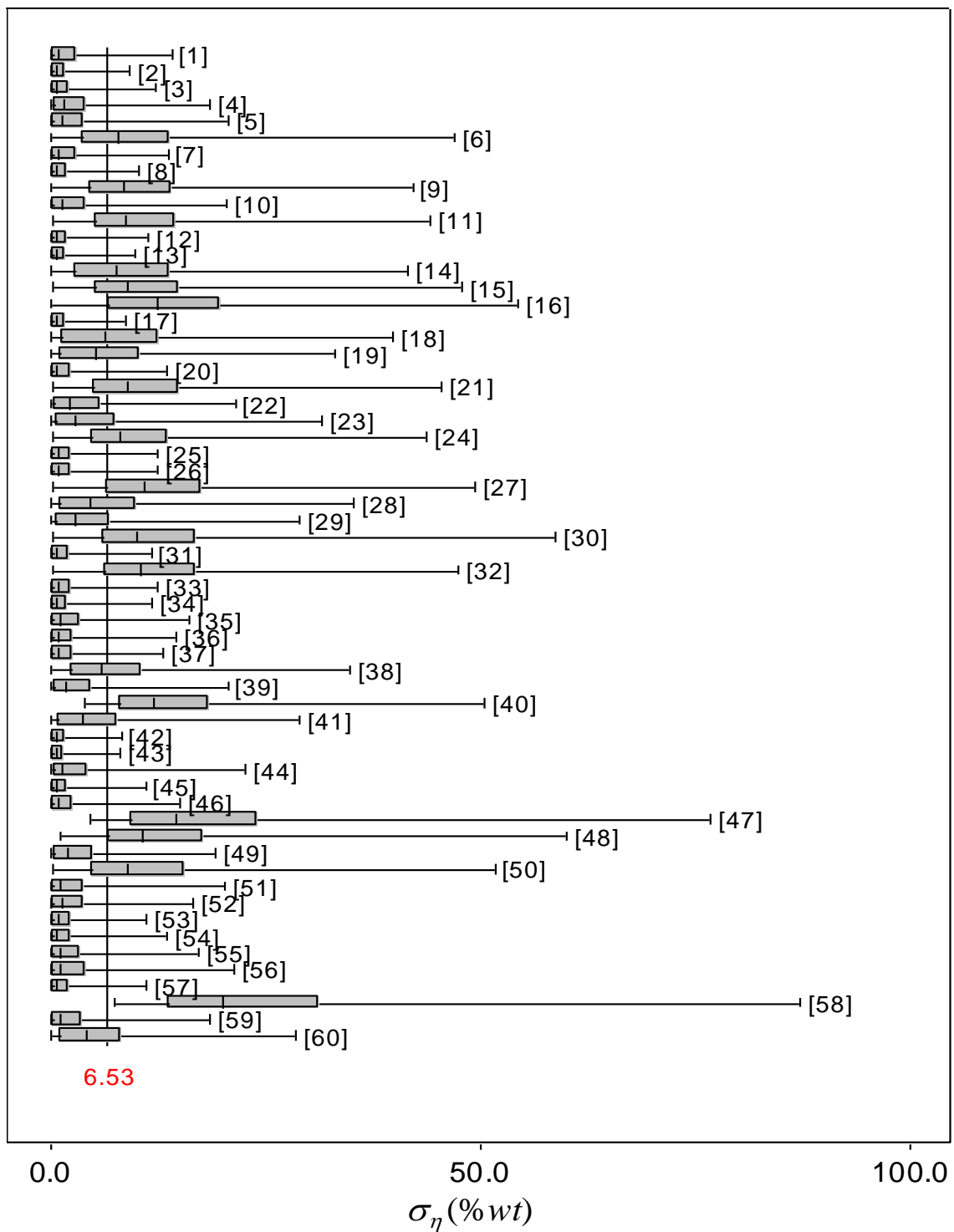


Figure 3.17 Box plot of the components of parameter vector σ_η of Case 2

Similar to Case 1, the median values of the marginal posterior distributions of a_i , b_i and t_{oi} were substituted into Eq. (3.7) (with the model error term set to zero) to predict the actual depths of the defects at different times. The comparison between the predicted and field-measured depths in 2011 along with the 1:1 line and the two bounding lines corresponding to field-measured depth $\pm 10\%wt$ is shown in Fig. 3.18. As shown in this figure, approximately 78% (47) of the predicted depths for the 60 defects fall within the two bounding lines.

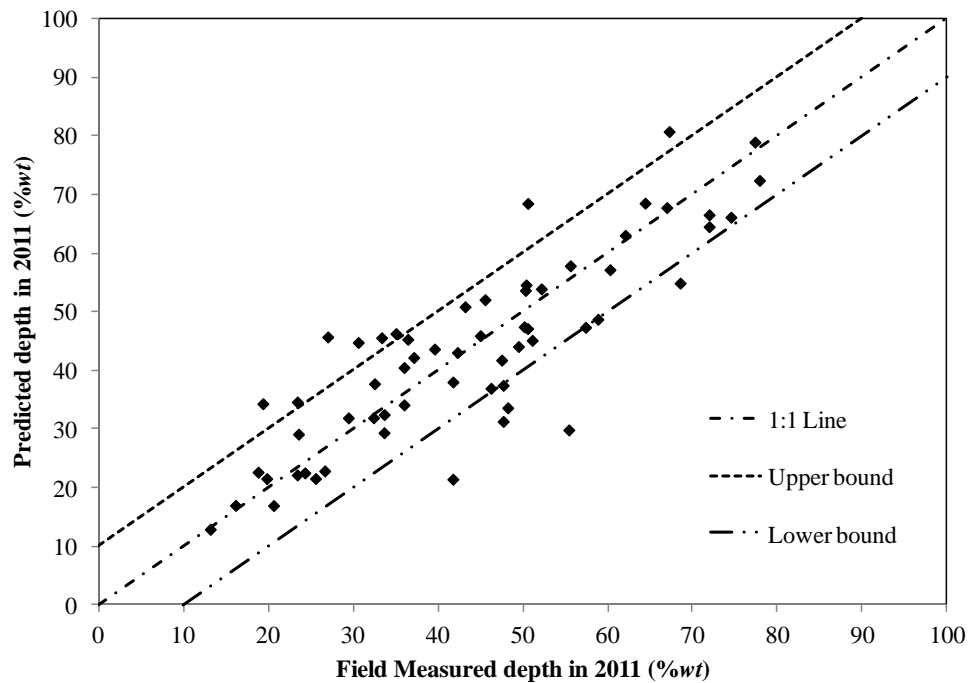
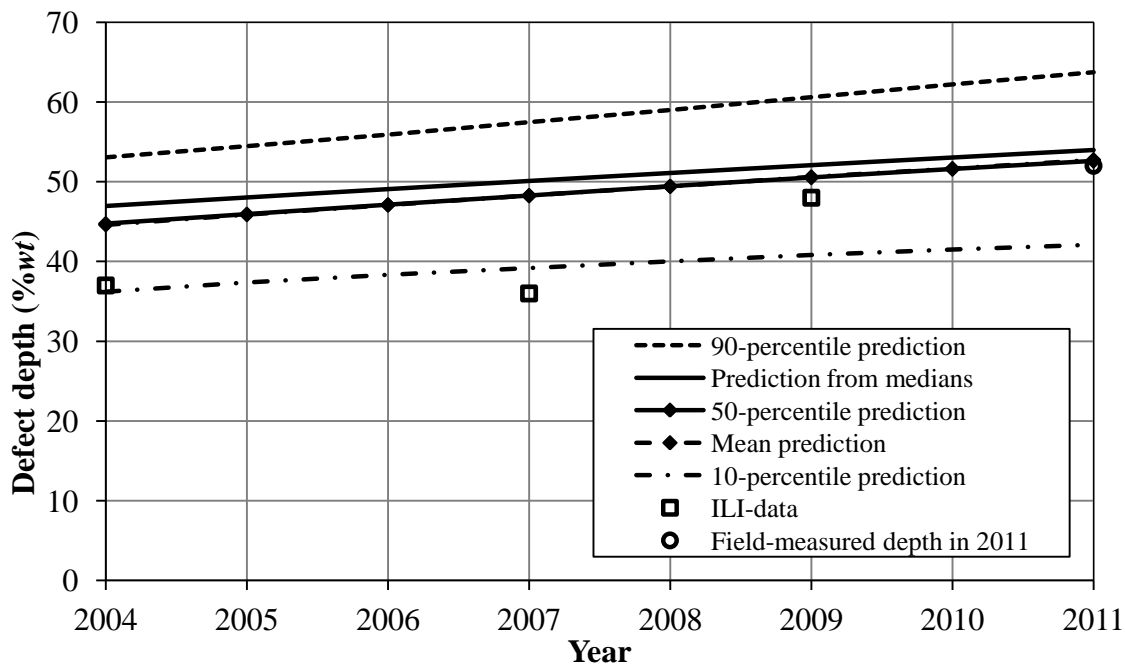


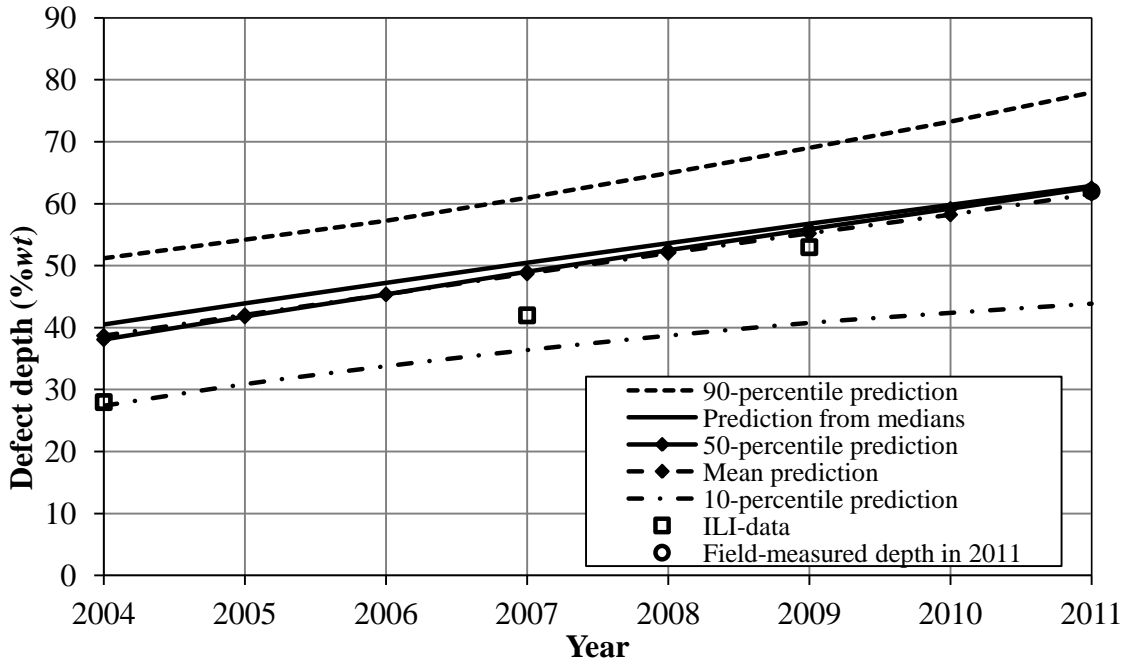
Figure 3.18 Comparison between the predicted and field-measured depths in 2011 for Case 2

The predicted growth paths, including the predictions from medians (obtained in the same way as the predicted depths shown in Fig. 3.18), the 10-, 50- and 90-percentile as well as mean predictions, the ILI data, and the corresponding field-measured depth in

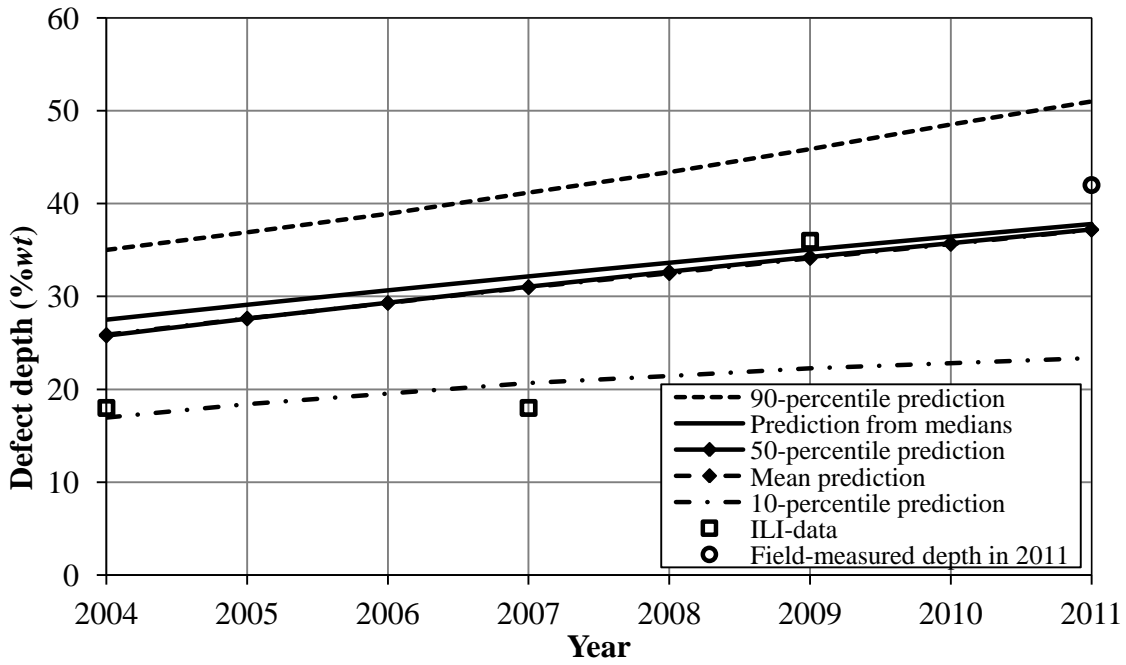
2011 for five selected defects (defects #13, #23, #35, #50 and #56) are shown in Fig. 3.19. This figure suggests that the prediction for defects #13, #23 and #35 is fairly good but the prediction for defects #50 and #56 deviates by about 12%wt from the corresponding field-measured depths. Unfortunately the defects located on this pipeline could not be classified according to the POF criteria because the length and width of these defects were not provided in the dig report. Therefore, it is unclear whether the poor predictions for some defects can be attributed to the large measurement errors of ILI data for certain types of defects (e.g. pinholes).



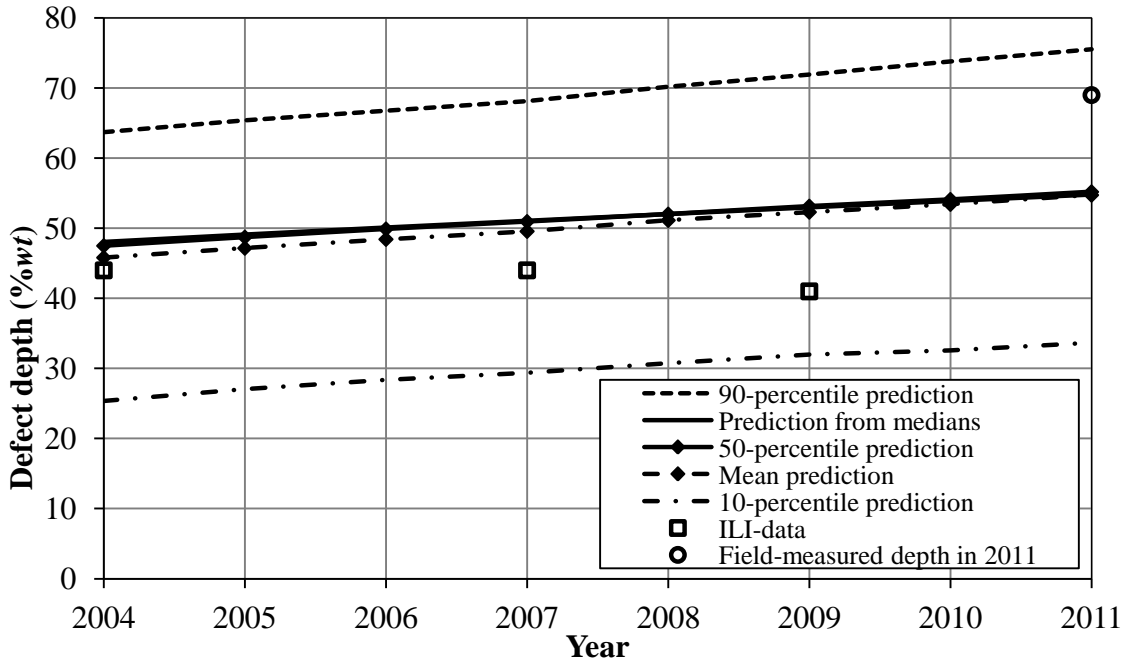
a) Defect #13



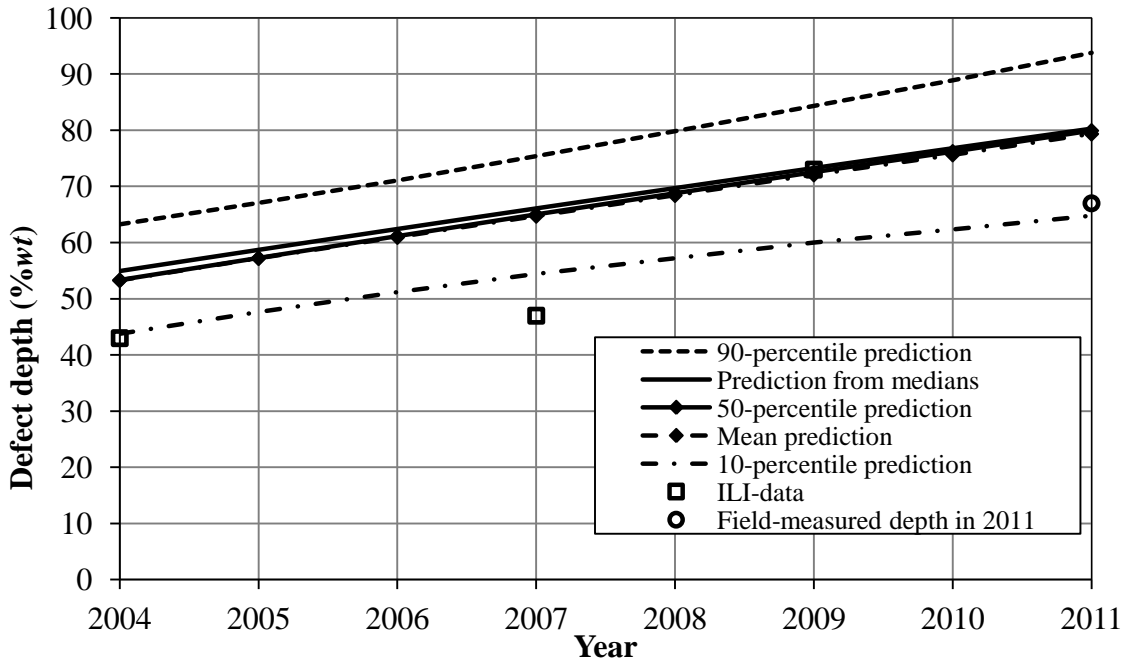
b) Defect #23



c) Defect #35



d) Defect #50



e) Defect #56

Figure 3.19 Predicted growth paths for defect #13, #23, #35, #50 and #56 on pipeline of Case 2

3.5.4 Effect of Correlation among the Random Scattering Measurement Errors

In Sections 3.5.2 and 3.5.3, the Bayesian updating of the corrosion growth models for Case 1 and Case 2 incorporated the partial correlations among the random scattering errors associated with different ILI tools. To investigate the impact of such correlations on the growth model, two additional scenarios, i.e. fully-correlated and independent scattering errors, were considered. The posterior distributions of the parameters of the growth models corresponding to these two scenarios were evaluated using OpenBUGS for Case 1 and Case 2. The median values of the marginal posterior distributions of a_i , b_i and t_{oi} were then substituted into Eq. (3.7) (with model error set to zero) to predict the depths of the defects at the times of the corresponding field measurements.

The comparison between the field-measured and predicted depths for the growth models considering partially-correlated (based on the calibration of the ILI tools), fully-correlated and independent random scattering errors are shown in Figs. 3.20 and 3.21 for the defects of Case 1 and Case 2, respectively. The results indicate that the percentages of predicted depths falling within $\pm 10\%$ of the field-measured depths are the same for the models with partially-correlated and fully-correlated random scattering errors for both Case 1 (89%) and Case 2 (78%). But this percentage decreases slightly for the model with independent random scattering errors: 84% and 75% of the predicted depths fall within the two bounding lines for Case 1 and Case 2, respectively.

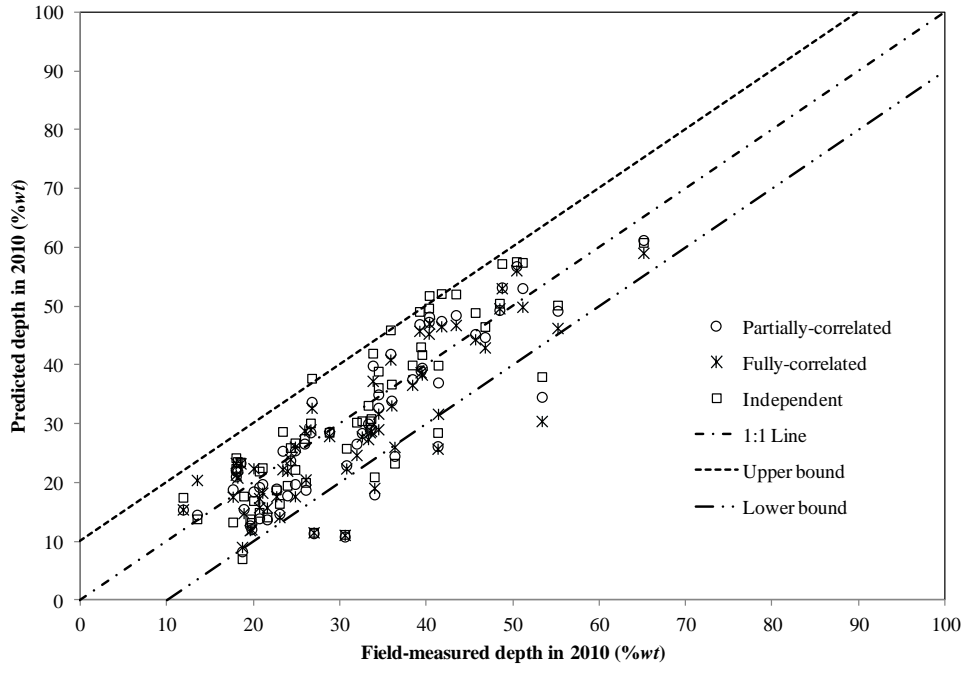


Figure 3.20 Comparison of the predicted depths from the models with partially-correlated, fully-correlated and independent random scattering errors with field-measured depths in 2010 for the corrosion defects in Case 1

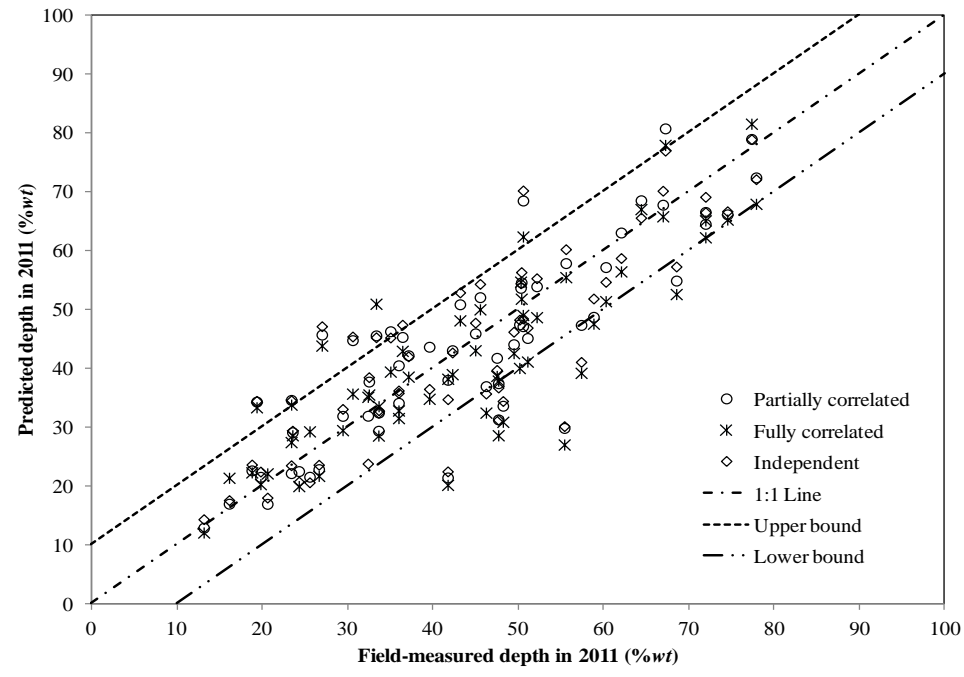


Figure 3.21 Comparison of the predicted depths from the models with partially-correlated, fully-correlated and independent random scattering errors with field-measured depths in 2011 for the corrosion defects in Case 2

Because the percentage of the predicted depths falling within the $\pm 10\% wt$ bounds does not vary significantly among the three models, the mean squared error of prediction (MSEP) (Bunke and Droge 1984; Harville and Jeske 1992; Wallach and Goffinet 1987) was selected as a metric to further evaluate the predictive ability of these models. The MSEP is given by

$$MSEP = \frac{1}{l} \sum_{i=1}^l (x_i - \hat{x}_i)^2 \quad (3.10)$$

where x denotes the actual value of a given parameter of interest; \hat{x} is the value of the parameter predicted from a certain model, and l is the sample size. The smaller is the MSEP, the better is the predictive ability of the corresponding model (van der Voet 1994).

Equation (3.10) was employed on the datasets of Case 1 and Case 2 to evaluate the MSEP's for the growth models with partially-correlated, fully-correlated and independent random scattering errors. The results are shown in Table 3.1. The model with the partially-correlated random scattering errors results in the smallest MSEP for both Case 1 and Case 2, although the differences in MSEP between different models for a given case are relatively small.

Table 3.1 MSEP's for the models with partially-correlated, fully-correlated and independent random scattering errors

Model	Case 1 (% wt) ²	Case 2 (% wt) ²
Partially-correlated	46.7	78.0
Fully-correlated	50.7	88.4
Independent	50.2	80.7

The statistical significance of the difference in MSEPs between different models can be examined using the hypothesis testing technique (Montgomery and Runger 2010). van der Voet (1994) proposed a randomization *t*-test for the hypothesis testing and used this approach to evaluate the predictive performance of different models by comparing the corresponding MSEPs. This approach was adopted in the current study to investigate the statistical significance levels of the differences in MSEPs corresponding to different growth models. As MSEP for the partially-correlated model is the smallest, comparisons were made with respect to MSEP of this model. The null and alternative hypotheses were specified as follows:

Null hypothesis, H_0 : $MSEP_1 = MESP_2$ ($MSEP_1 = MESP_3$)

Alternative hypothesis, H_a : $MSEP_1 < MESP_2$ ($MSEP_1 < MESP_3$)

where the subscripts “1”, “2” and “3” represent the models with partially-correlated, fully-correlated and independent random scattering errors, respectively. Note that the alternative hypothesis is a one-sided hypothesis.

The hypothesis testing procedure for comparing $MSEP_1$ and $MESP_2$ is outlined below (van der Voet 1994):

1. Calculate $\delta_i = (da_{1i} - \widehat{da}_{1i})^2 - (da_{2i} - \widehat{da}_{2i})^2$, $i = 1, 2, \dots, m$; where da and \widehat{da} are the actual (i.e. field-measured) and predicted depths, respectively;
2. compute $T_{obs} = \frac{1}{m} \sum_{i=1}^m \delta_i$;
3. for $j = 1, 2, \dots, s$, where $s = 2^m$ in theory but can be reasonably assumed to equal 199, do the following:

- a. randomly assign a positive or negative sign to δ_i ;
 - b. calculate $T_j = \frac{1}{m} \sum_{i=1}^m \delta_i$;
4. sort the vector $\mathbf{T} = [T_j, T_{obs}]$ in ascending order and find the rank of T_{obs} , say k ,
and
 5. compute the p -value as $k/(s+1)$.

The p -values obtained for the datasets of Case 1 and Case 2 are shown in Table 3.2. In this study, the specified significance level was set equal to 10% (Montgomery and Runger 2010) for the null hypothesis. The results in Table 3.2 suggest that the differences in MSEP's of the models with partially-correlated and independent random scattering errors are statistically insignificant for both Case 1 and Case 2. On the other hand, the difference in MESP's of the models with the partially-correlated and fully-correlated random scattering errors is statistically significant for Case 2. These results suggest that it is more reasonable to assume the random scattering errors of different ILI tools to be mutually independent in the corrosion growth modeling than to assume the scattering errors to be fully-correlated, if the partial correlations among the scattering errors of different tools are not quantified.

Table 3.2 p -values of the null hypothesis, $H_0: MSEP_1 = MESP_2$ ($MSEP_1 = MESP_3$) and alternative hypothesis $H_a: MSEP_1 < MESP_2$ ($MSEP_1 < MESP_3$)

Model	Case 1	Case 2
1 (Partially-correlated)	-	-
2 (Fully-correlated)	0.15	0.05
3 (Independent)	0.18	0.28

3.6 Comparison with Industry Practice

In practice, the depths reported by two ILI runs (typically successive) are often used to calculate a growth rate for a given defect (Coleman and Miller 2010; Fenyvesi and Dumalski 2005; Huysse and Roodselaar 2010; Nessim et al. 2008). To take into account the systematic measurement errors of the ILI tools, i.e. the constant and non-constant biases of the measurement error (see Eq. (3.4)), the growth rate for defect i , r_i , is estimated as follows:

$$r_i = \frac{\frac{1}{\beta_2}(dm_{i2} - \alpha_2) - \frac{1}{\beta_1}(dm_{i1} - \alpha_1)}{t_2 - t_1} \geq 0 \quad (3.11)$$

where dm_{i1} and dm_{i2} are the depths of the i^{th} defect reported by the ILI tools at time t_1 and t_2 , respectively, and α_1 (α_2) and β_1 (β_2) are the constant and non-constant biases associated with the ILI tool used at time t_1 (t_2), respectively. Because the actual depth of a defect cannot decrease, a lower bound of zero is set for the calculated growth rate in Eq. (3.11). The growth rate obtained from Eq. (3.11) is then used to predict the depth of the defect in the future as follows, assuming the defect to follow a linear growth path:

$$d_{i, t_2 + \Delta t} = \frac{1}{\beta_2}(dm_{i2} - \alpha_2) + r_i \Delta t \quad (3.12)$$

where $d_{i, t_2 + \Delta t}$ is the predicted depth of defect i at a given time in the future, i.e. $t_2 + \Delta t$.

The corrosion growth rates of the defects considered in Case 1 and Case 2 were calculated using Eq. (3.11) based on the two most recent successive ILI datasets respectively, i.e. the 2004 and 2007 datasets in Case 1 and the 2007 and 2009 datasets in Case 2. The calculated growth rates were then substituted into Eq. (3.12) to predict the

depths of the defects in 2010 for Case 1, and the depths of the defects in 2011 for Case 2. The predicted depths are compared with the corresponding field-measured depths in Figs. 3.22 and 3.23 for Case 1 and 2, respectively. Figure 3.22 indicates that only about 76% of the predicted depths fall within the $\pm 10\%wt$ bounding lines, compared with 89% of the predicted depths falling within the same bounding lines in the case of the Bayesian power-law growth model proposed in this study (see Fig. 3.11). The prediction based on the industry practice is also poor for Case 2 as indicated in Fig. 3.23: only 65% of the predicted depths fall within the $\pm 10\%wt$ bounding lines compared with 78% of the predictions falling within the same bounding lines based on the power-law growth model (see Fig. 3.18).

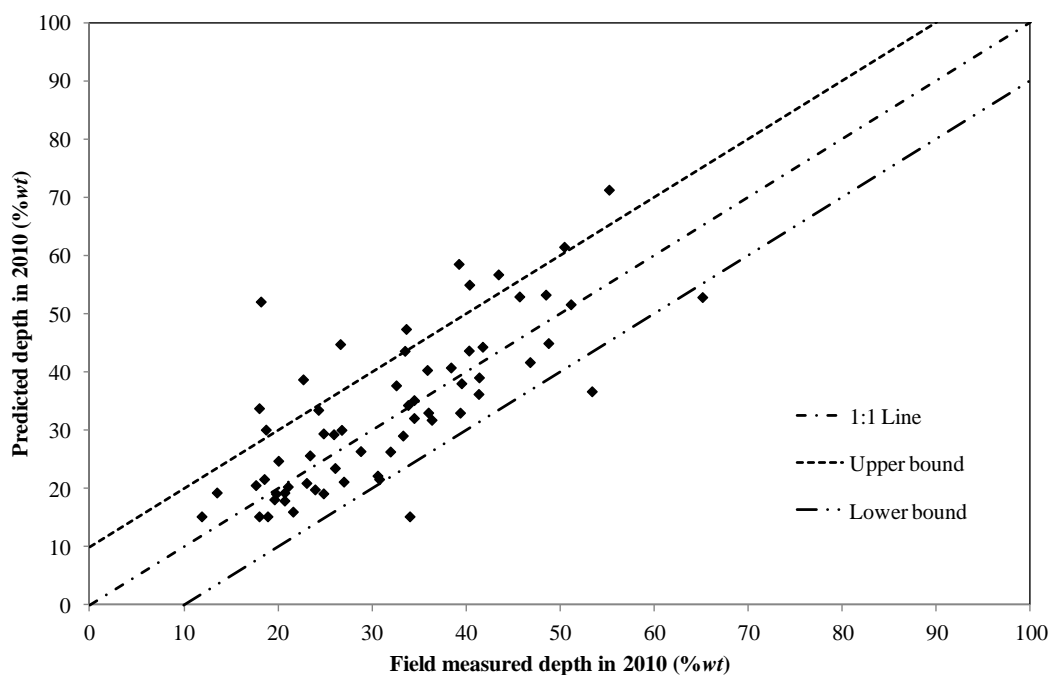


Figure 3.22 Comparison between the predicted depths from the linear growth model and field-measured depths in 2010 for the corrosion defects in Case 1

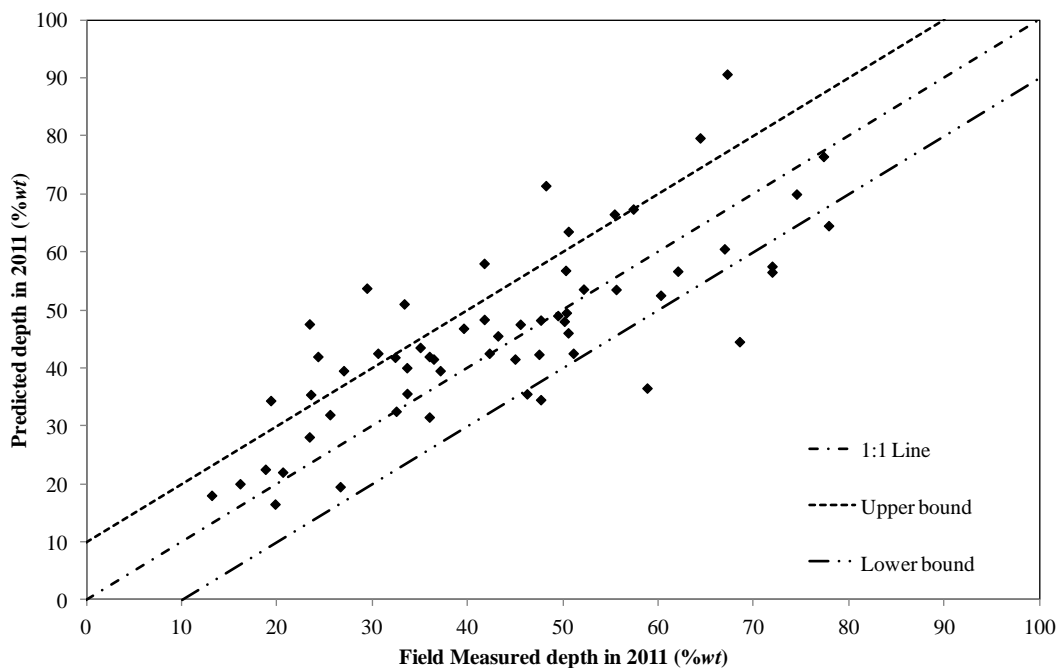


Figure 3.23 Comparison between the predicted depths from the linear growth model and field-measured depths in 2011 for the corrosion defects in Case 2

3.7 Conclusion

This chapter describes a Bayesian model to characterize the growth of the depth of individual metal-loss corrosion defect on underground energy pipelines. The depth of an active corrosion defect was assumed to follow a power-law function of time; the parameters of the growth model were evaluated using the hierarchical Bayesian method based on data obtained from multiple in-line inspections for a given pipeline. The measurement errors associated with the ILI data and potential correlations between the random scattering measurement errors associated with different tools were accounted for in the formulation of the model. The Markov Chain Monte Carlo (MCMC) simulation

was employed to carry out the Bayesian updating and to make statistical inferences of the model parameters.

The application of the proposed model was demonstrated in two case studies that involve two underground natural gas pipelines currently in service. The parameters of the growth models were developed for a relatively large number of external corrosion defects (62 and 60 defects in Cases 1 and 2, respectively). The defect depths predicted from the growth models were compared with the field-measured depths for these sets of defects, where the field-measured depths were assumed to be free of measurement errors and equal the corresponding actual depths. The results suggest that the proposed model is able to predict the corrosion growth with reasonable accuracy; for example, 89% and 78% of the predictions falling within the bounds of actual depth $\pm 10\%$ *wt* in Case 1 and 2, respectively. The prediction was found to be relatively poor for pinhole and circumferential grooving type defects due to the large measurement errors associated with the ILI data for these types of defects.

The effect of the correlation between the random scattering measurement errors associated with different ILI tools was investigated by comparing the mean squared errors of prediction (MSEP) of the growth models with partially-correlated, fully-correlated and independent scattering errors. The results indicate that the predictive accuracy is higher for the model with partially-correlated random scattering errors as compared to the models with fully-correlated and independent random scattering errors. Furthermore, the difference in MESP of the models with fully-correlated and partially-correlated scattering errors is statistically significant for Case 2, whereas the difference in

MESPs of the models with independent and partially-correlated scattering errors is statistically insignificant for both Case 1 and Case 2.

The proposed Bayesian hierarchical power-law growth model was compared with the linear growth model that is commonly used in the pipeline industry. The results suggest that the proposed model is more accurate than the linear growth model. For instance, 89% of the predicted depths fall within the $\pm 10\%$ bounding lines based on the power-law growth model, compared with about 76% of the predicted depths falling within the same bounding lines based on the linear growth model for the 62 defects considered in Case 1.

The proposed growth model is able to incorporate the accumulated ILI data as well as the measurement uncertainties associated with these data to predict the growth path of individual corrosion defect on pipelines and quantify the uncertainty associated with the growth path. The model will facilitate the pipeline corrosion management program in terms of reducing the number of unnecessary mitigation actions while maintaining the structural integrity of the pipeline to an acceptable level.

References

Achterbosch, G. G. J., and Grzelak, L. A., 2006. Determination of the Corrosion Rate of a MIC Influenced Pipeline Using Four Consecutive Pig Runs. *Proceedings of International Pipeline Conference (IPC2006)*, ASME, Alberta, Canada, pp. 209-217.

Banerjee, S., Carlin, B. P., and Gelfand, A. E., 2004. *Hierarchical modeling and analysis for spatial data*. Chapman & Hall/CRC, New York, NY, USA.

Bayes, M., and Price, M., 1763. An Essay towards Solving a Problem in the Doctrine of Chances. By the Late Rev. Mr. Bayes, F. R. S. Communicated by Mr. Price, in a Letter to John Canton, A. M. F. R. S. *Philosophical Transactions*, 53, pp. 370-418.

Bernardo, J., and Smith, A. F. M., 2007. *Bayesian Theory*. John Wiley & Sons Inc, New York, NY, USA.

Bunke, O., and Droge, B., 1984. Estimators of the Mean Squared Error of Prediction in Linear Regression. *Technometrics*, 26(2), pp. 145-155.

Caleyo, F., Alfonso, L., Espina-Hernández, J. H., and Hallen, J. M., 2007. Criteria for performance assessment and calibration of in-line inspections of oil and gas pipelines. *Measurement Science and Technology*, 18(7).

Caleyo, F., Velázquez, J. C., Valor, A., and Hallen, J. M., 2009. Probability distribution of pitting corrosion depth and rate in underground pipelines: A Monte Carlo study. *Corrosion Science*, 51(9), pp. 1925-1934.

Carlin, B. P., and Louis, T. A., 2000. *Bayes and Empirical Bayes methods for data analysis*. Chapman & Hall/CRC, London, UK.

Coleman, G. A., and Miller, S. J., 2010. ILI Tool Tolerance and Repeatability Effect on Corrosion Growth Rates. *Proceedings of 8th International Pipeline Conference*, ASME, Calgary, Alberta, Canada, pp. 549-556.

Demichelis, F., Magni, P., Piergiorgi, P., Rubin, M., Bellazzi, R., 2006. A hierarchical Naive Bayes Model for handling sample heterogeneity in classification problems: an application to tissue microarrays. *BMC Bioinformatics*, 7(1), p. 514.

Desjardins, G., 2001. Corrosion Rate and Severity Results from In-Line Inspection Data. *CORROSION 2001*, NACE International.

Fenyvesi, L., and Dumalski, S., 2005. Determining Corrosion Growth Accurately and Reliably. *Corrosion2005*, NACE International.

Fuller, W. A., 1987. *Measurement error models*. Jhon Wiley & Sons, Inc., New York, NY, USA.

Gelman, A., Carlin, J. B., Stern, H. S., and Rubin, D. B., 2004. *Bayesian data analysis*. Chapman & Hall/CRC, Boca Raton, Florida, USA.

Harville, D. A., and Jeske, D. R., 1992. Mean Squared Error of Estimation or Prediction Under a General Linear Model. *Journal of the American Statistical Association*, 87(419), pp. 724-731.

Hoff, P. D., 2009. *A First Course in Bayesian Statistical Methods*. Springer, New York, NY, USA.

Huyse, L., and Roodselaar, A. v., 2010. Effects of Inline Inspection Sizing Uncertainties on the Accuracy of the Largest Features and Corrosion Rate Statistics. *Proceedings of 8th International Pipeline Conference*, ASME, Calgary, Alberta, Canada, pp. 403-413.

Jaech, J. L., 1985. *Statistical analysis of measurement errors*. Jhon Wiley & Sons, Inc., New York, NY, USA.

Kariyawasam, S., and Peterson, W., 2010. Effective Improvements to Reliability Based Corrosion Management. *Proceedings of 8th International Pipeline Conference*, ASME, Calgary, Alberta, Canada, pp. 603-615.

Kiefner, J. F., Mesloh, R. E., and Kiefner, B. A., 2001. Analysis of DOT Reportable Incidents for Gas Transmission and Gathering System Pipelines, 1985 Through 1997, *Report to the Pipeline Research Council International, Inc. (PRCI)*, p. 75.

Lunn, D., Spiegelhalter, D., Thomas, A., and Best, N., 2009. The BUGS project: Evolution, critique and future directions. *Statistics in Medicine*, 28(25), pp. 3049-3067.

Maes, M. A., Dann, M. R., Breitung, K. W., and Brehm, E., 2008. Hierarchical modeling of stochastic deterioration. *Proceedings of the 6th international probabilistic workshop* Eds C.A. Graubner, H. Schmidt, D. Proske, T.U. Darmstadt, pp. 111-124.

Maes, M. A., Faber, M. H., and Dann, M. R., 2009. Hierarchical Modeling of Pipeline Defect Growth Subject to ILI Uncertainty. *Proceedings of 28th International Conference on Ocean, Offshore and Arctic Engineering (OMAE2009)*, ASME, Honolulu, Hawaii, USA, pp. 375-384.

Montgomery, D. C., and Runger, G. C., 2010. *Applied Statistics and Probability for Engineers*. John Wiley & Sons, New York, NY, USA.

Nessim, M., Dawson, J., Mora, R., and Hassanein, S., 2008. Obtaining Corrosion Growth Rates From Repeat In-Line Inspection Runs and Dealing With the Measurement Uncertainties. *Proceedings of 7th International Pipeline Conference*, ASME, Calgary, Alberta, Canada, pp. 593-600.

Ntzoufras, I., 2011. *Bayesian Modeling Using WinBUGS*. John Wiley & Sons, Hoboken, New Jersey, USA.

Pipeline Operators Forum (POF), 2009. Specification and requirements for intelligent pig inspection of pipelines.

Robert, C. P., 2007. *The Bayesian Choice: From Decision-Theoretic Foundations to Computational Implementation*. Springer, New York, NY, USA.

Romanoff, M., 1989. *Underground corrosion*. NACE, Houston, TX, USA.

Soares, C. G., and Garbatov, Y., 1999. Reliability of maintained, corrosion protected plates subjected to non-linear corrosion and compressive loads. *Marine Structures*, 12(6), pp. 425-445.

Spencer, K., Kariyawasam, S., Tetreault, C., and Wharf, J., 2010. A Practical Application to Calculating Corrosion Growth Rates by Comparing Successive ILI Runs

From Different ILI Vendors. *Proceedings of 8th International Pipeline Conference*, ASME, Calgary, Alberta, Canada, pp. 467-473.

Spiegelhalter, D. J., 1998. Bayesian graphical modelling: a case-study in monitoring health outcomes. *Journal of the Royal Statistical Society: Series C (Applied Statistics)*, 47(1), pp. 115-133.

van der Voet, H., 1994. Comparing the predictive accuracy of models using a simple randomization test. *Chemometrics and Intelligent Laboratory Systems*, 25(2), pp. 313-323.

Wallach, D., and Goffinet, B., 1987. Mean Squared Error of Prediction in Models for Studying Ecological and Agronomic Systems. *Biometrics*, 43(3), pp. 561-573.

Worthingham, R., Morrison, T., and Desjardins, G., 2000. Comparison of Estimates from a Growth Model 5 Years after the Previous Inspection. *Proceedings of International Pipeline Conference*, ASME, Calgary, Alberta, Canada.

Chapter 4 Time-dependent System Reliability Analysis of a Corroding Pipeline

4.1 Introduction

Metal-loss corrosion is considered one of the most common attributing factors to failures of energy pipeline, especially for the aging underground pipelines (Nessim et al. 2008; PHMSA 2012). The reliability-based corrosion management program has received increasing attention from pipeline operators (Kariyawasam and Peterson 2008) over the last decade. Such a program typically consists of three cyclic steps: firstly, detecting and sizing corrosion defects on a pipeline using the in-line inspection (ILI) technology; secondly, evaluating the failure probability of the pipeline as a result of the corrosion defects; and finally, mitigating the defects, if the failure probability exceeds a certain allowable level. To this end, implementation of the reliability-based corrosion management program requires accurate evaluation of the failure probability of pipelines due to corrosion defects so that defect repairs can be scheduled to meet the required safety levels while optimizing the allocation of limited resources for repair and mitigation.

The failure mechanisms of a pressurized pipeline containing an active corrosion defect can be broadly classified into two categories: small leak and burst (CSA 2007). Small leak occurs if the defect penetrates the pipe wall; burst occurs if the internal pressure exceeds the burst resistance at the corrosion defect, resulting in plastic collapse of the pipe wall. A burst can be further categorized as a rupture or a large leak. Rupture

occurs if the through-wall defect resulting from the burst extends unstably in the longitudinal direction of the pipeline, whereas large leak is the plastic collapse of the pipe wall without unstable axial extension of the defect (CSA 2007). It is important to distinguish small leak, large leak and rupture in that the consequences associated with these failure modes differ significantly, especially for natural gas pipelines (Nessim et al. 2009; Rothwell and Stephens 2006; Zhou 2011), with the consequences of ruptures generally being the most severe and those of small leaks being the least severe. Different allowable failure probabilities (or target reliability levels) have been proposed for different failure modes of natural gas pipelines to address the differences in the corresponding failure consequences (CSA 2007): more stringent allowable failure probabilities for ruptures and large leaks, and less stringent values for small leaks (CSA 2007).

Corrosion growth modeling plays an important role in forecasting the failure probability of a corroding pipeline (Kariyawasam and Peterson 2010; Nessim et al. 2008). The most commonly used corrosion growth model in practice is the linear growth model (Coleman and Miller 2010; Fenyvesi and Dumalski 2005; Huyse and Roodselaar 2010; Nessim et al. 2008), where the defect depth and length are assumed to grow at constant growth rates over time. The probabilistic characteristics of such growth rates have been reported in the literature. Several researchers (Caleyo et al. 2009; Maes et al. 2009; Romanoff 1989; Soares and Garbatov 1999) reported that the growth of metal-loss corrosion can be better characterized by the non-linear model than by the linear model. Furthermore, the growth paths vary from defect to defect (Ahammed 1998; Southwell and Bultman 1975).

Extensive research has been carried out in the past to evaluate the reliability of pressurized pipeline containing active metal-loss corrosion defects (Ahammed 1998; Caleyó et al. 2002; Hong 1997; Stephens and Nessim 2006; Zhou 2010). As far as the author of this thesis is aware, the corrosion defects were assumed to grow in a linear fashion in all previous investigations involving the evaluation of burst probabilities of corroding pipelines. Furthermore, the same probability distribution of the growth rate is typically applied to different defects considered in the reliability analysis. The consideration of non-linear defect-specific growth models in the reliability analysis of corroding pipelines has not been reported in the literature.

The main objective of the work reported in this chapter was to develop a methodology that can be used to evaluate the time-dependent system reliability of a segment of pipeline containing multiple active corrosion defects by incorporating a non-linear defect-specific corrosion growth model developed based on data obtained from repeated ILIs. The depth of the corrosion defect was assumed to follow a power-law growth path over time. The failure probabilities associated with three distinctive failure modes, namely small leak, large leak and rupture, were evaluated using a simulation-based approach that consists of both the simple Monte Carlo simulation for generating random samples of the pipe geometric and material properties as well as the defect length and Markov Chain Monte Carlo (MCMC) simulation for generating random samples of the defect depth. The methodology was illustrated using a numerical example that involves a corroding natural gas pipeline segment.

This chapter is organized in seven sections. The limit state functions associated with small leak, large leak and rupture are presented in Section 4.2. The capacity models for burst and rupture are discussed in Section 4.3. Section 4.4 describes the Bayesian power-law growth model for the depths of corrosion defects. Section 4.5 includes the basic assumptions adopted in the reliability analysis as well as the procedure of evaluating the system reliability using a combination of the conventional Monte Carlo simulation and MCMC simulation techniques. A numerical example is given in Section 4.6 to illustrate the proposed methodology. Results of the sensitivity analysis with respect to the spatial variability of the model error associated with the burst capacity model and maximum-to-average depth ratio are also presented in Section 4.6. The main findings of the study are summarized in Section 4.7.

4.2 Limit State Functions

Metal-loss corrosion on pipeline causes volumetric loss of metal in the pipe wall. The geometry of a typical metal-loss corrosion defect on a pipeline is illustrated in Fig. 4.1. The length, width and depth of the defect are measured in the longitudinal, circumferential and through-wall thickness directions, respectively, of the pipeline. Based on the above-defined defect dimensions, the limit state functions of a pressurized pipeline containing a single active corrosion defect are developed in the following.

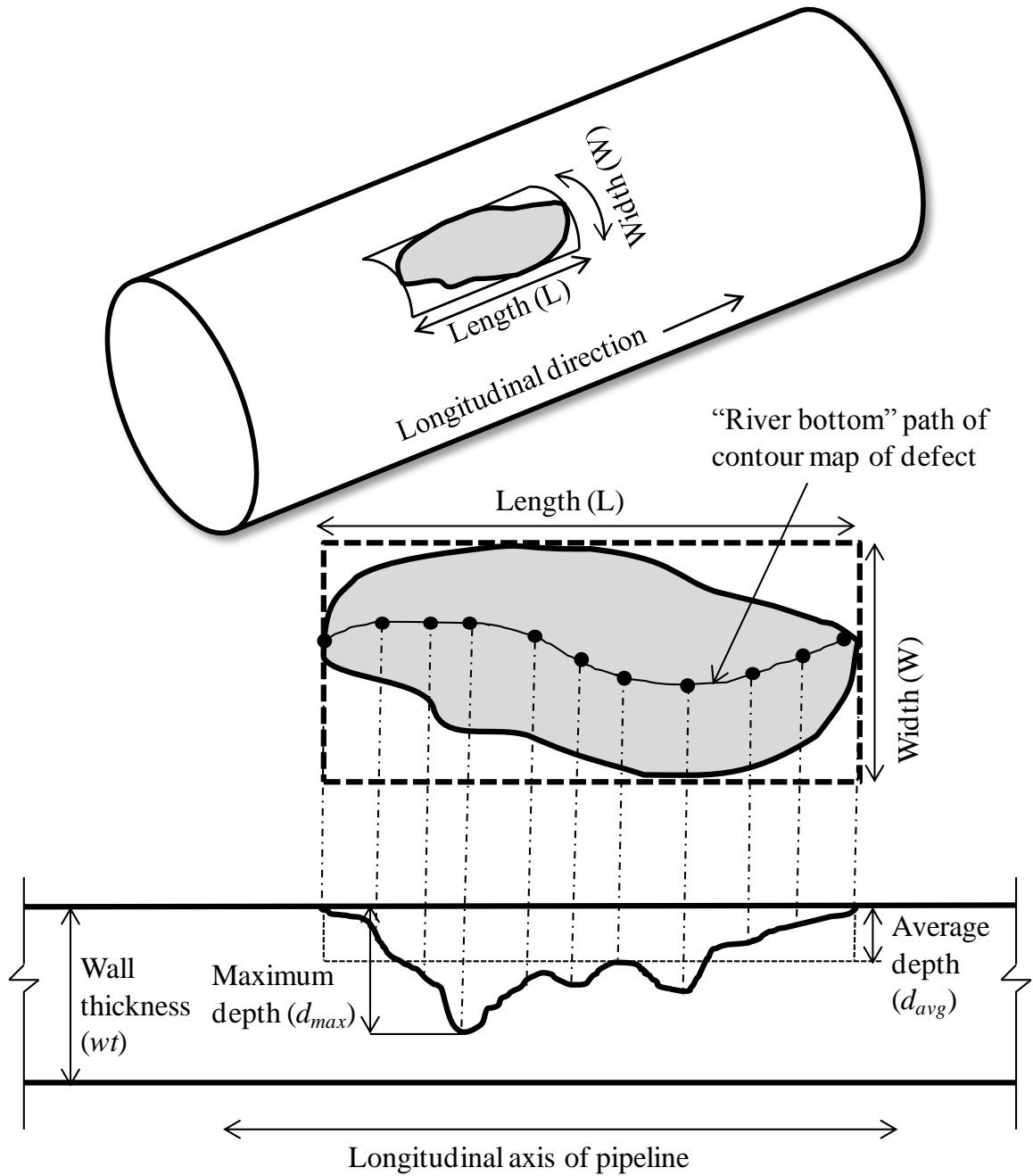


Figure 4.1 Dimensions of a typical corrosion defect on pipeline

The limit state function, $g_1(t)$, for the corrosion defect penetrating the pipe wall at a given time t is

$$g_1(t) = wt - d_{max}(t) \quad (4.1)$$

where wt is the wall thickness of the pipeline, and $d_{max}(t)$ is the maximum depth of the corrosion defect (see Fig. 4.1) at time t .

The limit state function, $g_2(t)$, for plastic collapse under internal pressure at the defect at time t is given by

$$g_2(t) = r_b(t) - p \quad (4.2)$$

where $r_b(t)$ denotes the burst pressure resistance of the pipe at the defect at time t , and p is the internal pressure of the pipeline and assumed to be time-independent in this study. The burst pressure resistance is a function of geometric and material properties of the pipeline, and the defect depth and length (see Fig. 4.1). Because the defect size monotonically increases over time, the burst pressure resistance monotonically decreases over time.

Given a burst, the unstable axial extension of the through-wall defect that results from the burst is defined as a rupture and is governed by the limit state function $g_3(t)$ as follows:

$$g_3(t) = r_{rp}(t) - p \quad (4.3)$$

where $r_{rp}(t)$ is the pressure resistance of the pipeline at the location of the through-wall defect resulting from the burst at time t . A burst is classified as a rupture if $g_3(t) \leq 0$; otherwise, it is a large leak.

Based on the limit state functions defined by Eqs. (4.1) through (4.3), failure of a pipeline can be categorized into three modes, namely small leak, large leak and rupture. Because these limit state functions involve monotonically increasing defect geometry and monotonically decreasing pipe resistance, and because the internal pressure is assumed to be time-independent, the probabilities of small leak, large leak and rupture within a time interval $[0, t]$, $P_{sl}(t)$, $P_{ll}(t)$ and $P_{rp}(t)$ respectively, are defined as follows:

$$P_{sl}(t) = \text{Prob}[g_1(t) \leq 0 \cap g_2(t) > 0] \quad (4.4a)$$

$$P_{ll}(t) = \text{Prob}[g_1(t) > 0 \cap g_2(t) \leq 0 \cap g_3(t) > 0] \quad (4.4b)$$

$$P_{rp}(t) = \text{Prob}[g_1(t) > 0 \cap g_2(t) \leq 0 \cap g_3(t) \leq 0] \quad (4.4c)$$

where “ \cap ” represents the intersection (i.e. joint event). In estimating the probabilities of small leak and burst, it is assumed that the occurrences of burst and small leak at a given defect are mutually exclusive (Zhou 2011).

4.3 Burst and Rupture Pressure Models

In this study, the burst pressure resistance model suggested in Annex O of the Canadian pipeline standard CSA Z662-07 (CSA 2007) was selected to evaluate r_b in Eq. (4.2). Instead of using the two-term model error (i.e. the additive and multiplicative model errors) recommended in Annex O of CSA Z662-07, a single multiplicative model error reported by Huang (2011) was employed in this study. The pressure resistance r_b is calculated as follows:

$$r_b = er_{bc} \quad (4.5a)$$

$$r_{bc} = r_0 \left(\frac{1 - \frac{d_{avg}}{wt}}{1 - \frac{d_{avg}}{Mwt}} \right) = r_0 \left(\frac{1 - \frac{d_{max}}{\xi wt}}{1 - \frac{d_{max}}{\xi Mwt}} \right) \quad (4.5b)$$

$$r_0 = \frac{2wt\sigma_f}{D} \quad (4.5c)$$

$$M = \begin{cases} \sqrt{1 + 0.6275 \frac{l^2}{Dwt} - 0.003375 \frac{l^4}{(Dwt)^2}} & \frac{l^2}{Dwt} \leq 50 \\ 3.293 + 0.032 \frac{l^2}{Dwt} & \frac{l^2}{Dwt} > 50 \end{cases} \quad (4.5d)$$

$$\sigma_f = \begin{cases} 1.15\sigma_y & SMYS \leq 241 \text{ MPa} \\ 0.9\sigma_u & SMYS > 241 \text{ MPa} \end{cases} \quad (4.5e)$$

where r_{bc} is the predicted burst pressure without model error; r_0 is the burst pressure resistance of a defect-free pipe; σ_f , σ_y and σ_u are the flow stress, yield stress and tensile strength of the pipe material, respectively; SMYS is the specified minimum yield strength; e is the multiplicative model error defined as the ratio of actual-to-predicted burst pressure; D is the outside diameter of the pipeline; d_{avg} is the average depth of the defect (see Fig. 4.1) and can be calculated from the corresponding maximum depth, d_{max} , using the maximum-to-average depth ratio ξ , i.e. $d_{avg} = d_{max}/\xi$; l is the length of the defect, and M is the Folias factor or bulging factor.

The rupture pressure resistance model recommended in Annex O of CSA Z662-07 was employed in this study. This model was developed by Kiefner and Vieth (1989) based on the flow stress-dependent failure criterion for pressurized pipelines containing through-wall flaws. The rupture pressure resistance, r_{rp} , is calculated as follows:

$$r_{rp} = \frac{2wt\sigma_f}{MD} \quad (4.6)$$

The Folias factor M in Eq. (4.6) can be calculated using Eq. (4.5d). The model error for Eq. (4.6) was ignored in the analysis due to a lack of relevant information.

4.4 Corrosion Growth Model

The maximum depth of corrosion defect i , $d_{max,i}(t)$, was assumed to follow a power-law growth path defined as follows:

$$d_{max,i}(t) = a_i(t - t_{oi})^{b_i} + \eta_i(t) \quad (4.7)$$

where t (years) is the time elapsed since the time of installation; $\eta_i(t)$ represents the model error of the power-law growth model associated with defect i at time t , which is assumed to follow a normal distribution with a zero mean and a variance of $\sigma_{\eta_i}^2$, and a_i , b_i and t_{oi} define the growth path for defect i . The parameter a_i ($a_i > 0$) is indicative of the growth of the defect depth within one year from the defect initiation; b_i ($b_i > 0$) defines the rate of change of the growth path; that is, $b_i = 1$, $b_i > 1$ and $0 < b_i < 1$ characterize a linear, an accelerating and a decelerating growth path respectively, and t_{oi} (years) represents the corrosion initiation time (e.g. the time interval between the installation and the time at which defect i starts to grow). The parameters of the growth models, i.e. a_i , b_i , t_{oi} and $\sigma_{\eta_i}^2$, can be evaluated using the hierarchical Bayesian model based on the data collected from multiple ILIs as described in Chapter 3.

A linear growth was assumed for the defect length; that is, the length of a corrosion defect was assumed to grow at a constant (but uncertain) rate over time (Caleyo et al. 2002; Hong 1997; Zhou 2011). Therefore, the length of defect i can be predicted as follows:

$$l_i(\tau) = l_{oi} + r_l \tau \quad (4.8)$$

where τ is the time elapsed since the last inspection (i.e. the forecasting year); $l_i(\tau)$ is the length of the defect i at the forecasting year τ , l_{oi} is the length of the defect i at the time of last inspection (i.e. initial length), and r_l denotes the length growth rate.

4.5 System Reliability Analysis

4.5.1 Basic Assumptions

In this study, the system reliability of a pipeline was evaluated on a joint-by-joint basis; that is, a pipe joint containing multiple active corrosion defects was considered as a system. The typical length of a pipe joint is 10-20 meters. Because failure of any defect on a pipe joint implies failure of the joint, it follows that the pipe joint is a series system. The internal operating pressure of the pipeline was assumed to be a time-independent random variable. The internal pressure, pipe geometry and material properties (i.e. diameter, wall thickness, yield strength and ultimate tensile strength), maximum-to-average depth ratio, and the model error associated with the burst pressure model were assumed to be mutually independent for a given defect. Each of these parameters was further assumed to be fully correlated for all the defects in a given joint.

4.5.2 Analysis Procedure

A combination of the simple Monte Carlo simulation and MCMC simulation techniques was used to evaluate the system reliability of a given pipe joint containing multiple active corrosion defects. Because the parameters of the growth model for the

defect depth were obtained from the Bayesian updating using the MCMC technique (see Chapter 3), it's advantageous to retain the random samples of these parameters generated from MCMC and incorporate the samples in the reliability analysis. Furthermore, the correlations among these parameters are fully preserved by directly using the MCMC samples in the reliability analysis. The simple Monte Carlo technique was used to generate random samples for the other parameters in the reliability analysis such as the pipe wall thickness, yield strength and model error.

The samples of $d_{max,i}(t)$ were obtained by substituting MCMC samples of a_i , b_i and t_{oi} , and random samples of $\eta_i(t)$ into Eq. (4.7) for different t values corresponding to the forecasting years. Note that the random samples of $\eta_i(t)$ were generated from the normal distribution with a zero mean and a variance of $\sigma_{\eta_i}^2$, with the values of $\sigma_{\eta_i}^2$ obtained from MCMC. Because the model error, $\eta_i(t)$, associated with the power-law model is normally distributed, the random samples of $d_{max,i}(t)$ may be less than zero or greater than $100\%wt$, which are impossible in reality. To address this, the distribution of $d_{max,i}(t)$ was truncated at the lower bound of zero and upper bound of $100\%wt$.

To calculate the system reliability of a pipe joint containing m active corrosion defects over a forecasting period of T years since the last inspection, the follow analysis procedure was employed:

- 1) Generate N random samples of the maximum depth for each of the m defects at each year within the forecasting period T using the procedure described in the previous paragraph;

- 2) set $sl(\tau)$, $ll(\tau)$ and $rp(\tau) = 0$, where $sl(\tau)$, $ll(\tau)$ and $rp(\tau)$ denote the counters of small leaks, large leaks and ruptures, respectively, that occur in a given forecasting year τ ($\tau = 1, 2, \dots, T$);
- 3) for a given simulation trial k ($k = 1, 2, \dots, N$), check if the system has failed and determine the corresponding failure mode within the forecasting period T as follows:
 - 3.1) generate samples of the material properties (e.g. σ_y , σ_u) and geometric properties (e.g. wt and D) of the pipeline, initial lengths l_{oi} ($i = 1, 2, \dots, m$) and length growth rates r_{li} of the defects, the internal operating pressure p , maximum-to-average depth ratio ξ , and the model error e ;
 - 3.2) start from the forecasting year $\tau = 1$, carry out the following:
 - a) obtain a set of m random samples of the maximum defect depth, $d_{max,i}$ ($i = 1, 2, \dots, m$) at τ , one for each of the m defects;
 - b) calculate the lengths of the defects l_i at τ using Eq. (4.8);
 - c) calculate $g_1 = wt - \max_i \{d_{max,i}\}$;
 - d) substitute the values of wt , D , ξ , e , σ_y (σ_u), l_i and $d_{max,i}$ into Eq. (4.5); calculate $g_2 = \min_i \{r_{b,i}\} - p$;
 - e) if $g_1 > 0$ and $g_2 > 0$, set $\tau = \tau + 1$ and repeat steps 3.2a) through 3.2d); if $g_1 = 0$ and $g_2 > 0$, set $sl(\tau) = sl(\tau) + 1$; if $g_2 \leq 0$, calculate $g_3 = \widetilde{r}_{rp} - p$, where \widetilde{r}_{rp} is the rupture pressure of the defect with the lowest burst pressure at τ , set $ll(\tau) = ll(\tau) + 1$ if $g_2 \leq 0$ and $g_3 > 0$; set $rp(\tau) = rp(\tau) + 1$ if $g_2 \leq 0$ and $g_3 \leq 0$, and

4) repeat steps 3.1) to 3.2) for N simulation trials.

Once the counts of $sl(\tau)$, $ll(\tau)$ and $rp(\tau)$ are obtained for the N simulation trials, the cumulative probabilities of small leak, large leak and rupture up to a given forecasting year τ , $P_{sl}(\tau)$, $P_{ll}(\tau)$ and $P_{rp}(\tau)$, are evaluated as follows:

$$P_{sl}(\tau) \approx \frac{1}{N} \sum_{j=1}^{\tau} sl(j) \quad (4.9a)$$

$$P_{ll}(\tau) \approx \frac{1}{N} \sum_{j=1}^{\tau} ll(j) \quad (4.9b)$$

$$P_{rp}(\tau) \approx \frac{1}{N} \sum_{j=1}^{\tau} rp(j) \quad (4.9c)$$

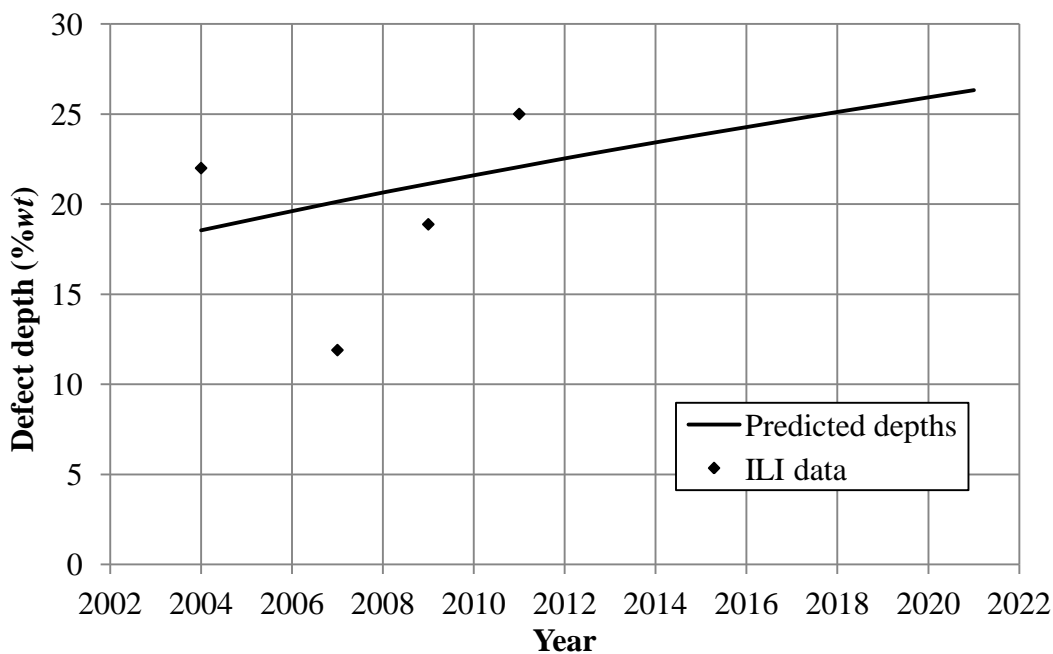
4.6 Numerical Example

4.6.1 General

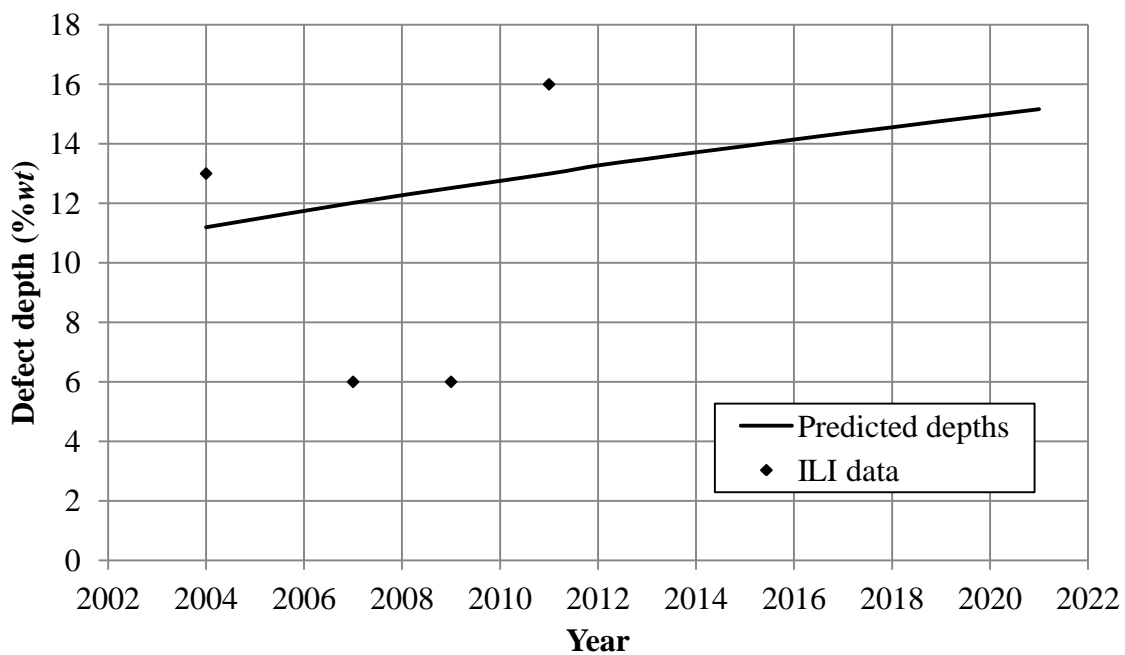
The time-dependent system reliability of a joint of a natural gas pipeline located in Alberta was evaluated using the methodology described in Section 4.5. The subject pipeline has a nominal outside diameter of 508 mm (20 inches) and an operating pressure of 5.654 MPa, and is made from API 5L Grade X52 steel with an SMYS of 359 MPa and an SMTS of 456 MPa. The selected joint is 18.13 m long, has a nominal wall thickness of 5.56 mm, and contains ten individual external corrosion defects. The pipe joint was inspected by high-resolution MFL tools in 2004, 2007, 2009 and 2011.

4.6.2 Growth Mode for the Defect Depth

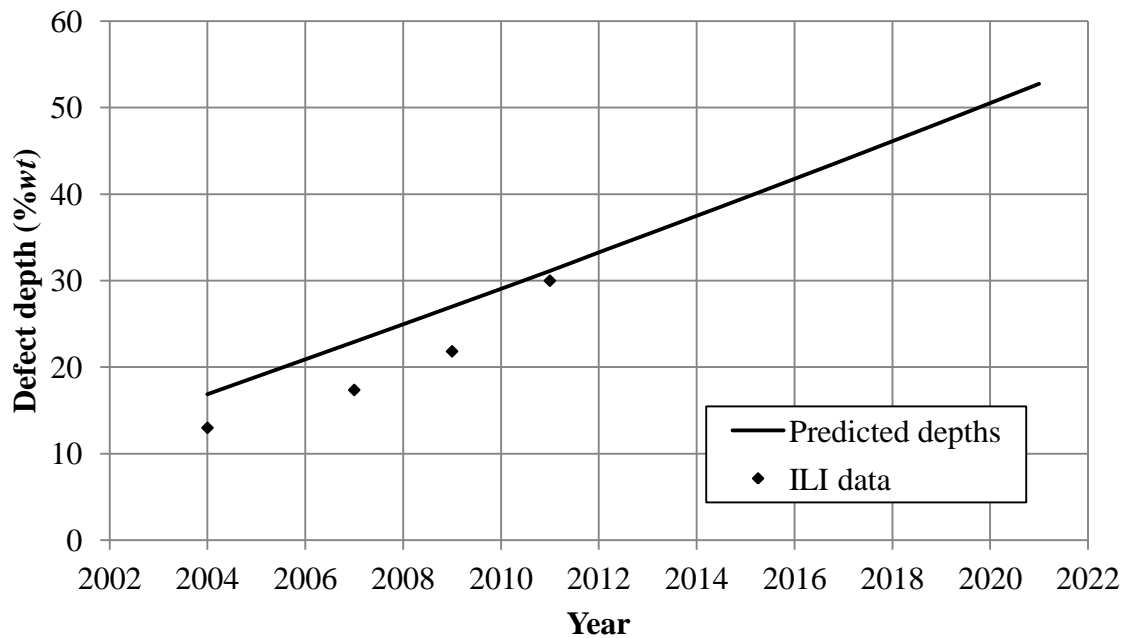
The ILI data of 2004, 2007, 2009 and 2011 were used to develop the power-law depth growth model based on the hierarchical Bayesian methodology described in Chapter 3. The maximum depths of the defects were predicted for a period of 10 years from the last inspection (i.e. 2011). The growth paths obtained from the median values of the marginal posterior distributions of the parameters in the growth model for four selected defects (i.e. defects #2, #4, #5 and #7) are shown in Fig. 4.2. The ILI-reported depths of these defects are also shown in this figure. This figure indicates that the growth paths of these defects vary significantly according to the growth model; for example, the depths of defects #2 and #4 are predicted to grow by less than 5%wt from 2011 to 2021, whereas the depths of defects #5 and #7 are predicted to grow by more than 20%wt from 2011 to 2021.



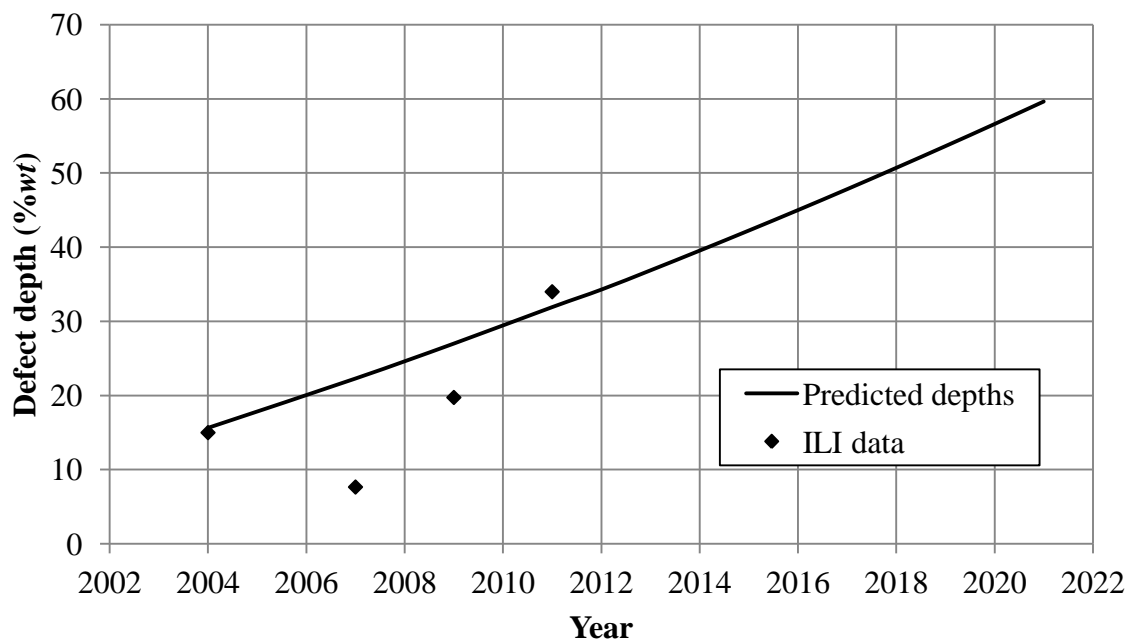
a) Defect #2



b) Defect #4



c) Defect #5



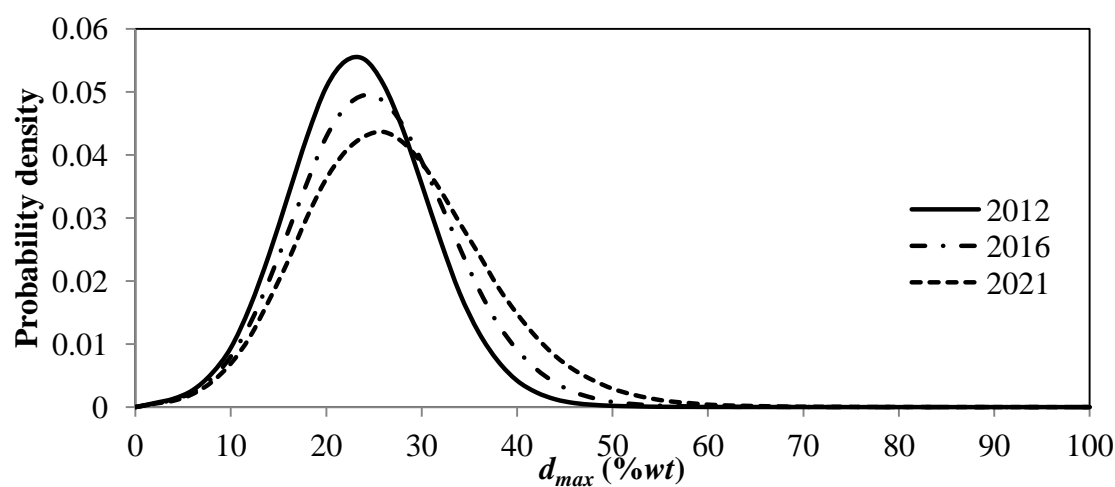
d) Defect #7

Figure 4.2 Predicted growth paths for defects #2, #4, #5 and #7 on the selected pipe joint

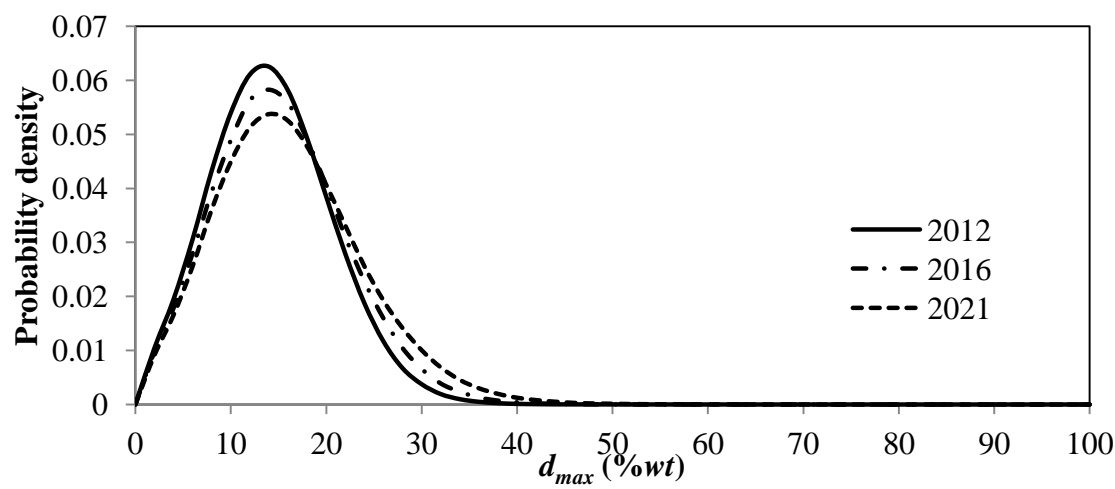
Two Markov chains were run simultaneously to generate 25,000,000 MCMC samples (after the burn in period of 10,000) of the defect depth in each chain for each defect at every forecasting year. A thinning interval of 50 was then applied to the generated samples to reduce the autocorrelation so that the samples from different sequences can be approximately considered to be independent of each other, allowing them to be used in the same way as the samples generated from the simple Monte Carlo simulation. Therefore, a thinning interval of 50 results in 500,000 samples in each chain to be stored, which makes a total of 1,000,000 samples for each defect at each forecasting year. The autocorrelation of the 500,000 samples in each chain was found to be no greater than 0.4-

0.6 for all the defects considered. The thinning interval of 50 was therefore deemed adequate.

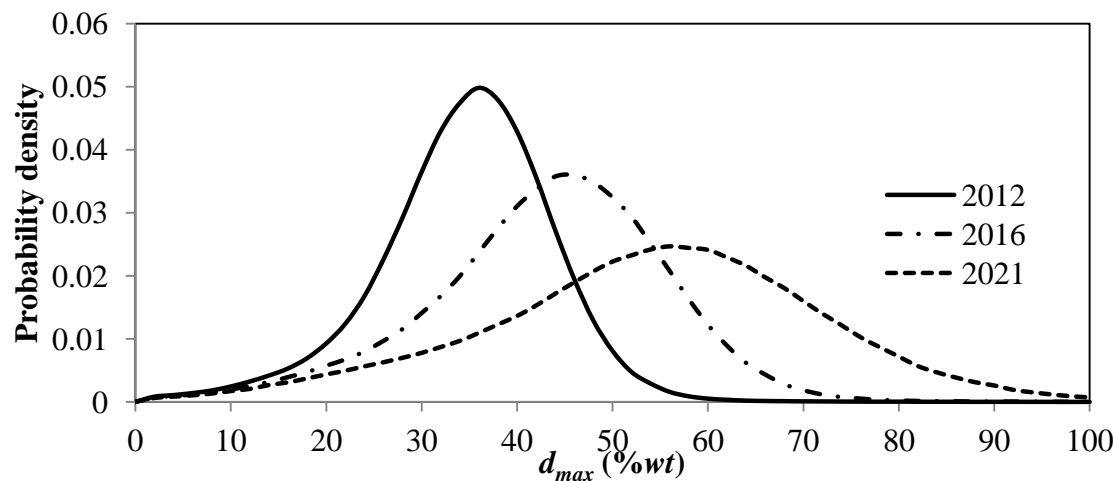
The probability density functions (PDF) of the predicted depths of the four defects (defects #2, #4, #5 and #7) in 2012, 2016 and 2021 are shown in Figs. 4.3. These figures indicate that the PDF curves move toward larger depths with time and that the spread of these curves also increases over time (i.e. the uncertainty in the predicted depth increases with time).



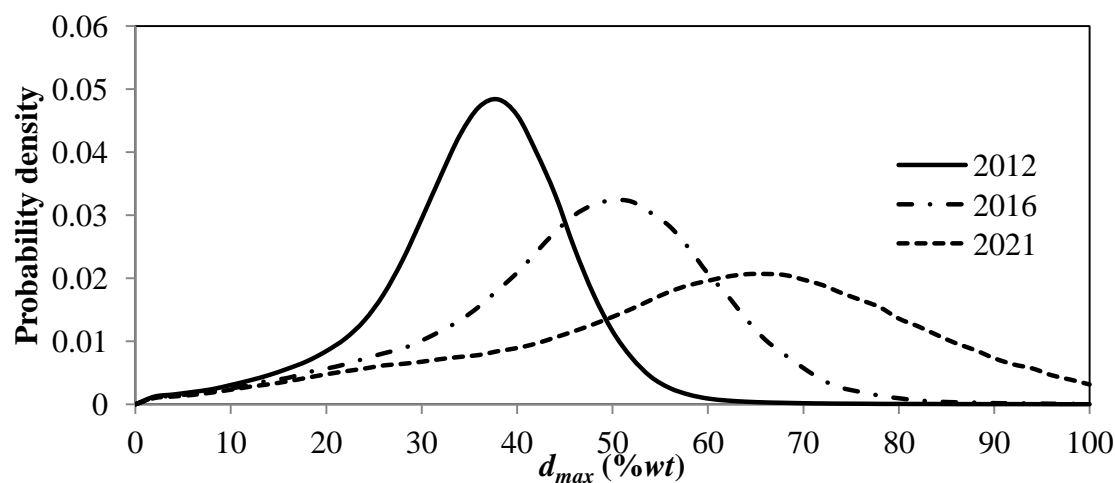
a) Defect #2



b) Defect #4



c) Defect #5



d) Defect #7

Figure 4.3 Marginal posterior probability density functions of predicted depths in 2012, 2016 and 2021 for defects #2, #4, #5 and #7

4.6.3 Probabilistic Characteristics of Input Parameters

The statistical characteristics of the basic random variables involved in the numerical example are listed in Table 4.1. The statistical information about the pipeline geometry, material strength and defect geometry were obtained from previous studies indicated in

the table. The nominal values of the parameters are shown in Table 4.2. The nominal values of the initial lengths of the defects were obtained from the ILI carried out in 2011.

Table 4.1 Probabilistic characteristics of the basic random variables used in the reliability analysis

Parameter	Distribution Type	Mean-to-nominal ratio	Coefficient of variation (COV)	Source
Diameter	Deterministic	1.00	-	Jiao et al. (1995)
Wall thickness	Normal	1.00	1.5%	Zhou (2010)
Yield stress	Normal	1.11	3.4%	Jiao et al. (1997)
Tensile strength	Normal	1.12	3%	Jiao et al. (1995)
Initial length of defect	Truncated Normal (lower bound = 0)	1.00	ILI tool specification ^a	Kariyawasam and Peterson (2010)
Defect length growth rates	Lognormal	3.0 ^b (mm/yr)	50%	Zhou (2011)
Internal pressure	Gumbel	1.02	2%	CSA (2007)
Burst capacity model error	Lognormal	1.103 ^b	17.2%	Huang (2011)
Maximum-to-average defect depth ratio	Shifted lognormal (lower bound = 1.0)	2.08 ^b	50%	CSA (2007)

^a +/- 10mm with 80% confidence

^b Mean value

Table 4.2 Nominal values of the input parameters used in the reliability analysis

Parameter		Nominal value	Unit
Diameter		508	mm
Wall thickness		5.56	
SMYS		359	MPa
SMTS		455	
Internal pressure		5.654	
Initial lengths of defects	defect #1	21	mm
	defect #2	19	
	defect #3	24	
	defect #4	19	
	defect #5	29	
	defect #6	41	
	defect #7	21	
	defect #8	18	
	defect #9	25	
	defect #10	29	

4.6.4 Results

A total of 1,000,000 simulation trials were carried out to evaluate the probabilities of small leak, large leak and rupture of the pipe joint. The cumulative failure probabilities corresponding to the three different failure modes are shown in Fig. 4.4. This figure indicates that the probability of small leak is the highest of those of the three failure modes. Furthermore, the probability of rupture for the first four years of the forecasting

period is too small to be calculated reasonably accurately using 1,000,000 simulation trials.

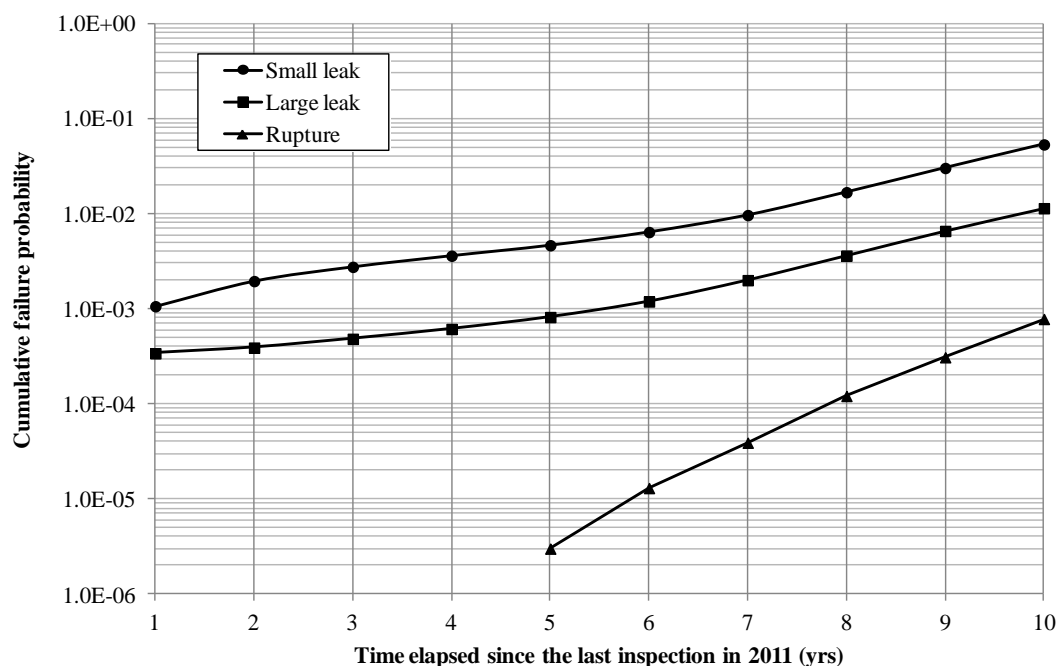


Figure 4.4 Cumulative failure probabilities of the pipe segment for three different failure modes

4.6.5 Sensitivity analysis

The model error associated with burst pressure model was assumed to be fully correlated among the different defects in obtaining the analysis results shown in Fig. 4.4. In reality, the model errors for different defects are expected to be partially correlated because the model error has been found (Huang 2011) to depend on the defect geometry, which varies from defect to defect, and the pipe strength, which is likely the same (or highly correlated) for all the defects in the same pipe joint. To investigate the impact of the correlation between the model errors for different defects on the system reliability, two bounding scenarios, i.e. fully-correlated and independent model errors, were

considered. The failure probabilities of the pipe joint corresponding to independent model errors were evaluated and are compared with the failure probabilities corresponding to fully-correlated model errors in Fig.4.6. This figure indicates that the probability of large leak corresponding to independent model errors is substantially higher than that corresponding to fully-correlated model errors and that the difference between the failure probabilities corresponding to these two scenarios decreases with time. On the other hand, the correlation between the model errors has almost no impact on the probability of small leak, which is expected because the model error has little impact on the probability of small leak in the first place (see Eq. (4.1)). The correlation between the model errors has a negligible impact on the probability of ruptures for this example, which can be attributed to the fact that the defects considered are all relatively short, making large leak the dominant failure mode given burst.

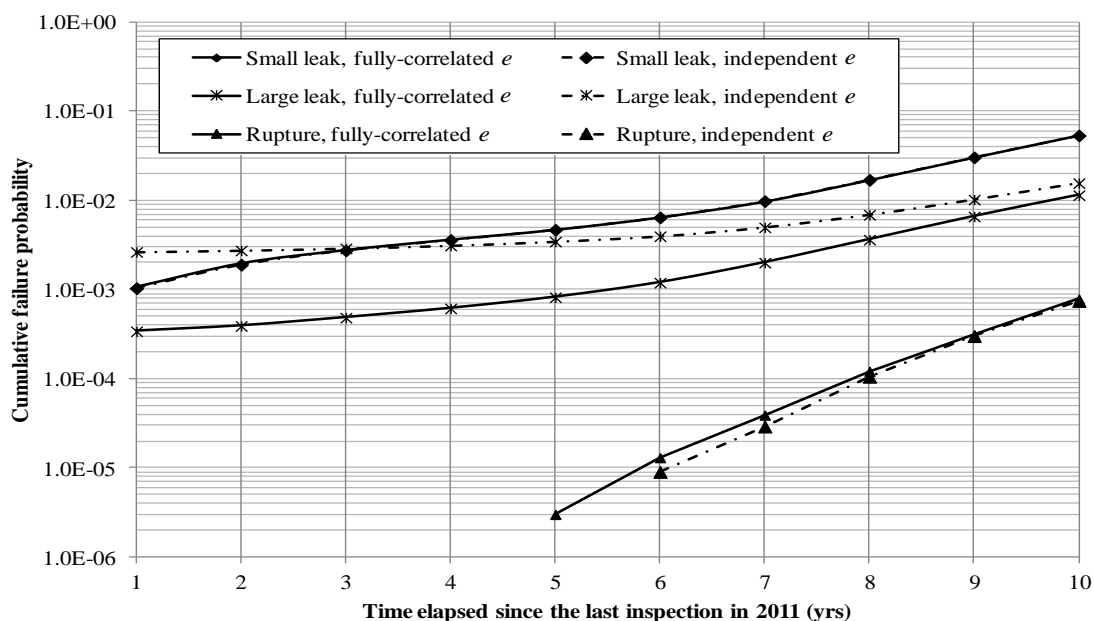


Figure 4.5 Impact of correlation between the model errors of the burst capacity models, e , for different defects on the system reliability

Additional sensitivity analyses were carried out to examine the impact of the correlation between the maximum-to-average depth ratios for different defects. For this purpose, the probabilities of small leak, large leak and rupture were evaluated considering independent maximum-to-average depth ratios and then compared with those of the baseline case where maximum-to-average depth ratios for different defects were assumed to be fully correlated. The comparison is shown in Fig. 4.6. Note that in these two cases fully-correlated model errors were assumed for different defects. Figure 4.6 suggests that the correlation between the maximum-to-average depth ratios has a negligible impact on the system reliability of the pipe joint.

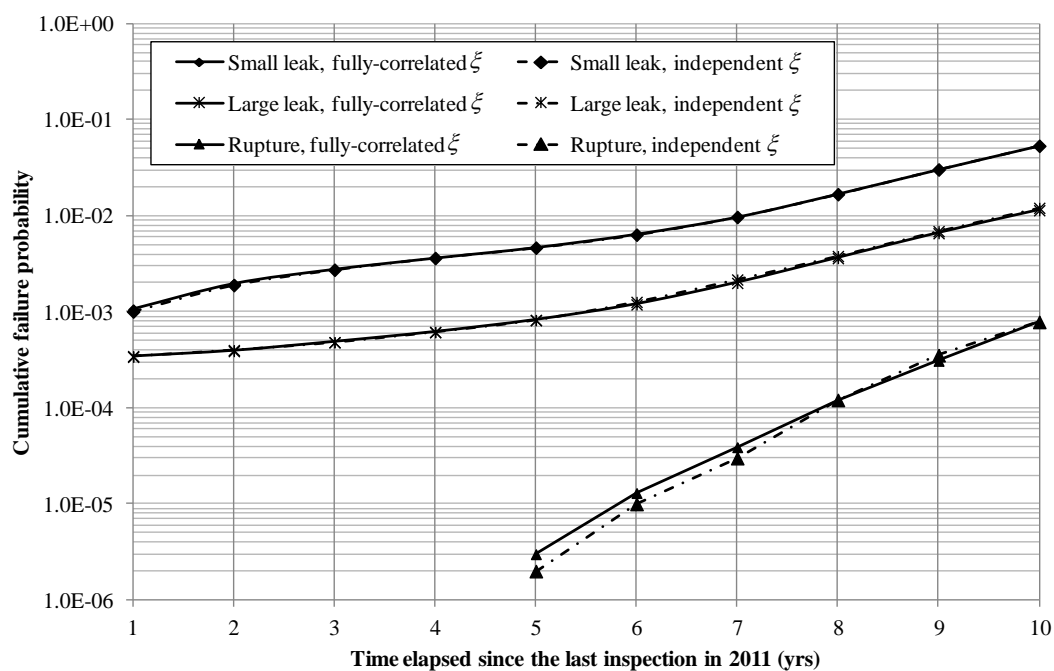


Figure 4.6 Impact of correlation between the maximum-to-average depth ratios, ξ , for different defects on the system reliability

4.7 Conclusion

A methodology was proposed to evaluate the time-dependent system reliability of a pressurized pipeline segment containing multiple active corrosion defects. The growth of the depth of individual corrosion defect on the pipeline segment was characterized by a power-law function of time, and the parameters of the growth model were quantified from the Bayesian updating based on data obtained from multiple in-line inspections. The pipeline segment was modeled as a series system with three distinctive failure modes, namely small leak, large leak and rupture. A simulation-based approach was employed to calculate the probabilities of small leak, large leak and rupture of the pipe segment, whereby random samples of the all input parameters except the defect depth were generated from the simple Monte Carlo simulation and the random samples of the defect depth were generated from the Markov Chain Monte Carlo simulation. The proposed methodology can be used in risk- and reliability-based pipeline corrosion management programs to facilitate defect repair and mitigation that satisfy both safety and economic constraints.

The methodology was illustrated using a numerical example that involves a natural gas pipeline joint containing ten active external corrosion defects. Two sensitivity analyses were carried out to examine the impact on the system reliability due to the correlation between the model errors of the burst capacity models associated with different defects and the correlation of maximum-to-average depth ratios for different defects. The results indicate that the probability of large leak is sensitive to the correlation between the model errors: the probability of large leak corresponding to

independent model errors is markedly higher than that corresponding to fully-correlated model errors. On the other hand, the correlation between the model errors has no impact on the probability of small leak. The results also suggest that the failure probability of the pipe joint is insensitive to the correlation between the maximum-to-average depth ratios for different defects.

References

Ahammed, M., 1998. Probabilistic estimation of remaining life of a pipeline in the presence of active corrosion defects. *International Journal of Pressure Vessels and Piping*, 75(4), pp. 321-329.

Caleyo, F., González, J. L., and Hallen, J. M., 2002. A study on the reliability assessment methodology for pipelines with active corrosion defects. *International Journal of Pressure Vessels and Piping*, 79(1), pp. 77-86.

Caleyo, F., Velázquez, J. C., Valor, A., and Hallen, J. M., 2009. Probability distribution of pitting corrosion depth and rate in underground pipelines: A Monte Carlo study. *Corrosion Science*, 51(9), pp. 1925-1934.

Coleman, G. A., and Miller, S. J., 2010. ILI Tool Tolerance and Repeatability Effect on Corrosion Growth Rates. *Proceedings of 8th International Pipeline Conference*, ASME, Calgary, Alberta, Canada, pp. 549-556.

CSA, 2007. *CSA-Z662 Oil and Gas Pipeline Systems*. Canadian Standards Associations, Rexdale, Ontario.

Fenyvesi, L., and Dumalski, S., 2005. Determining Corrosion Growth Accurately and Reliably. *Corrosion2005*, NACE International.

Hong, H. P., 1997. Reliability based Optimal Inspection and Maintenance for Pipeline under Corrosion. *Civil Engineering Systems*, 14(4), pp. 313-334.

Huang, G., 2011, Model Error Assessment of Burst Capacity Models for Energy Pipelines, *MESc Thesis*, The University of Western Ontario, London, Ontario, Canada.

Huyse, L., and Roodselaar, A. v., 2010. Effects of Inline Inspection Sizing Uncertainties on the Accuracy of the Largest Features and Corrosion Rate Statistics. *Proceedings of 8th International Pipeline Conference*, ASME, Calgary, Alberta, Canada, pp. 403-413.

Jiao, G., Sotberg, T., Bruschi, R., and Igland, R. T., 1997. The Superb Project: Linepipe Statistical Properties and Implications in Design of Offshore Pipelines. *Proceedings of Proceedings of the Sixteenth International Conference on Offshore Mechanics and Arctic Engineering.*, ASME, pp. 45-56.

Jiao, G., Sotberg, T., and Igland, R. T., 1995. *SUPERB 2M Statistical Data- Basic Uncertainty Measures for Reliability Analysis of Offshore Pipelines.*

Kariyawasam, S., and Peterson, W., 2008. Revised Corrosion Management With Reliability Based Excavation Criteria. *Proceedings of 7th International Pipeline Conference*, ASME, Calgary, Alberta, Canada, pp. 489-500.

Kariyawasam, S., and Peterson, W., 2010. Effective Improvements to Reliability Based Corrosion Management. *Proceedings of 8th International Pipeline Conference*, ASME, Calgary, Alberta, Canada, pp. 603-615.

Maes, M. A., Faber, M. H., and Dann, M. R., 2009. Hierarchical Modeling of Pipeline Defect Growth Subject to ILI Uncertainty. *Proceedings of 28th International Conference on Ocean, Offshore and Arctic Engineering (OMAE2009)*, ASME, Honolulu, Hawaii, USA, pp. 375-384.

Nessim, M., Dawson, J., Mora, R., and Hassanein, S., 2008. Obtaining Corrosion Growth Rates From Repeat In-Line Inspection Runs and Dealing With the Measurement Uncertainties. *Proceedings of 7th International Pipeline Conference*, ASME, Calgary, Alberta, Canada, pp. 593-600.

Nessim, M., Zhou, W., Zhou, J., and Rothwell, B., 2009. Target Reliability Levels for Design and Assessment of Onshore Natural Gas Pipelines. *Journal of Pressure Vessel Technology*, 131(6), pp. 061701-061712.

PHMSA, 2012, Pipeline Incidents and Mileage Reports, March 2012. *Pipeline & Hazardous Materials Safety Administration*, <http://primis.phmsa.dot.gov/comm/reports/safety/PSI.html>.

Romanoff, M., 1989. *Underground corrosion*. NACE, Houston, TX, USA.

Rothwell, B., and Stephens, M., 2006. Risk Analysis of Sweet Natural Gas Pipelines: Benchmarking Simple Consequence Models. *Proceedings of International Pipeline Conference (IPC2006)* ASME, Calgary, Alberta, Canada, pp. 911-919.

Soares, C. G., and Garbatov, Y., 1999. Reliability of maintained, corrosion protected plates subjected to non-linear corrosion and compressive loads. *Marine Structures*, 12(6), pp. 425-445.

Southwell, C. R., and Bultman, J. D., 1975. Corrosion of Metals in Tropical Environments: Final report of 16- year exposures, *Naval Research Laboratory*, Washington D. C., USA.

Stephens, M., and Nessim, M., 2006. A Comprehensive Approach to Corrosion Management Based on Structural Reliability Methods. *Proceedings of International Pipeline Conference (IPC2006)*, ASME, Calgary, Alberta, Canada, pp. 695-704.

Zhou, W., 2010. System reliability of corroding pipelines. *International Journal of Pressure Vessels and Piping*, 87(10), pp. 587-595.

Zhou, W., 2011. Reliability Evaluation of Corroding Pipelines Considering Multiple Failure Modes and Time-Dependent Internal Pressure. *Journal of Infrastructure Systems*, ASCE, 17(4), pp. 216-224.

Chapter 5 Summary and Conclusions

5.1 General

Characterization of the growth of metal-loss corrosion defects on energy pipelines is a key focus for pipeline operators because defect growth rates are paramount to a number of critical corrosion management actions such as determination of location and timing of defect mitigations, development of re-inspection intervals and evaluation of time-dependent failure probability of the pipeline. In-line inspection (ILI) has been widely used to collect corrosion data on pipeline for the past few decades. In the study reported in this thesis, a calibration model was developed to quantify the measurement errors associated with the ILI data; a Bayesian model was then developed to characterize the growth of depths of corrosion defects based on the ILI data by incorporating the measurement errors associated with the data, and finally a methodology was proposed to evaluate the time-dependent system reliability of a pipeline segment containing multiple active corrosion defects by incorporating the developed corrosion growth model.

5.2 Bayesian Model for Calibration of ILI Tools

In Chapter 2, a Bayesian model was developed to calibrate the ILI tool and quantify the measurement errors associated with the ILI data. The calibration was carried out by comparing ILI-reported depths with the corresponding field-measured depths for a set of recoated defects. The measurement error associated with the field measurement was quantified first using Jaech's method (Jaech 1985), and found to be negligibly small. Therefore, the field-measured depth was assumed to equal the actual depth of the defect.

The ILI-reported depth was assumed to be a linear function of the corresponding field-measured depth with an intercept representing the constant bias and a slope representing the non-constant bias plus a random scattering error. The model was developed in a Bayesian framework. The Bayesian updating was carried out using Markov Chain Monte Carlo (MCMC) simulation techniques. The probabilistic characteristics of constant and non-constant biases, standard deviations of the random scattering errors as well as the correlation coefficients between the random scattering errors of different ILI tools were evaluated based on the MCMC samples. The mean value of the marginal posterior distribution of each parameter was considered as the point estimate.

In two case studies, the proposed model was applied to the ILI tools that were used to inspect the corrosion defects on two in-service pipelines located in Alberta. Each pipeline has been inspected multiple times by high-resolution Magnetic Flux Leakage (MFL) tools that were from two different ILI vendors. The ILI tools used in 2004, 2007, 2009 and 2011 on the subject pipeline of Case 1, and the ILI tools used in 2004, 2007 and 2009 on the subject pipeline of Case 2 were calibrated. The results of calibration indicate that the accuracies of the ILI tools vary markedly. For example, the ILI tool used in 2004 on the subject pipeline of Case 1 is the most accurate among the four ILI tools considered in that the corresponding constant and non-constant biases (2.04% *wt* and 0.97 respectively) are closer to zero and unity, respectively, than those of the other three tools, and the standard deviation of the scattering error is the second lowest (5.97% *wt*) among the four ILI tools and only slightly higher than the lowest standard deviation (5.94% *wt*). On the other hand, the measurement error of the ILI tool used on the subject pipeline of Case 1 in 2007 is relatively large because the constant and non-constant biases (-

15.28%wt and 1.40 respectively) are significantly different from zero and unity, respectively, and the standard deviations of the scattering error (9.05%wt) is large. Furthermore, it was found that the random scattering errors associated with different ILI tools used in the same pipeline are highly correlated: the corresponding correlation coefficients are consistently greater than or equal to 0.70 for both cases. It was further observed that the correlation coefficient is slightly higher for the tools from the same vendor than those of the tools from different vendors. For Case 1, for example, the correlation coefficient between the random scattering errors associated with the ILI tools of 2004 and 2011, which are from the same vendor, is 0.82, whereas the correlation coefficient is 0.70 between the ILI tools of 2004 and 2007, which are from different vendors.

Any number of ILI tools can be calibrated simultaneously using the proposed Bayesian model. The model will assist the ILI vendors in improving the sizing algorithms of the ILI tools used on a particular pipeline, and facilitate the development of a reliable corrosion growth model based on ILI data by accurately quantifying the measurement errors of the ILI tools as well as the correlation between the measurement errors of different tools.

5.3 Hierarchical Bayesian Corrosion Growth Model Based on In-line Inspection Data

In Chapter 3, a defect-specific growth model was developed to predict the depth of individual corrosion defect on underground energy pipelines. A power-law growth path over time, characterized by two power-law coefficients and the defect initiation time, was

assumed for the depths of active corrosion defects on pipeline. The parameters of the growth model were evaluated based on the data obtained from multiple in-line inspections using the hierarchical Bayesian method. The model was formulated to account for the constant and non-constant biases and random scattering errors of the ILI data, as well as the potential correlation between the random scattering errors associated with different ILI tools. The MCMC simulation was carried out to make statistical inference of the model parameters.

Two case studies, involving ILI data for corrosion defects on two natural gas pipelines currently in service, were carried out to illustrate the application of the proposed growth model. In Case 1, the growth models for 62 external corrosion defects were developed based on the corresponding ILI data obtained in 2000, 2004 and 2007, whereas the growth models for 60 external corrosion defects were developed based on the corresponding ILI data obtained in 2004, 2007 and 2009 in Case 2. The measurement errors associated with the ILI tools as well as the correlation coefficient between the measurement errors of different ILI tools were obtained from the Bayesian calibration model described in Chapter 2. To validate the growth model, the depths of the 62 defects of Case 1 in 2010 were predicted using the growth models and compared with the corresponding defect depths obtained from field measurements carried out in 2010, assuming that the field measurements are error free. For Case 2, the depths of the 60 defects in 2011 were predicted using the growth models and compared with the corresponding field-measured depths in 2011.

The comparison suggests that the growth model can predict the actual depth of the defect reasonable well; for example, 89% and 78% of the predicted depths fall within the bounds of actual depth $\pm 10\%$ *wt* in Cases 1 and 2, respectively. Because the measurement error associated with pinholes and circumferential grooving type of defects is relatively larger (Maes et al. 2008), the prediction was found to be relatively poor for these types of defects.

To examine the merit of accounting for the correlations among the random scattering errors associated with different ILI tools in the growth model, two additional analyses were performed considering fully-correlated and independent scattering errors respectively. The mean squared error of prediction (MESP) was adopted as a metric to evaluate the predictive accuracies of the models with partially-correlated (with the correlation coefficient obtained from Bayesian calibration), fully-correlated and independent random scattering errors among different ILI tools. The results indicate that the predictive accuracy is higher for the model with partially-correlated random scattering errors (i.e. the corresponding MSEP is lower) as compared to the models with fully-correlated and independent random scattering errors. Furthermore, hypothesis testing was carried out to examine the statistical significance of the difference in MSEP's of different models. The results suggest that the difference in MESP's of the models with fully-correlated and partially-correlated scattering errors is statistically significant for Case 2, whereas the difference in MESP's of the models with independent and partially-correlated scattering errors is statistically insignificant for both Case 1 and Case 2. Therefore, it is recommended to assume the random scattering errors between different

ILI tools to be independent of each other, if the partial correlations between the scattering errors are not quantified.

The predictive accuracy of the Bayesian hierarchical power-law growth model was compared with that of the linear growth model commonly used in the pipeline industry. It was found that the prediction of the proposed model is more accurate than that of the linear growth model. For example, 78% of the predicted depths fall within the $\pm 10\%$ *w*t bounding lines based on the power-law growth model, compared with about 65% of the predicted depths falling within the same bounding lines based on the linear growth model for the 60 defects considered in Case 2.

The proposed growth model will facilitate the application of defect-based pipeline corrosion management program by maintaining the structural integrity of the pipelines while achieving optimal allocation of the limited resources for maintenance.

5.4 Time-dependent System Reliability Analysis of a Corroding Pipeline

In Chapter 4, a methodology was developed to evaluate the time-dependent system reliability of a segment of a pressurized pipeline containing multiple active corrosion defects. A defect-specific power-law model was employed to characterize the growth of the depth of individual corrosion defect, whereas the length of the defect was assumed to grow in a linear fashion. The parameters of the power-law model were evaluated from the Bayesian updating based on the data from multiple in-line inspections. A combination of the conventional Monte Carlo simulation and Markov Chain Monte Carlo simulation techniques was employed to evaluate the failure probabilities of the pipeline

segment in terms of three distinctive failure modes, namely small leak, large leak and rupture.

The proposed methodology was demonstrated using a numerical example whereby the time-dependent system reliability of a joint of an in-service underground natural gas pipeline containing ten active external corrosion defects was evaluated. The burst and rupture pressure capacity models recommended in Annex O of the Canadian pipeline standard CSA Z662-07 (CSA 2007) were adopted in this study. The impact on the system reliability due to the correlation between the model errors associated with the burst capacity models at different defects and the correlation of maximum-to-average depth ratios for different defects was investigated in two sensitivity analyses. The results suggest that the probability of large leak is sensitive to the correlation between the model errors in that independent model errors result in markedly higher probability of large leak than fully-correlated model errors. On the other hand, the probability of small leak is insensitive to the correlation between the model errors. The results also indicate that the correlation between the maximum-to-average depth ratios for different defects has a negligible impact on the failure probability of the pipe joint.

5.5 Recommendations for Future Work

The recommended work for future investigations includes the following.

1. Further investigations are needed to quantify the measurement errors of the ILI tool for specific types of defects (e.g. pinholes and circumferential grooving type of defects) to improve the predictive accuracy of the defect growth model.

2. The potential spatial correlations among the defects of close proximity need to be investigated and incorporated in the corrosion growth model.
3. Because external corrosion on underground pipelines is largely influenced by the protective coating on the pipeline and characteristics of the surrounding soils, the corrosion growth model can be improved by incorporating the properties of the coating and surrounding soils (e.g. soil type, water content, pH value, etc.) in the model.
4. Research is needed to characterize the growth of the length of individual corrosion defect based on the ILI data.
5. Due to the unavailability of field measurements for internal corrosion defects, the corrosion growth model proposed in this study was validated for external corrosion defects only; therefore, further studies should be carried out to validate the model for internal corrosion on pipeline.

References

CSA, 2007. *CSA-Z662 Oil and Gas Pipeline Systems*. Canadian Standards Associations, Rexdale, Ontario.

Jaech, J. L., 1985. *Statistical analysis of measurement errors*. Jhon Wiley & Sons, Inc., New York, NY, USA.

Maes, M. A., Dann, M. R., Breitung, K. W., and Brehm, E., 2008. Hierarchical modeling of stochastic deterioration. *Proceedings of the 6th international probabilistic workshop* Eds C.A. Graubner, H. Schmidt, D. Proske, T.U. Darmstadt, pp. 111-124.

Appendix 2A Algorithms for Performing Markov Chain Monte Carlo Simulation

2A.1 Metropolis-Hastings Algorithm

The Metropolis-Hastings (M-H) algorithm is the most general Markov chain based simulation technique. The algorithm was first introduced and formulated by Metropolis et al. (1953) and later generalized by Hastings (1970). This simulation method is applicable to any distribution types including multivariate distributions and suitable for the high dimensional Bayesian models. The Metropolis-Hastings algorithm uses two distributions, namely the proposal or jumping distribution (Chib and Greenberg 1995) and the stationary or target distribution that is the posterior distribution in this study. The initial value of the parameter of interest θ is chosen arbitrarily and denoted as $\theta^{(0)}$. At each iteration i , the value of θ in the next iteration, $\theta^{(i+1)}$, is chosen by generating a candidate value θ^* from the proposal distribution $\pi(\bullet|\theta^{(i)})$, and checking if θ^* will be accepted as $\theta^{(i+1)}$ based on the acceptance criterion. If the candidate value is accepted then $\theta^{(i+1)}$ is set as θ^* , otherwise $\theta^{(i+1)} = \theta^i$. The acceptance function is defined as,

$$\phi(\theta^{(i)}, \theta^*) = \min\left(1, \frac{p(\theta^*)\pi(\theta^{(i)}|\theta^*)}{p(\theta^{(i)})\pi(\theta^*|\theta^{(i)})}\right) \quad (2A.1)$$

where $\phi(\theta^{(i)}, \theta^*)$ is the probability of accepting θ^* as an updated value of $\theta^{(i)}$ at step i , and $p(\bullet)$ is the probability density function of the target distribution (i.e. posterior distribution).

If the posterior probability is larger for the candidate value (θ^*) than the current value ($\theta^{(i)}$), i.e. numerator is higher than the denominator in Eq. (2A.1), the candidate value

will be automatically accepted in the next iteration, i.e. $\theta^{(i+1)} = \theta^*$. However, even if ϕ is less than unity, the candidate value may still be accepted. This is determined by drawing a random sample from a standard uniform distribution, $U(0,1)$, and comparing the sample with ϕ . The M-H algorithm is summarized as follows:

1. Select the initial value $\theta^{(0)}$ and set $\theta^{(1)} = \theta^{(0)}$;
2. for $i = 1, 2, 3, \dots, N$, repeat the following steps:
 - a. generate a candidate value θ^* from the proposal distribution conditional on the current value, i.e. $\pi(\bullet|\theta^{(i)})$;
 - b. calculate the acceptance ratio as follows:
$$\phi = \min\left(1, \frac{p(\theta^*)\pi(\theta^{(i)}|\theta^*)}{p(\theta^{(i)})\pi(\theta^*|\theta^{(i)})}\right)$$
 - c. draw a random sample ζ from a standard uniform distribution $U(0, 1)$, and
 - d. if $\phi \geq \zeta$, set $\theta^{(i+1)} = \theta^*$; otherwise $\theta^{(i+1)} = \theta^{(i)}$.

The proposal distribution can take any form. But the proper choice of the proposal distribution will increase the rate of convergence to the target distribution and reduce the autocorrelation between the generated samples. Most commonly used proposal distributions are the uniform, normal and student t distributions.

Recall the example of count data in Section 2.2.1. Assume that $\mathbf{y} = (1, 3, 2)$ are the count data, and that the shape and scale parameters of the gamma prior distribution for the count rate λ are $\kappa = 2$ and $\theta = 2$, respectively. Now we will generate MCMC samples for λ using the M-H algorithm. Consider a normal distribution with a variance of unity as the proposal distribution.

The target distribution is $p(\lambda) \propto e^{-(n+\theta)\lambda} \lambda^{n\bar{y}+\kappa-1} \propto e^{-5\lambda} \lambda^7$

The proposal distribution is $\pi(x|m, 1) \propto e^{-\frac{1}{2}(x-m)^2}$

The algorithm proceeds as follows:

- Assume an initial value $\lambda^{(0)} = 2.0$ and set $\lambda^{(1)} = 2.0$;
- for $i = 1$
 - draw a candidate sample λ^* from $\pi(\lambda^* | \lambda^{(1)}, 1)$, i.e. $N(2.0, 1.0)$; $\lambda^* = 1.82$;
 - calculate $\phi = \min\left(1, \frac{e^{-5(\lambda^*)}(\lambda^*)^7 \times e^{-\frac{1}{2}(\lambda^{(1)}-\lambda^*)^2}}{e^{-5(\lambda^{(1)})}(\lambda^{(1)})^7 \times e^{-\frac{1}{2}(\lambda^*-\lambda^{(1)})^2}}\right)$; $\phi = 1.0$;
 - generate ζ from $U(0, 1)$; $\zeta = 0.35$, and
 - as $\phi \geq \zeta$, λ^* is accepted; $\lambda^{(2)} = \lambda^* = 1.82$, then the chain of λ becomes

$$\lambda = \begin{bmatrix} \lambda^{(1)} \\ \lambda^{(2)} \end{bmatrix} = \begin{bmatrix} 2.00 \\ 1.82 \end{bmatrix}$$

- for $i = 2$
 - draw a candidate sample λ^* from $N(1.82, 1)$; $\lambda^* = 3.24$;
 - calculate $\phi = \min\left(1, \frac{e^{-5(\lambda^*)}(\lambda^*)^7 \times e^{-\frac{1}{2}(\lambda^{(1)}-\lambda^*)^2}}{e^{-5(\lambda^{(1)})}(\lambda^{(1)})^7 \times e^{-\frac{1}{2}(\lambda^*-\lambda^{(1)})^2}}\right)$; $\phi = 0.05$;
 - generate ζ from $U(0, 1)$; $\zeta = 0.59$, and
 - as $\phi < \zeta$, the candidate point is rejected; $\lambda^{(3)} = \lambda^{(2)} = 1.82$, then the chain of λ becomes

$$\lambda = \begin{bmatrix} \lambda^{(1)} \\ \lambda^{(2)} \\ \lambda^{(3)} \end{bmatrix} = \begin{bmatrix} 2.00 \\ 1.82 \\ 1.82 \end{bmatrix}$$

The cycle continues for $i = 3, 4, \dots, N$ to generate N number of samples of λ .

2A.2 Gibbs Sampler

The Gibbs sampler (Gelfand and Smith 1990; Geman and Geman 1984; Gilks et al. 1993) is a special case of the Metropolis-Hastings algorithm. This sampling method is applicable where the full conditional distributions of the parameters are available in known distribution forms. The full conditional distribution can be written as $p(\theta_j | \boldsymbol{\theta}_{(-j)}, \mathbf{X})$, where $\boldsymbol{\theta}_{(-j)} = (\theta_1, \dots, \theta_{j-1}, \theta_{j+1}, \dots, \theta_k)$, where k is the total number of parameters. In Gibbs sampling approach, the full conditional distribution is used as the proposal distribution, so that the acceptance rate ϕ becomes unity; therefore, the candidate sample will always be accepted. The main advantages of Gibbs sampler are that it does not require specification of the proposal distribution; it is highly efficient in getting convergence as each candidate value is accepted, and the implementation is very easy due to the use of closed form distributions. The sampling procedure using Gibbs sampler is described below.

Suppose the joint distribution of $\boldsymbol{\theta} = (\theta_1, \theta_2, \dots, \theta_k)$ is uniquely determined by the full conditional distributions, $p_j(\theta_j | \boldsymbol{\theta}_{(-j)}, \mathbf{X})$ ($j = 1, 2, \dots, k$). Set the initial values as $\boldsymbol{\theta}^{(0)} = (\theta_1^{(0)}, \theta_2^{(0)}, \dots, \theta_k^{(0)})$. For each iteration i ($i = 1, 2, \dots, N$) do the following:

(1) Draw $\theta_1^{(i)}$ from $p_1(\theta_1 | \theta_2^{(i-1)}, \theta_3^{(i-1)}, \dots, \theta_k^{(i-1)}, \mathbf{X})$;

(2) draw $\theta_2^{(i)}$ from $p_2(\theta_2 | \theta_1^{(i)}, \theta_3^{(i-1)}, \dots, \theta_k^{(i-1)}, \mathbf{X})$;

(3) draw $\theta_3^{(i)}$ from $p_3(\theta_3 | \theta_1^{(i)}, \theta_2^{(i)}, \theta_4^{(i-1)}, \dots, \theta_k^{(i-1)}, \mathbf{X})$;

...

- ...
- (j) draw $\theta_j^{(i)}$ from $p_j(\theta_j | \theta_1^{(i)}, \theta_2^{(i)}, \dots, \theta_{j-1}^{(i)}, \theta_{j+1}^{(i-1)}, \dots, \theta_k^{(i-1)}, \mathbf{X})$;
- ...
- ...
- (k) draw $\theta_k^{(i)}$ from $p_k(\theta_k | \theta_1^{(i)}, \theta_2^{(i)}, \dots, \theta_{k-1}^{(i)}, \mathbf{X})$;

Let's consider a simple fixed effect linear model $y_i = \mu + \varepsilon_i$, where ε_i follows a normal distribution with zero mean and variance of σ_ε^2 , i.e. $\varepsilon_i \sim N(0, \sigma_\varepsilon^2)$. Assume that the prior distributions of μ and σ_ε^2 follow a normal and an inverse-gamma distribution, respectively. Therefore, the model can be summarized as follows:

$$\text{Likelihood of data: } p(y_i | \mu, \sigma_\varepsilon^2) = \prod_{i=1}^n \frac{1}{\sqrt{2\pi}\sigma_\varepsilon} \exp\left(-\frac{1}{2}\left(\frac{y_i - \mu}{\sigma_\varepsilon}\right)^2\right)$$

$$\text{Prior distribution of } \mu: p(\mu) = \frac{1}{\sqrt{2\pi}b} \exp\left(-\frac{1}{2}\left(\frac{\mu - a}{b}\right)^2\right)$$

$$\text{Prior distribution of } \sigma_\varepsilon^2: p(\sigma_\varepsilon^2) = \frac{1}{(\sigma_\varepsilon^2)^{c+1}} \exp\left(-\frac{d}{\sigma_\varepsilon^2}\right)$$

$$\text{The joint posterior distribution of } \mu \text{ and } \sigma_\varepsilon^2: p(\mu, \sigma_\varepsilon^2 | y_i) = \prod_{i=1}^n p(y_i | \mu, \sigma_\varepsilon^2) p(\mu) p(\sigma_\varepsilon^2)$$

where a and b are the mean and standard deviation of the normal prior distribution of μ ; c and d are the shape and scale parameters of the inverse-gamma prior distribution of σ_ε^2 . a , b , c and d are called the *hyper-parameters* of the model and are all known quantities.

The full conditional distributions of μ and σ_ε^2 can be evaluated as follows:

$$\begin{aligned}
p(\mu|\sigma_\varepsilon^2, y_i) &\propto \prod_{i=1}^n p(y_i|\mu, \sigma_\varepsilon^2)p(\mu) \\
&\propto \prod_{i=1}^n \left(\frac{1}{\sigma_\varepsilon} \exp\left(-\frac{1}{2}\left(\frac{y_i-\mu}{\sigma_\varepsilon}\right)^2\right) \right) \left(\frac{1}{b} \exp\left(-\frac{1}{2}\left(\frac{\mu-a}{b}\right)^2\right) \right) \\
&\propto \exp\left[-\frac{1}{2}\left\{\frac{1}{\sigma_\varepsilon^2}\sum_{i=1}^n (y_i - \mu)^2 + \frac{1}{b^2}(\mu - a)^2\right\}\right] \\
&\propto \exp\left[-\frac{1}{2}\left\{\frac{\mu^2(nb^2+\sigma_\varepsilon^2)-2\mu(b^2\sum_{i=1}^n y_i+a\sigma_\varepsilon^2)}{\sigma_\varepsilon^2 b^2}\right\}\right]
\end{aligned}$$

and

$$\begin{aligned}
p(\sigma_\varepsilon^2|\mu, y_i) &\propto p(y_i|\mu, \sigma_\varepsilon^2)p(\sigma_\varepsilon^2) \\
&\propto \prod_{i=1}^n \left(\frac{1}{\sqrt{\sigma_\varepsilon^2}} \exp\left(-\frac{1}{2}\left(\frac{y_i-\mu}{\sigma_\varepsilon}\right)^2\right) \right) \left(\frac{1}{(\sigma_\varepsilon^2)^{c+1}} \exp\left(-\frac{d}{\sigma_\varepsilon^2}\right) \right) \\
&\propto \left(\frac{1}{\sqrt{\sigma_\varepsilon^2}}\right)^n \frac{1}{(\sigma_\varepsilon^2)^{c+1}} \exp\left(-\frac{1}{2}\frac{1}{\sigma_\varepsilon^2}\sum_{i=1}^n (y_i - \mu)^2 - \frac{d}{\sigma_\varepsilon^2}\right) \\
&\propto (\sigma_\varepsilon^2)^{-\frac{n}{2}-c-1} \exp\left(-\frac{\sum_{i=1}^n (y_i-\mu)^2+2d}{2\sigma_\varepsilon^2}\right)
\end{aligned}$$

From the above we can conclude that

$$p(\mu|\sigma_\varepsilon^2, y_i) \sim N\left(\frac{b^2\sum_{i=1}^n y_i+a\sigma_\varepsilon^2}{nb^2+\sigma_\varepsilon^2}, \frac{\sigma_\varepsilon^2 b^2}{nb^2+\sigma_\varepsilon^2}\right) \quad (2A.2)$$

$$p(\sigma_\varepsilon^2|\mu, y_i) \sim IG\left(\frac{n}{2} + c, \frac{\sum_{i=1}^n (y_i-\mu)^2+2d}{2}\right) \quad (2A.3)$$

Once the full conditional distributions are available the MCMC samples can be generated using the Gibbs sampler that is outlined below:

- Set the initial values $\mu^{(0)}$ and $(\sigma_\varepsilon^2)^{(0)}$;
- for $t = 1, 2, \dots, N$ do the following steps:
 - generate $\mu^{(t)}$ from $N\left(\frac{b^2 \sum_{i=1}^n y_i + a(\sigma_\varepsilon^2)^{(t-1)}}{nb^2 + (\sigma_\varepsilon^2)^{(t-1)}}, \frac{(\sigma_\varepsilon^2)^{(t-1)}b^2}{nb^2 + (\sigma_\varepsilon^2)^{(t-1)}}\right)$;
 - generate $(\sigma_\varepsilon^2)^{(t)}$ from $IG\left(\frac{n}{2} + c, \frac{\sum_{i=1}^n (y_i - \mu^{(t)})^2 + 2d}{2}\right)$;

For a given Bayesian method, the full conditional distributions of the parameters of the model are not necessarily all closed-form distributions in most of the cases. In such a case a combination of Metropolis-Hastings and Gibbs sampler, which is known as Metropolis within Gibbs procedure (Ntzoufras 2011), is used, whereby Gibbs sampler is used to generate samples for the parameters with closed-form full conditional distributions and Metropolis-Hastings is used for the rest of the parameters.

References

- Chib, S., and Greenberg, E., 1995. Understanding the Metropolis-Hastings Algorithm. *The American Statistician*, 49(4), pp. 327-335.
- Gelfand, A., and Smith, A., 1990. Sampling-Based Approaches to Calculating Marginal Densities. *Journal of the American Statistical Association*, 85(410), pp. 398-409.
- Geman, S., and Geman, D., 1984. Stochastic relaxation, Gibbs distributions, and the Bayesian restoration of images. *IEEE Trans. Pattern Anal. Mach. Intell.*, 6, pp. 721-741.
- Gilks, W. R., Wang, C. C., Yvonnet, B., and Coursaget, P., 1993. Random-Effects Models for Longitudinal Data Using Gibbs Sampling. *Biometrics*, 49(2), pp. 441-453.
- Hastings, W. K., 1970. Monte Carlo sampling methods using Markov chains and their applications. *Biometrika*, 57(1), pp. 97-109.
- Hoff, P. D., 2009. *A First Course in Bayesian Statistical Methods*. Springer, New York, NY, USA.

Metropolis, N., Rosenbluth, A., Rosenbluth, M., Teller, A., and Teller, E., 1953. Equation of State Calculations by Fast Computing Machines. *The Journal of Chemical Physics*, 21(6), pp. 1087-1092.

Ntzoufras, I., 2011. *Bayesian Modeling Using WinBUGS*. John Wiley & Sons, Hoboken, New Jersey, USA.

Appendix 2B Grubbs' Estimator and Jaech's Estimator

2B.1 Grubbs' Estimator

The statistical approach to quantify the random scattering measurement errors associated with two measuring devices was first introduced by Grubbs (1948). The methodology uses the method of moment to estimate the variance of the random scattering measurement error associated with each tool. The methodology is described below.

Consider that a given parameter (e.g. depth of a corrosion defect) is measured by two different measuring tools, Tool 1 and Tool 2 for m different items (e.g. defects). The relationships between the actual and measured values of the parameter are as follows:

$$y_{1i} = x_i + \varphi_{1i} \quad (2B.1a)$$

$$y_{2i} = x_i + \varphi_{2i} \quad (2B.1b)$$

where y_{1i} and y_{2i} ($i = 1, 2, \dots, m$) are the measurements reported by Tool 1 and Tool 2, respectively, for item i ; φ_{1i} and φ_{2i} are the random scattering errors associated with Tool 1 and Tool 2, respectively, and x_i is the actual value of item i . It is assumed that 1) φ_{1i} and φ_{2i} are independent of each other and also among themselves; 2) φ_{1i} and φ_{2i} are independent of x_i , and 3) the mean values of φ_{1i} and φ_{2i} are zero.

If m is sufficiently large, the variances of the random scattering errors associated with the two tools can be estimated as follows:

$$\sigma_{\varphi_1}^2 = s_1^2 - s_{12} \quad (2B.2a)$$

$$\sigma_{\varphi 2}^2 = s_2^2 - s_{12} \quad (2B.2b)$$

where $\sigma_{\varphi 1}^2$ and $\sigma_{\varphi 2}^2$ are the estimated variances of random scattering errors associated with Tool 1 and Tool 2, respectively; s_1^2 and s_2^2 are the sample variances of y_{1i} and y_{2i} , respectively, and s_{12} is the sample covariance between y_{1i} and y_{2i} .

For m measured items the unbiased sample variances and covariance are given as follows:

$$s_1^2 = \frac{1}{m-1} \left[\sum_{i=1}^m (y_{1i})^2 - \frac{1}{m} (\sum_{i=1}^m y_{1i})^2 \right] \quad (2B.3a)$$

$$s_2^2 = \frac{1}{m-1} \left[\sum_{i=1}^m (y_{2i})^2 - \frac{1}{m} (\sum_{i=1}^m y_{2i})^2 \right] \quad (2B.3b)$$

$$s_{12} = \frac{1}{m-1} \left[\sum_{i=1}^m (y_{1i})(y_{2i}) - \frac{1}{m} (\sum_{i=1}^m y_{1i})(\sum_{i=1}^m y_{2i}) \right] \quad (2B.3c)$$

2B.2 Jaech's Estimator

Grubbs' method results in negative value of the variance of random scattering error, which is unrealistic, if the sample covariance is greater than the sample variance (i.e. $s_1^2 < s_{12}$ or $s_2^2 < s_{12}$). To overcome this problem, Jaech (1985) introduced the so-called constrained expected likelihood (CEL) estimation method to estimate the variances of the random measurement errors, whereby the expectation of the variance is restricted to the space of nonnegative values only. In this estimation process a proportion quantity ν is defined such that the total scatter is distributed to each tool in the proportion of ν and $1-\nu$. The quantity ν is bounded between 0 and 1 to ensure that the variance of the measurement error is greater than zero for each tool for all values of ν .

Let S denote the total scatter associated with both tools. Therefore the quantity v is defined such that

$$\sigma_{\varphi_1}^2 = vS; \quad 0 \leq v \leq 1 \quad (2B.4a)$$

$$\sigma_{\varphi_2}^2 = (1 - v)S \quad (2B.4b)$$

The total scatter S can be calculated from the sample variances and covariance as follows:

$$S = \frac{m-1}{m}(s_1^2 + s_2^2 - s_{12}) \quad (2B.5)$$

Based on the likelihood function the so-called sharing function, $f(v)$, can be derived as follows (Jaech 1985):

$$f(v) = \left[\frac{mSv^2}{m-1} + 2v(s_{12} - s_1^2) + s_1^2 \right]^{-0.5m} \quad (2B.6)$$

The estimates of $\sigma_{\varphi_1}^2$ and $\sigma_{\varphi_2}^2$ can be then obtained as follows:

$$\sigma_{\varphi_1}^2 = \frac{\int_0^1 v f(v) dv}{\int_0^1 f(v) dv} \quad (2B.7)$$

$$\sigma_{\varphi_2}^2 = \frac{\int_0^1 (1-v) f(v) dv}{\int_0^1 f(v) dv} = S - \sigma_{\varphi_1}^2 \quad (2B.8)$$

References

Grubbs, F. E., 1948. On Estimating Precision of Measuring Instruments and Product Variability. *Journal of the American Statistical Association*, 43(242), pp. 243-264.

Jaech, J. L., 1985. *Statistical analysis of measurement errors*. Jhon Wiley & Sons, Inc., New York, NY, USA.

Appendix 2C Derivation of the Conditional Posterior Distributions of Parameters of Bayesian Calibration Model

1. $\alpha_1, \alpha_2, \dots, \alpha_n$

Likelihood: $\mathbf{d}\mathbf{m}_i \sim MVN(\boldsymbol{\alpha} + \boldsymbol{\beta}da_i, \boldsymbol{\Sigma}_\varepsilon)$

Prior distribution: $\alpha_1, \alpha_2, \dots, \alpha_n \stackrel{iid}{\sim} N(a, b^2)$

where $\boldsymbol{\alpha} = (\alpha_1, \alpha_2, \dots, \alpha_n)^T$ and $\boldsymbol{\beta} = (\beta_1, \beta_2, \dots, \beta_n)^T$.

Therefore, the posterior distribution of α_i is as follows:

$$\begin{aligned}
 p(\alpha_1 | \bullet) &\propto \prod_{i=1}^m p(\mathbf{d}\mathbf{m}_i | \bullet) p(\alpha_1) \\
 &\propto \prod_{i=1}^m (2\pi)^{-\frac{n}{2}} |\boldsymbol{\Sigma}_\varepsilon|^{-\frac{1}{2}} \exp \left[-\frac{1}{2} \{ \mathbf{d}\mathbf{m}_i - (\boldsymbol{\alpha} + \boldsymbol{\beta}da_i) \}^T \boldsymbol{\Sigma}_\varepsilon^{-1} \{ \mathbf{d}\mathbf{m}_i - (\boldsymbol{\alpha} + \boldsymbol{\beta}da_i) \} \right] \times \\
 &\quad \frac{1}{\sqrt{2\pi}b} \exp \left[-\frac{1}{2} \frac{(\alpha_1 - a)^2}{b^2} \right] \\
 &\propto \exp \left[-\frac{1}{2} \sum_{i=1}^m \{ (\mathbf{d}\mathbf{m}_i - \boldsymbol{\beta}da_i) - \boldsymbol{\alpha} \}^T \boldsymbol{\Sigma}_\varepsilon^{-1} \{ (\mathbf{d}\mathbf{m}_i - \boldsymbol{\beta}da_i) - \boldsymbol{\alpha} \} \right] \times \exp \left[-\frac{1}{2} \frac{(\alpha_1^2 - 2\alpha_1 a)}{b^2} \right] \\
 &\propto \exp \left[-\frac{1}{2} \sum_{i=1}^m \{ (\mathbf{d}\mathbf{m}_i - \boldsymbol{\beta}da_i)^T \boldsymbol{\Sigma}_\varepsilon^{-1} (\mathbf{d}\mathbf{m}_i - \boldsymbol{\beta}da_i) - (\mathbf{d}\mathbf{m}_i - \boldsymbol{\beta}da_i)^T \boldsymbol{\Sigma}_\varepsilon^{-1} \boldsymbol{\alpha} - \right. \\
 &\quad \left. \boldsymbol{\alpha}^T \boldsymbol{\Sigma}_\varepsilon^{-1} (\mathbf{d}\mathbf{m}_i - \boldsymbol{\beta}da_i) + \boldsymbol{\alpha}^T \boldsymbol{\alpha} \} \right] \times \exp \left[-\frac{1}{2} \frac{(\alpha_1^2 - 2\alpha_1 a)}{b^2} \right] \\
 &\propto \exp \left[-\frac{1}{2} \sum_{i=1}^m \{ \boldsymbol{\alpha}^T \boldsymbol{\alpha} - 2\boldsymbol{\alpha}^T \boldsymbol{\Sigma}_\varepsilon^{-1} (\mathbf{d}\mathbf{m}_i - \boldsymbol{\beta}da_i) \} - \frac{1}{2} \frac{(\alpha_1^2 - 2\alpha_1 a)}{b^2} \right]
 \end{aligned}$$

Now consider $(\mathbf{d}\mathbf{m}_i - \boldsymbol{\beta}da_i) = (x_{i1}, x_{i2}, \dots, x_{in})^T$ and

$$\boldsymbol{\Sigma}_\varepsilon^{-1} = \begin{bmatrix} C_{11} & C_{12} & \cdots & C_{1n} \\ C_{21} & C_{22} & \cdots & C_{2n} \\ \vdots & \vdots & \ddots & \vdots \\ C_{n1} & C_{n2} & \cdots & C_{nn} \end{bmatrix}$$

So,

$$p(\alpha_1|\bullet) \propto \exp \left[-\frac{1}{2} \sum_{i=1}^m \{ \alpha_1^2 + \alpha_2^2 + \cdots + \alpha_n^2 - 2(\alpha_1 C_{11} x_{i1} + \alpha_2 C_{21} x_{i1} + \cdots + \alpha_n C_{n1} x_{i1} + \alpha_1 C_{12} x_{i2} + \alpha_2 C_{22} x_{i2} + \cdots + \alpha_n C_{n2} x_{i2} + \cdots + \alpha_1 C_{1n} x_{in} + \alpha_2 C_{2n} x_{in} + \cdots + \alpha_n C_{nn} x_{in}) \} - \frac{1}{2} \frac{(\alpha_1^2 - 2\alpha_1 a)}{b^2} \right]$$

$$\propto \exp \left[-\frac{1}{2} \sum_{i=1}^m \{ \alpha_1^2 - 2\alpha_1 (C_{11} x_{i1} + C_{12} x_{i2} + \cdots + C_{1n} x_{in}) \} - \frac{1}{2} \frac{(\alpha_1^2 - 2\alpha_1 a)}{b^2} \right]$$

$$\propto \exp \left[-\frac{1}{2} \left\{ \left(m + \frac{1}{b^2} \right) \alpha_1^2 - 2\alpha_1 \left(\sum_{i=1}^m (C_{11} x_{i1} + C_{12} x_{i2} + \cdots + C_{1n} x_{in}) + \frac{a}{b^2} \right) \right\} \right]$$

$$\propto \exp \left[-\frac{1}{2} \left\{ \left(m + \frac{1}{b^2} \right) \alpha_1^2 - 2\alpha_1 \left(\sum_{i=1}^m (C_{11} (dm_{i1} - \beta_1 da_i) + C_{12} (dm_{i2} - \beta_2 da_i) + \cdots + C_{1n} (dm_{in} - \beta_n da_i)) + \frac{a}{b^2} \right) \right\} \right]$$

Therefore, $\alpha_1 \sim N \left(\left(m + \frac{1}{b^2} \right)^{-1} \left(\sum_{i=1}^m (C_{11} (dm_{i1} - \beta_1 da_i) + C_{12} (dm_{i2} - \beta_2 da_i) + \right. \right.$

$$\left. \left. C_{1n} (dm_{in} - \beta_n da_i) \right) + \frac{a}{b^2} \right), \left(m + \frac{1}{b^2} \right)^{-1}$$

Similarly for $j = 2, 3, \dots, n$ the posterior distribution of α_j is

$$\alpha_j \sim N \left(\left(m + \frac{1}{b^2} \right)^{-1} \left(\sum_{i=1}^m (C_{j1} (dm_{i1} - \beta_1 da_i) + C_{j2} (dm_{i2} - \beta_2 da_i) + \right. \right.$$

$$\left. \left. C_{jn} (dm_{in} - \beta_n da_i) \right) + \frac{a}{b^2} \right), \left(m + \frac{1}{b^2} \right)^{-1}$$

2. $\beta_1, \beta_2, \dots, \beta_n$

Likelihood: $\mathbf{d}\mathbf{m}_i \sim MVN(\boldsymbol{\alpha} + \boldsymbol{\beta} da_i, \boldsymbol{\Sigma}_\varepsilon)$

Prior distribution: $\beta_1, \beta_2, \dots, \beta_n \stackrel{iid}{\sim} Be(c, d, l, u)$

Therefore, the posterior distribution of β_1 is as follows:

$$\begin{aligned}
p(\beta_1 | \bullet) &\propto \prod_{i=1}^m p(\mathbf{d}\mathbf{m}_i | \bullet) p(\beta_1) \\
&\propto \prod_{i=1}^m (2\pi)^{-\frac{n}{2}} |\boldsymbol{\Sigma}_\varepsilon|^{-\frac{1}{2}} \exp \left[-\frac{1}{2} \{ \mathbf{d}\mathbf{m}_i - (\boldsymbol{\alpha} + \boldsymbol{\beta} da_i) \}^T \boldsymbol{\Sigma}_\varepsilon^{-1} \{ \mathbf{d}\mathbf{m}_i - (\boldsymbol{\alpha} + \boldsymbol{\beta} da_i) \} \right] \times \\
&\quad \frac{1}{B(c, d)} \frac{(\beta_1 - l)^{c-1} (u - \beta_1)^{d-1}}{(u - l)^{c+d-1}} \\
&\propto \exp \left[-\frac{1}{2} \sum_{i=1}^m \{ (\mathbf{d}\mathbf{m}_i - \boldsymbol{\alpha}) - \boldsymbol{\beta} da_i \}^T \boldsymbol{\Sigma}_\varepsilon^{-1} \{ (\mathbf{d}\mathbf{m}_i - \boldsymbol{\alpha}) - \boldsymbol{\beta} da_i \} \right] \times (\beta_1 - l)^{c-1} \times \\
&\quad (u - \beta_1)^{d-1} \\
&\propto \exp \left[-\frac{1}{2} \sum_{i=1}^m \{ (\mathbf{d}\mathbf{m}_i - \boldsymbol{\alpha})^T \boldsymbol{\Sigma}_\varepsilon^{-1} (\mathbf{d}\mathbf{m}_i - \boldsymbol{\alpha}) - (\mathbf{d}\mathbf{m}_i - \boldsymbol{\alpha})^T \boldsymbol{\Sigma}_\varepsilon^{-1} \boldsymbol{\beta} da_i - \right. \\
&\quad \left. (\boldsymbol{\beta} da_i)^T \boldsymbol{\Sigma}_\varepsilon^{-1} (\mathbf{d}\mathbf{m}_i - \boldsymbol{\alpha}) + (\boldsymbol{\beta} da_i)^T (\boldsymbol{\beta} da_i) \} \right] \times (\beta_1 - l)^{c-1} (u - \beta_1)^{d-1} \\
&\propto \exp \left[-\frac{1}{2} \sum_{i=1}^m \{ (\boldsymbol{\beta} da_i)^T (\boldsymbol{\beta} da_i) - 2(\boldsymbol{\beta} da_i)^T \boldsymbol{\Sigma}_\varepsilon^{-1} (\mathbf{d}\mathbf{m}_i - \boldsymbol{\alpha}) \} \right] \times (\beta_1 - l)^{c-1} \times \\
&\quad (u - \beta_1)^{d-1} \\
&\propto \exp \left[-\frac{1}{2} \sum_{i=1}^m da_i \{ \beta_1^2 da_i - 2\beta_1 (C_{11}(dm_{i1} - \alpha_1) + C_{12}(dm_{i2} - \alpha_2) + \dots + \right. \\
&\quad \left. C_{1n}(dm_{in} - \alpha_n)) \} \right] \times (\beta_1 - l)^{c-1} (u - \beta_1)^{d-1}
\end{aligned}$$

$$\text{where } \Sigma_{\varepsilon}^{-1} = \begin{bmatrix} C_{11} & C_{12} & \cdots & C_{1n} \\ C_{21} & C_{22} & \cdots & C_{2n} \\ \vdots & \vdots & \ddots & \vdots \\ C_{n1} & C_{n2} & \cdots & C_{nn} \end{bmatrix}$$

Similarly for $j = 2, 3, \dots, n$, the posterior distribution of β_j is

$$p(\beta_j | \bullet) \propto \exp \left[-\frac{1}{2} \sum_{i=1}^m da_i \{ \beta_j^2 da_i - 2\beta_j (C_{j1}(dm_{i1} - \alpha_1) + C_{j2}(dm_{i2} - \alpha_2) + \cdots + C_{jn}(dm_{in} - \alpha_n)) \} \right] \times (\beta_j - l)^{c-1} (u - \beta_j)^{d-1}$$

3. Σ_{ε}

The prior distribution for $\Sigma_{\varepsilon}^{-1}$ was assigned as follows:

$$\Sigma_{\varepsilon}^{-1} \sim \text{Wishart}(\mathbf{R}^{-1}, k)$$

Therefore the prior distribution of the covariance matrix Σ_{ε} follows an inverse-Wishart (\mathbf{R}, k) distribution. The inverse-Wishart density is given by

$$p(\Sigma_{\varepsilon}) = \frac{|\mathbf{R}|^{k/2}}{2^{\frac{kn}{2}} \Gamma_n\left(\frac{k}{2}\right)} |\Sigma_{\varepsilon}|^{-\frac{k+n+1}{2}} \exp \left\{ -\frac{1}{2} \text{tr}(\mathbf{R}\Sigma_{\varepsilon}^{-1}) \right\}$$

where Σ_{ε} and \mathbf{R} are $n \times n$ positive definite matrices; $\Gamma_n(\bullet)$ is the multivariate gamma function; $\Gamma_n\left(\frac{k}{2}\right) = \pi^{n(n-1)/4} \prod_{j=1}^n \left[\frac{k}{2} + \frac{(1-j)}{2} \right]$, and $\text{tr}(\bullet)$ denotes the *trace* of a square matrix \bullet , i.e. the sum of the diagonal elements of \bullet .

$$\begin{aligned}
p(\boldsymbol{\Sigma}_\varepsilon|\bullet) &\propto \prod_{i=1}^m p(\mathbf{d}\mathbf{m}_i|\bullet)p(\boldsymbol{\Sigma}_\varepsilon) \\
&\propto \prod_{i=1}^m (2\pi)^{-\frac{n}{2}} |\boldsymbol{\Sigma}_\varepsilon|^{-\frac{1}{2}} \exp\left[-\frac{1}{2}\{\mathbf{d}\mathbf{m}_i - (\boldsymbol{\alpha} + \boldsymbol{\beta}d\mathbf{a}_i)\}^T \boldsymbol{\Sigma}_\varepsilon^{-1} \{\mathbf{d}\mathbf{m}_i - (\boldsymbol{\alpha} + \boldsymbol{\beta}d\mathbf{a}_i)\}\right] \times \\
&\quad \frac{|\mathbf{R}|^{k/2}}{2^{\frac{kn}{2}} \Gamma_n(\frac{k}{2})} |\boldsymbol{\Sigma}_\varepsilon|^{-\frac{k+n+1}{2}} \exp\left\{-\frac{1}{2} \text{tr}(\mathbf{R}\boldsymbol{\Sigma}_\varepsilon^{-1})\right\} \\
&\propto |\boldsymbol{\Sigma}_\varepsilon|^{-\frac{m}{2}} \exp\left[-\frac{1}{2} \sum_{i=1}^m \{\mathbf{d}\mathbf{m}_i - (\boldsymbol{\alpha} + \boldsymbol{\beta}d\mathbf{a}_i)\}^T \boldsymbol{\Sigma}_\varepsilon^{-1} \{\mathbf{d}\mathbf{m}_i - (\boldsymbol{\alpha} + \boldsymbol{\beta}d\mathbf{a}_i)\}\right] \times \\
&\quad |\boldsymbol{\Sigma}_\varepsilon|^{-\frac{k+n+1}{2}} \exp\left\{-\frac{1}{2} \text{tr}(\mathbf{R}\boldsymbol{\Sigma}_\varepsilon^{-1})\right\}
\end{aligned}$$

Following the matrix algebra it can be proved (Hoff 2009) that

$$\sum_{i=1}^m \{\mathbf{d}\mathbf{m}_i - (\boldsymbol{\alpha} + \boldsymbol{\beta}d\mathbf{a}_i)\}^T \boldsymbol{\Sigma}_\varepsilon^{-1} \{\mathbf{d}\mathbf{m}_i - (\boldsymbol{\alpha} + \boldsymbol{\beta}d\mathbf{a}_i)\} = \text{tr}(\mathbf{S}\boldsymbol{\Sigma}_\varepsilon^{-1}), \text{ where}$$

$$\mathbf{S} = \sum_{i=1}^m \{\mathbf{d}\mathbf{m}_i - (\boldsymbol{\alpha} + \boldsymbol{\beta}d\mathbf{a}_i)\} \{\mathbf{d}\mathbf{m}_i - (\boldsymbol{\alpha} + \boldsymbol{\beta}d\mathbf{a}_i)\}^T$$

Therefore,

$$\begin{aligned}
p(\boldsymbol{\Sigma}_\varepsilon|\bullet) &\propto |\boldsymbol{\Sigma}_\varepsilon|^{-\frac{m+k+n+1}{2}} \exp\left[-\frac{1}{2} \text{tr}(\mathbf{S}\boldsymbol{\Sigma}_\varepsilon^{-1})\right] \times \exp\left\{-\frac{1}{2} \text{tr}(\mathbf{R}\boldsymbol{\Sigma}_\varepsilon^{-1})\right\} \\
&\propto |\boldsymbol{\Sigma}_\varepsilon|^{-\frac{m+k+n+1}{2}} \exp\left[-\frac{1}{2} \text{tr}((\mathbf{S} + \mathbf{R})\boldsymbol{\Sigma}_\varepsilon^{-1})\right]
\end{aligned}$$

Therefore we have

$$\boldsymbol{\Sigma}_\varepsilon \sim \text{inverse - Wishart}(\mathbf{S} + \mathbf{R}, m + k)$$

Appendix 2D OpenBUGS code for Bayesian calibration model of Case 1

Model specification

model{

likelihood function

for(i in 1 : m) {

for(j in 1 : n) {

dm[i , 1:n] ~ dmnorm(mu[i , 1:n], tau[,]) # tau is the precision

matrix

mu[i , j] <- alpha[j] + beta[j] * df[i]

}

}

Prior distribution specification

tau[1:n , 1:n] ~ dwish(R[,], n)

for(k in 1 : n) {

alpha[k] ~ dnorm(0, 1.0E-4)

beta1[k] ~ dbeta(5, 5)

beta[k] <- 2 * beta1[k]

```

    }

# Output analysis

Sigma.epsilon[1:n , 1:n] <- inverse(tau[ , ])

for (s in 1 : n){
  for (t in 1 : n) {
    rho [s, t]<-Sigma.epsilon[s, t] / sqrt(Sigma.epsilon[s, s] *
Sigma.epsilon[t, t])
  }
}

}# End of the model

# Data

list(dm = structure(

.Data = c(dm[1, 1], dm[1, 2], ..., dm[1, n],

dm[2, 1], dm[2, 2], ..., dm[2, n],

...

...

dm[m-1, 1], dm[m-1, 2], ..., dm[m-1, n],

dm[m, 1], dm[m, 2], ..., dm[m, n]),

```

```
.Dim = c(m, n),  
  
df = c(df[1], df[2], ..., df[i], ..., df[m]),  
  
m = 128, n = 4,  
  
R = structure(  
  
.Data = c(0.001, 0, 0, 0,  
  
0, 0.001, 0, 0,  
  
0, 0, 0.001, 0,  
  
0, 0, 0, 0.001),  
  
.Dim=c(4, 4))  
  
# Assignment of initial values for chain1  
  
list(tau = structure(  
  
.Data = c(0.01, 0, 0, 0,  
  
0, 0.01, 0, 0,  
  
0, 0, 0.01, 0,  
  
0, 0, 0, 0.01),  
  
.Dim = c(4, 4)),
```

```
alpha = c(0, 0, 0, 0), beta1= c(0.5, 0.5, 0.5, 0.5))
```

```
# Assignment of initial values for chain1
```

```
list(tau=structure(
```

```
.Data = c(0.05, 0, 0, 0,
```

```
0, 0.05, 0, 0,
```

```
0, 0, 0.05, 0,
```

```
0, 0, 0, 0.05),
```

```
.Dim = c(4, 4)),
```

```
alpha = c(1, 1, 1, 1), beta1= c(0.3, 0.3, 0.3, 0.3))
```

Appendix 2E OpenBUGS code for Bayesian calibration model of Case 2

```
# Model specification
```

```
model{
```

```
# likelihood function
```

```
  for( i in 1 : m ) {
```

```
    for( j in 1 : n ) {
```

```
      dm[i , 1:n] ~ dnmnorm(mu[i , 1:n], tau[ , ])# tau is the precision
```

```
matrix
```

```
      mu[i , j] <- alpha[j] + beta[j] * df[i]
```

```
    }
```

```
  }
```

```
# Prior distribution specification
```

```
tau[1:n , 1:n] ~ dwish(R[ , ], n)
```

```
for( k in 1 : n ) {
```

```
  alpha[k] ~ dnorm(0, 1.0E-4)
```

```
  beta1[k] ~ dbeta(5, 5)
```

```
  beta[k] <- 2 * beta1[k]
```

```

    }

# Output analysis

Sigma.epsilon[1:n , 1:n] <- inverse(tau[ , ])

for (s in 1 : n){
  for (t in 1 : n) {
    rho [s, t]<-Sigma.epsilon[s, t] / sqrt(Sigma.epsilon[s, s] *
Sigma.epsilon[t, t])
  }
}

}# End of the model

# Data

list(dm = structure(

.Data = c(dm[1, 1], ...,dm[1, n],

dm[2, 1], ..., dm[2, n],

...

...

dm[m-1, 1], ..., dm[m-1, n],

dm[m, 1], ..., dm[m, n],

```

```
.Dim = c(m, n),  
  
df = c(df[1], df[2], ..., df[i], ..., df[m]),  
  
m = 128, n = 3,  
  
R = structure(  
  
.Data = c(0.001, 0, 0,  
  
          0, 0.001, 0,  
  
          0, 0, 0.001),  
  
.Dim = c(3, 3))  
  
# Assignment of initial values for chain1  
  
list (tau = structure(  
  
.Data = c(0.01, 0, 0,  
  
          0, 0.01, 0,  
  
          0, 0, 0.01),  
  
.Dim = c(3, 3)),  
  
alpha = c(0, 0, 0), beta1 = c(0.5, 0.5, 0.5))
```



```
# Assignment of initial values for chain2
```

```
list(tau = structure(
```

```
  .Data = c(0.05, 0, 0,
```

```
    0, 0.05, 0,
```

```
    0, 0, 0.05),
```

```
  .Dim = c(3, 3)),
```

```
  alpha = c(1, 1, 1), beta1= c(0.3, 0.3, 0.3))
```

Appendix 3A Derivation of the Conditional Posterior Distributions of the HBM corrosion growth model

1. da_{ij}

Likelihood: $\mathbf{d}\mathbf{m}_i \sim MVN(\boldsymbol{\alpha} + \boldsymbol{\beta}d\mathbf{a}_i, \boldsymbol{\Sigma}_\varepsilon)$

By combining Eqs. (3.7) and (3.8d), we can write the prior distribution of da_{ij} as follows:

$da_{ij} \sim N\left(a_i(t_j - t_{oi})^{b_i}, \sigma_{\eta i}^2\right)$, which is *iid* for $i = 1, 2, \dots, m$; and independent for $j = 1, 2, \dots, n$.

Therefore, the conditional posterior distribution of da_{ij} ($i = 1, 2, \dots, m; j = 1, 2, \dots, n$) can be derived as follows:

$$\begin{aligned}
 p(da_{ij}|\bullet) &\propto p(\mathbf{d}\mathbf{m}_i|\mathbf{d}\mathbf{a}_i, \boldsymbol{\Sigma}_\varepsilon) p(da_{ij}|a_i, b_i, t_{oi}, \sigma_{\eta i}^2) \\
 &\propto (2\pi)^{-\frac{n}{2}} |\boldsymbol{\Sigma}_\varepsilon|^{-\frac{1}{2}} \exp\left[-\frac{1}{2}\{\mathbf{d}\mathbf{m}_i - (\boldsymbol{\alpha} + \boldsymbol{\beta}d\mathbf{a}_i)\}^T \boldsymbol{\Sigma}_\varepsilon^{-1} \{\mathbf{d}\mathbf{m}_i - (\boldsymbol{\alpha} + \boldsymbol{\beta}d\mathbf{a}_i)\}\right] \times \\
 &\quad \frac{1}{\sqrt{2\pi}\sigma_{\eta i}} \exp\left[-\frac{1}{2} \frac{\{da_{ij} - (a_i(t_j - t_{oi})^{b_i})\}^2}{\sigma_{\eta i}^2}\right] \\
 &\propto \exp\left[-\frac{1}{2} \left[\{\mathbf{d}\mathbf{m}_i - (\boldsymbol{\alpha} + \boldsymbol{\beta}d\mathbf{a}_i)\}^T \boldsymbol{\Sigma}_\varepsilon^{-1} \{\mathbf{d}\mathbf{m}_i - (\boldsymbol{\alpha} + \boldsymbol{\beta}d\mathbf{a}_i)\} + \frac{\{da_{ij} - (a_i(t_j - t_{oi})^{b_i})\}^2}{\sigma_{\eta i}^2} \right] \right]
 \end{aligned}$$

2. a_i

Likelihood: $da_{ij} \sim N\left(a_i(t_j - t_{oi})^{b_i}, \sigma_{\eta i}^2\right)$

Prior distribution: $a_i \stackrel{iid}{\sim} N(\mu_a, \sigma_a^2); a_i > 0$

Conditional posterior distribution:

$$\begin{aligned}
p(a_i|\bullet) &\propto \prod_{j=1}^n p(da_{ij}|a_i, b_i, t_{oi}, \sigma_{\eta i}^2) p(a_i|\mu_a, \sigma_a^2) \\
&\propto \prod_{j=1}^n \left(\frac{1}{\sqrt{\sigma_{\eta i}^2}} \exp \left(-\frac{1}{2} \left(\frac{da_{ij} - a_i(t_j - t_{oi})^{b_i}}{\sigma_{\eta i}} \right)^2 \right) \right) \times \frac{1}{\sqrt{\sigma_a^2}} \exp \left(-\frac{1}{2} \left(\frac{a_i - \mu_a}{\sigma_a} \right)^2 \right) \\
&\propto \exp \left[-\frac{1}{2} \left\{ \sum_{j=1}^n \left(\frac{da_{ij} - a_i(t_j - t_{oi})^{b_i}}{\sigma_{\eta i}} \right)^2 + \left(\frac{a_i - \mu_a}{\sigma_a} \right)^2 \right\} \right] \\
&\propto \exp \left[-\frac{1}{2} \left\{ \frac{\sigma_a^2 \sum_{j=1}^n \left\{ (a_i(t_j - t_{oi})^{b_i})^2 - 2da_{ij}a_i(t_j - t_{oi})^{b_i} + \sigma_{\eta i}^2(a_i^2 - 2a_i\mu_a) \right\}}{\sigma_{\eta i}^2 \sigma_a^2} \right\} \right] \\
&\propto \exp \left[-\frac{1}{2} \left\{ \frac{\sigma_a^2 a_i^2 \sum_{j=1}^n (t_j - t_{oi})^{2b_i} - 2a_i \sigma_a^2 \sum_{j=1}^n da_{ij}(t_j - t_{oi})^{b_i} + \sigma_{\eta i}^2(a_i^2 - 2a_i\mu_a)}{\sigma_{\eta i}^2 \sigma_a^2} \right\} \right] \\
&\propto \exp \left[-\frac{1}{2} \left\{ \frac{a_i^2 (\sigma_a^2 \sum_{j=1}^n (t_j - t_{oi})^{2b_i} + \sigma_{\eta i}^2) - 2a_i (\sigma_a^2 \sum_{j=1}^n da_{ij}(t_j - t_{oi})^{b_i} + \mu_a \sigma_{\eta i}^2)}{\sigma_{\eta i}^2 \sigma_a^2} \right\} \right]
\end{aligned}$$

Hence,

$$a_i \sim N \left(\frac{2a_i (\sigma_a^2 \sum_{j=1}^n da_{ij}(t_j - t_{oi})^{b_i} + \mu_a \sigma_{\eta i}^2)}{\sigma_a^2 \sum_{j=1}^n (t_j - t_{oi})^{2b_i} + \sigma_{\eta i}^2}, \frac{\sigma_{\eta i}^2 \sigma_a^2}{\sigma_a^2 \sum_{j=1}^n (t_j - t_{oi})^{2b_i} + \sigma_{\eta i}^2} \right)$$

3. b_i

Likelihood: $da_{ij} \sim N \left(a_i(t_j - t_{oi})^{b_i}, \sigma_{\eta i}^2 \right)$

Prior distribution: $b_i \stackrel{iid}{\sim} N(\mu_b, \sigma_b^2)$; $b_i > 0$

Conditional posterior distribution:

$$\begin{aligned}
 p(b_i|\bullet) &\propto \prod_{j=1}^n p(da_{ij}|a_i, b_i, t_{oi}, \sigma_{\eta i}^2) p(b_i|\mu_b, \sigma_b^2) \\
 &\propto \prod_{j=1}^n \left(\frac{1}{\sqrt{\sigma_{\eta i}^2}} \exp \left(-\frac{1}{2} \left(\frac{da_{ij} - a_i(t_j - t_{oi})^{b_i}}{\sigma_{\eta i}} \right)^2 \right) \right) \times \frac{1}{\sqrt{\sigma_b^2}} \exp \left(-\frac{1}{2} \left(\frac{b_i - \mu_b}{\sigma_b} \right)^2 \right) \\
 &\propto \exp \left[-\frac{1}{2} \left\{ \sum_{j=1}^n \left(\frac{da_{ij} - a_i(t_j - t_{oi})^{b_i}}{\sigma_{\eta i}} \right)^2 + \left(\frac{b_i - \mu_b}{\sigma_b} \right)^2 \right\} \right] \\
 &\propto \exp \left[-\frac{1}{2} \left\{ \frac{\sigma_b^2 \sum_{j=1}^n \{ (a_i(t_j - t_{oi})^{b_i})^2 - 2da_{ij}(a_i(t_j - t_{oi})^{b_i}) \} + \sigma_{\eta i}^2 (b_i^2 - 2b_i\mu_b)}{\sigma_{\eta i}^2 \sigma_b^2} \right\} \right]
 \end{aligned}$$

4. t_{oi}

Likelihood: $da_{ij} \sim N \left(a_i(t_j - t_{oi})^{b_i}, \sigma_{\eta i}^2 \right)$

Prior distribution: $t_{oi} \stackrel{iid}{\sim} U(0, t_1)$

Conditional posterior distribution:

$$\begin{aligned}
 p(t_{oi}|\bullet) &\propto \prod_{j=1}^n p(da_{ij}|a_i, b_i, t_{oi}, \sigma_{\eta i}^2) p(t_{oi}|t_1) \\
 &\propto \prod_{j=1}^n \left(\frac{1}{\sqrt{\sigma_{\eta i}^2}} \exp \left(-\frac{1}{2} \left(\frac{da_{ij} - a_i(t_j - t_{oi})^{b_i}}{\sigma_{\eta i}} \right)^2 \right) \right) \times \frac{1}{t_1}
 \end{aligned}$$

$$\propto \exp \left[-\frac{1}{2} \left\{ \sum_{j=1}^n \left(\frac{da_{ij} - a_i(t_j - t_{oi})^{b_i}}{\sigma_{\eta i}} \right)^2 \right\} \right]$$

5. $\sigma_{\eta i}^2$

Likelihood: $da_{ij} \sim N \left(a_i(t_j - t_{oi})^{b_i}, \sigma_{\eta i}^2 \right)$

Prior distribution of $1/\sigma_{\eta i}^2$: $1/\sigma_{\eta i}^2 \stackrel{iid}{\sim} G(o, p)$

Therefore, the prior distribution of $\sigma_{\eta i}^2$ is $\sigma_{\eta i}^2 \stackrel{iid}{\sim} IG(o, p')$, where $p' = 1/p$

Conditional posterior distribution:

$$\begin{aligned} p(\sigma_{\eta i}^2 | \bullet) &\propto \prod_{j=1}^n p(da_{ij} | a_i, b_i, t_{oi}, \sigma_{\eta i}^2) p(\sigma_{\eta i} | o, p') \\ &\propto \prod_{j=1}^n \left(\frac{1}{\sqrt{\sigma_{\eta i}^2}} \exp \left(-\frac{1}{2} \left(\frac{da_{ij} - a_i(t_j - t_{oi})^{b_i}}{\sigma_{\eta i}} \right)^2 \right) \right) \times \left(\frac{1}{(\sigma_{\eta i}^2)^{o+1}} \exp \left(-\frac{p'}{\sigma_{\eta i}^2} \right) \right) \\ &\propto \left(\frac{1}{\sqrt{\sigma_{\eta i}^2}} \right)^n \frac{1}{(\sigma_{\eta i}^2)^{o+1}} \exp \left(-\frac{\sum_{j=1}^n (da_{ij} - a_i(t_j - t_{oi})^{b_i}) + 2p'}{2\sigma_{\eta i}^2} \right) \\ &\propto (\sigma_{\eta i}^2)^{-\frac{n}{2} - o - 1} \exp \left(-\frac{\sum_{j=1}^n (da_{ij} - a_i(t_j - t_{oi})^{b_i}) + 2p'}{2\sigma_{\eta i}^2} \right) \end{aligned}$$

Hence,

$$\sigma_{\eta i}^2 \sim IG \left(\frac{n}{2} + o, \frac{\sum_{j=1}^n (da_{ij} - a_i(t_j - t_{oi})^{b_i}) + 2p'}{2} \right)$$

6. μ_a (μ_b)

Likelihood: $a_i \stackrel{iid}{\sim} N(\mu_a, \sigma_a^2); a_i > 0$

Prior distribution: $\mu_a \sim N(c, d^2)$

Conditional posterior distribution:

$$\begin{aligned}
 p(\mu_a | \bullet) &\propto \prod_{i=1}^m p(a_i | \mu_a, \sigma_a^2) p(\mu_a | c, d^2) \\
 &\propto \prod_{i=1}^m \left(\frac{1}{\sqrt{\sigma_a^2}} \exp\left(-\frac{1}{2} \left(\frac{a_i - \mu_a}{\sigma_a}\right)^2\right) \right) \times \left(\frac{1}{\sqrt{d^2}} \exp\left(-\frac{1}{2} \left(\frac{\mu_a - c}{d}\right)^2\right) \right) \\
 &\propto \exp \left[-\frac{1}{2} \left\{ \frac{1}{\sigma_a^2} \sum_{i=1}^m (a_i - \mu_a)^2 + \frac{1}{d^2} (\mu_a - c)^2 \right\} \right] \\
 &\propto \exp \left[-\frac{1}{2} \left\{ \frac{1}{\sigma_a^2} \sum_{i=1}^m (a_i^2 - 2a_i\mu_a + \mu_a^2) + \frac{1}{d^2} (\mu_a^2 - 2\mu_a c + c^2) \right\} \right] \\
 &\propto \exp \left[-\frac{1}{2} \left\{ \frac{1}{\sigma_a^2} \sum_{i=1}^m (\mu_a^2 - 2a_i\mu_a) + \frac{1}{d^2} (\mu_a^2 - 2\mu_a c) \right\} \right] \\
 &\propto \exp \left[-\frac{1}{2} \left\{ \frac{d^2(m\mu_a^2 - 2\mu_a \sum_{i=1}^m a_i) + \sigma_a^2(\mu_a^2 - 2\mu_a c)}{\sigma_a^2 d^2} \right\} \right] \\
 &\propto \exp \left[-\frac{1}{2} \left\{ \frac{\mu_a^2(md^2 + \sigma_a^2) - 2\mu_a(d^2 \sum_{i=1}^m a_i + c\sigma_a^2)}{\sigma_a^2 d^2} \right\} \right]
 \end{aligned}$$

Hence,

$$\mu_a \sim N\left(\frac{d^2 \sum_{i=1}^m a_i + c\sigma_a^2}{md^2 + \sigma_a^2}, \frac{\sigma_a^2 d^2}{md^2 + \sigma_a^2}\right)$$

Similarly,

$$\mu_b \sim N\left(\frac{h^2 \sum_{i=1}^m b_i + g\sigma_b^2}{mh^2 + \sigma_b^2}, \frac{\sigma_b^2 h^2}{mh^2 + \sigma_b^2}\right)$$

7. σ_a^2 (σ_b^2)

Likelihood: $a_i \stackrel{iid}{\sim} N(\mu_a, \sigma_a^2); a_i > 0$

Prior distribution of $1/\sigma_a^2$: $1/\sigma_a^2 \stackrel{iid}{\sim} G(e, f)$

Therefore, the prior distribution of σ_a^2 is $\sigma_a^2 \stackrel{iid}{\sim} IG(e, f')$, where $f' = 1/f$

Conditional posterior distribution:

$$\begin{aligned}
 p(\sigma_a^2 | \bullet) &\propto \prod_{i=1}^m p(a_i | \mu_a, \sigma_a^2) p(\sigma_a^2 | e, f') \\
 &\propto \prod_{i=1}^m \left(\frac{1}{\sqrt{\sigma_a^2}} \exp\left(-\frac{1}{2} \left(\frac{a_i - \mu_a}{\sigma_a}\right)^2\right) \right) \times \left(\frac{1}{(\sigma_a^2)^{e+1}} \exp\left(-\frac{f'}{\sigma_a^2}\right) \right) \\
 &\propto \left(\frac{1}{\sqrt{\sigma_a^2}} \right)^m \frac{1}{(\sigma_a^2)^{e+1}} \exp\left(-\frac{1}{2} \frac{1}{\sigma_a^2} \sum_{i=1}^m (a_i - \mu_a)^2 - \frac{f'}{\sigma_a^2}\right) \\
 &\propto (\sigma_a^2)^{-\frac{m}{2} - e - 1} \exp\left(-\frac{\sum_{i=1}^m (a_i - \mu_a)^2 + 2f'}{2\sigma_a^2}\right)
 \end{aligned}$$

Hence,

$$\sigma_a^2 \sim IG\left(\frac{m}{2} + e, \frac{\sum_{i=1}^m (a_i - \mu_a)^2 + 2f'}{2}\right)$$

Similarly,

$$\sigma_b^2 \sim IG\left(\frac{m}{2} + k, \frac{\sum_{i=1}^m (b_i - \mu_b)^2 + 2l'}{2}\right), \text{ where } l' = 1/l$$

Appendix 3B OpenBUGS code for HBM model of Case 1

model specification

model {

 for(i in 1 : m) {

 dm[i , 1:n]~dmnorm(mu[i, 1:n] , tau1[,]) #tau1 is the precision matrix, i.e. $\tau_1 = \Sigma_{\varepsilon}^{-1}$.

 for(j in 1: n) {

 mu[i, j]<-alpha[j] +beta[j]*da[i, j]

 da[i, j]~dnorm(dma[i, j], tau.eta[i])

 dma[i, j]<-a[i] *pow((t[i, j]-to[i]), b[i])

 }

 a[i]~dnorm(mu.a, tau.a)T(0,) # “T” denotes truncation

 b[i] ~dnorm(mu.b, tau.b)T(0,)

 to[i]~dunif(0, t1)

 tau.eta[i]~dgamma(0.001, 0.001)

 sigma.eta[i]<-1/sqrt(tau.eta[i])

 dp[i, 1]<-a[i] *pow((36-to[i]), b[i]) # Prediction depth

 dp[i, 2]<-a[i] *pow((37-to[i]), b[i])

 dp[i, 3]<-a[i] *pow((38-to[i]), b[i])

 dp[i, 4]<-a[i] *pow((39-to[i]), b[i])

 dp[i, 5]<-a[i] *pow((40-to[i]), b[i])

 }

 mu.a~dnorm(0, 0.0001)T(0,)


```

mu.b ~dnorm(0, 0.0001)T(0, )
tau.a~dgamma(0.01, 100)
tau.b~dgamma(0.01, 100)
tau1[1:n, 1:n]<-inverse(var[1:n, 1:n])
var[1, 1]<-35.73
var[1, 2]<-29.30
var[1, 3]<-37.88
var[2, 1]<-29.30
var[2, 2]<-35.73
var[2, 3]<-38.05
var[3, 1]<-37.88
var[3, 2]<-38.05
var[3, 3]<-82.28
}

# Data
list(alpha=c(2.04, 2.04, -15.28), beta=c(0.97, 0.97, 1.40),
dm = structure(
.Data = c(dm[1, 1], dm[1, 2], dm[1, 3],
dm[2, 1], dm[2, 2], dm[2, 3],
...
...
dm[m-1, 1], dm[m-1, 2], dm[m-1, 3],
dm[m, 1], dm[m, 2], dm[m, 3],

```



```

to=c(15, 15, 15, 15, 15, 15, 15, 15, 15, 15, 15, 15, 15, 15, 15, 15, 15, 15, 15, 15,
15, 15, 15, 15, 15, 15, 15, 15, 15, 15, 15, 15, 15, 15, 15, 15, 15, 15, 15, 15, 15,
15, 15, 15, 15, 15, 15, 15, 15, 15, 15, 15, 15, 15, 15, 15, 15, 15, 15, 15, 15, 15),

da=structure(

.Data=c(10, 15, 20,
10, 15, 20,
...
...
10, 15, 20),

.Dim=c(62, 3)))

# Assignment of initial values for chain2

list(mu.a =5, mu.b=0.5, tau.a=0.01, tau.b=0.01,
tau.eta=c(0.05, 0.05, 0.05, 0.05, 0.05, 0.05, 0.05, 0.05, 0.05, 0.05, 0.05, 0.05, 0.05,
0.05, 0.05, 0.05, 0.05, 0.05, 0.05, 0.05, 0.05, 0.05, 0.05, 0.05, 0.05, 0.05, 0.05,
0.05, 0.05, 0.05, 0.05, 0.05, 0.05, 0.05, 0.05, 0.05, 0.05, 0.05, 0.05, 0.05, 0.05, 0.05,
0.05, 0.05, 0.05, 0.05, 0.05, 0.05, 0.05, 0.05, 0.05, 0.05, 0.05, 0.05, 0.05, 0.05,
0.05),

da=structure(

.Data=c(10, 20, 30,
10, 15, 30,
10, 15, 30),
...
...

```


Appendix 3C OpenBUGS code for HBM model of Case 2

```

# model specification

model {

  for( i in 1 : m ) {

    dm[i , 1:n]~dmnorm(mu[i, 1:n] , tau1[, ])

    for(j in 1: n) {

      mu[i, j]<-alpha[j] +beta[j]*da[i, j]

      da[i, j]~dnorm(dma[i, j], tau.eta[i])

      dma[i, j]<-a[i] *pow((t[i, j]-to[i] ), b[i])

    }

    a[i]~dnorm(mu.a, tau.a)T(0, )

    b[i] ~dnorm(mu.b, tau.b)T(0, )

    to[i]~dunif(0, 28)

    dp[i, 1]<-a[i] *pow((38-to[i] ), b[i]) # Prediction depth

    dp[i, 2]<-a[i] *pow((39-to[i] ), b[i])

    dp[i, 3]<-a[i] *pow((40-to[i] ), b[i])

    tau.eta[i]~dgamma(0.001, 0.001)

    sigma.eta[i]<-1/sqrt(tau.eta[i])

  }

  mu.a~dnorm(0, 0.0001)T(0, )

  mu.b~dnorm(0, 0.0001)T(0, )

  tau.a~dgamma(0.01, 100)

```

```
tau.b~dgamma(0.01, 100)

tau1[1:n, 1:n]<-inverse(var[1:n, 1:n])

var[1, 1]<-28.35

var[1, 2]<-28.87

var[1, 3]<-31.44

var[2, 1]<-28.87

var[2, 2]<-50.75

var[2, 3]<-38.75

var[3, 1]<-31.44

var[3, 2]<-38.75

var[3, 3]<-58.71

}

# Data

list(alpha=c(-4.23, -9.50, -3.54), beta=c(0.89, 0.91, 1.00),

t = structure(

  .Data=c(32, 35, 37,

32, 35, 37,

...

...

32, 35, 37),

  .Dim = c(60, 3)),

m = 60, n = 3,

dm = structure(
```

```

.Data = c(dm[1, 1], dm[1, 2], dm[1, 3],
dm[2, 1], dm[2, 2], dm[2, 3],
...
...
dm[m-1, 1], dm[m-1, 2], dm[m-1, 3],
dm[m, 1], dm[m, 2], dm[m, 3],

.Dim = c(m, 3))

# Assignment of initial values for chain1

list(mu.a=5, mu.b=0.5, tau.a=0.01, tau.b=0.01,
tau.eta=c(0.01, 0.01, 0.01, 0.01, 0.01, 0.01, 0.01, 0.01, 0.01, 0.01, 0.01, 0.01, 0.01, 0.01,
0.01, 0.01, 0.01, 0.01, 0.01, 0.01, 0.01, 0.01, 0.01, 0.01, 0.01, 0.01, 0.01, 0.01, 0.01, 0.01,
0.01, 0.01, 0.01, 0.01, 0.01, 0.01, 0.01, 0.01, 0.01, 0.01, 0.01, 0.01, 0.01, 0.01, 0.01, 0.01,
0.01, 0.01, 0.01, 0.01, 0.01, 0.01, 0.01, 0.01, 0.01, 0.01, 0.01, 0.01, 0.01),
a=c(10, 10, 10, 10, 10, 10, 10, 10, 10, 10, 10, 10, 10, 10, 10, 10, 10, 10, 10, 10, 10, 10,
10, 10, 10, 10, 10, 10, 10, 10, 10, 10, 10, 10, 10, 10, 10, 10, 10, 10, 10, 10, 10, 10, 10,
10, 10, 10, 10, 10, 10, 10, 10, 10, 10, 10, 10, 10),
b=c(0.5, 0.5, 0.5, 0.5, 0.5, 0.5, 0.5, 0.5, 0.5, 0.5, 0.5, 0.5, 0.5, 0.5, 0.5, 0.5, 0.5, 0.5, 0.5,
0.5, 0.5, 0.5, 0.5, 0.5, 0.5, 0.5, 0.5, 0.5, 0.5, 0.5, 0.5, 0.5, 0.5, 0.5, 0.5, 0.5, 0.5, 0.5,
0.5, 0.5, 0.5, 0.5, 0.5, 0.5, 0.5, 0.5, 0.5, 0.5, 0.5, 0.5, 0.5, 0.5, 0.5, 0.5, 0.5, 0.5,
0.5),
to=c(10, 10, 10, 10, 10, 10, 10, 10, 10, 10, 10, 10, 10, 10, 10, 10, 10, 10, 10, 10, 10, 10,
10, 10, 10, 10, 10, 10, 10, 10, 10, 10, 10, 10, 10, 10, 10, 10, 10, 10, 10, 10, 10, 10, 10,
10, 10, 10, 10, 10, 10, 10, 10, 10, 10, 10, 10, 10),

```



```
.Data=c(10, 15, 25,  
10, 15, 25,  
...  
...  
10, 15, 25),  
.Dim=c(60, 3))
```

Curriculum Vitae

Name: Mohammad Al-Amin

Birth Place Brahmanbaria, Bangladesh

Date of Birth 06 June, 1986

Post-secondary Education: Bangladesh University of Engineering and Technology
Dhaka, Bangladesh
2004-2009, B.Sc. (Civil Engineering)

The University of Western Ontario
London, Ontario, Canada
2010-2012, M.E.Sc. (Structural Engineering)

Honours and Awards: Dutch-Bangla Bank Foundation Scholarship
2004-2009

Graduate Thesis Research Award
The University of Western Ontario
2011-2012

Related Work Experience Junior Engineer
PNJ Associates
Dhaka, Bangladesh
01/11/2009-15/08/2010

Research and Teaching Assistant
The University of Western Ontario
2010-2012